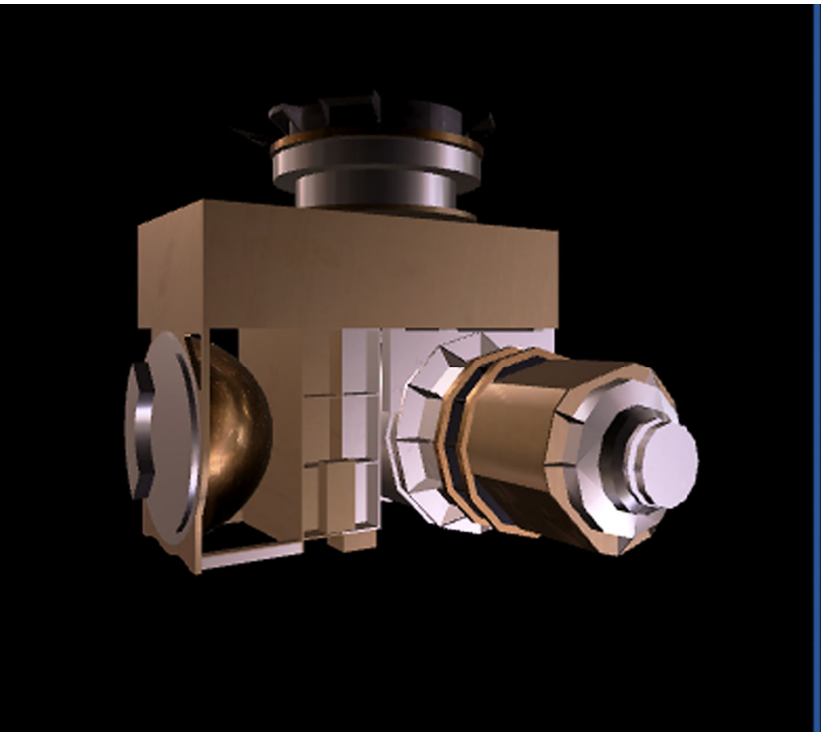

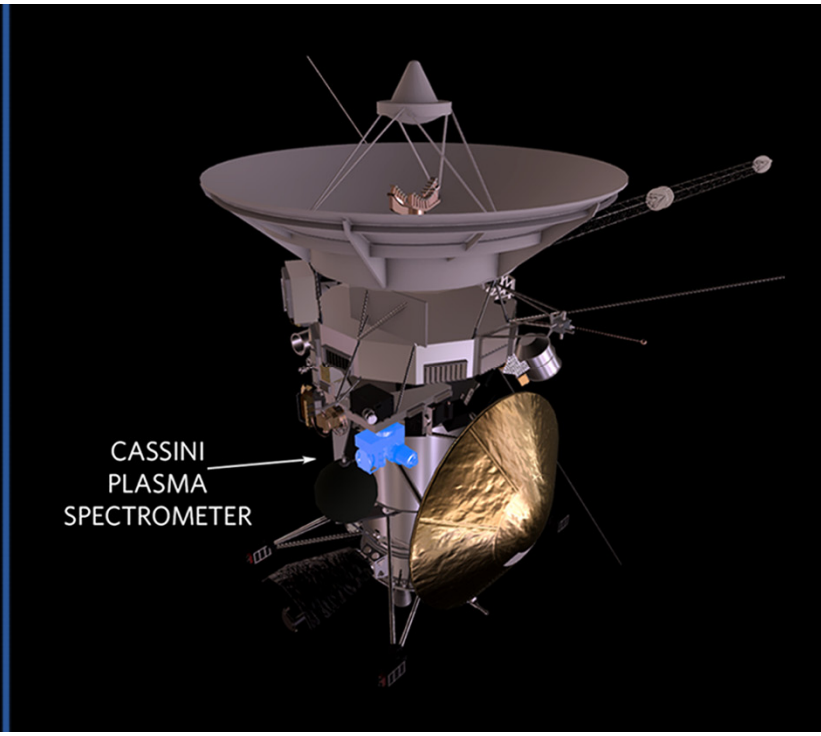

Cassini Plasma Spectrometer

The Cassini Plasma Spectrometer (CAPS) was an in situ instrument that investigated the plasma environment in and near Saturn's magnetosphere. CAPS made measurements of the plasma composition, density, flow velocity, and temperature. The **science objectives** of CAPS were to determine the sources of plasma in the magnetosphere, characterize dynamic magnetospheric processes, and study the interaction of plasma sources, including Enceladus, the rings, and Titan, with the magnetosphere.

CAPS comprised three sensors, a time-of-flight Ion Mass Spectrometer (IMS), an Electron Spectrometer (ELS), and an Ion Beam Spectrometer (IBS) that together measured the composition and velocity distributions of positively and negatively charged ions and electrons from approximately 1 eV to several tens of keV depending on the sensor. CAPS was mounted on an actuator platform that rotated the sensor fields-of-view parallel to the spacecraft Z-axis in order to compensate for 3-axis stabilization of the Cassini spacecraft.

CONTENTS

Figures

Tables

EXECUTIVE SUMMARY

The CAPS instrument was designed to make comprehensive three-dimensional mass-resolved measurements of the full variety of plasma phenomena found in Saturn's magnetosphere. The CAPS science objectives can be broken into four general categories: 1) investigate the structure, composition, and boundaries of the magnetosphere; 2) identify plasma sources and sinks and the physical processes by which they are created and quenched; 3) understand dynamical processes of plasma acceleration, transport, and loss; and 4) study the interactions of plasma sources, including Enceladus, the rings, and Titan, with the magnetosphere.

> … CAPS made significant discoveries and contributions to our understanding of a wide range of phenomena including the unexpected composition and interactions of the ionospheres of Titan, Enceladus, and the rings, as well as the structure and dynamics of the magnetosphere.

By the end of CAPS operations, the investigation met all of the goals and objectives listed above, thereby fulfilling objectives laid out in the Announcement of Opportunity (AO) and Cassini Solstice Mission (CSM). In doing so CAPS made significant discoveries and contributions to our understanding of a wide range of phenomena including the unexpected composition and interactions of the ionospheres of Titan, Enceladus, and the rings, as well as the structure and dynamics of the magnetosphere. Examples of the former include discovery of massive negative and positive ions at Titan and Enceladus, while the latter include radial transport driven by centrifugal interchange instabilities and the massive co-rotating magnetodisk in the middle magnetosphere. CAPS also showed itself to be uniquely capable of measuring the composition and energy distributions of hot plasmas found in the magnetotail and outer magnetosphere. During cruise to Saturn CAPS made the first observations of interstellar pickup ions beyond the orbit of Jupiter as well as the sun's hydrogen shadow.

CAPS operated from checkout through the Cruise phase (1997 through 2004), the primary mission (2004 through June 2008), the extended mission (2008 through 2010) and well into the Solstice Mission (2010 through 2012). Due to an unfortunate and very unusual power anomaly (see National Electrical Safety Code (NESC) RP-12-00803) CAPS did not operate from June 2012 through the end of mission.

During cruise CAPS measured the plasma environments inside the Earth's magnetosphere, and the upstream solar wind, bow shock and magnetosheath conditions at Jupiter. Following the Jupiter swing-by, CAPS made its first major discovery when it captured the first direct, mass-resolved observations of heliospheric pickup ions (H^+, He^+, He^{++}, and O^+) beyond the orbit of Jupiter [McComas et al. 2004]. The neutral interstellar atoms corresponding to these ion species were ionized by solar ultraviolet (UV) and then picked up by the solar wind. The observations were made

between 6.4 and 8.2 astronomical unit (AU) consistent with gravitational focusing of the neutral atoms by the Sun.

During orbital insertion on July 1, 2004, CAPS discovered a completely unexpected atmosphere and ionosphere hovering over the main rings [Young et al. 2005]. The ring plasma is created by photon sputtering of ring ices, creating O_2 molecules that are ionized by solar UV, leading to an admixture of O^+, OH^+, H_2O^+ and O_2^+ ions between the F-ring and G-ring [Tokar et al. 2005].

CAPS contributions to understanding the complexity of the magnetosphere began with the ring plasma, followed by further discoveries of unusual plasma populations and phenomena with each new satellite encounter. During the initial flyby of Titan, the ELS, which was designed to measure electron velocity distributions, showed that in fact the high-altitude (~1000 km) ionosphere is rich in negatively charged ions with masses up to and greater than 13,800 amu/q. At the same time the IBS, designed primarily for solar wind and high Mach number flows, identified heavy positive ions with masses up to 350 amu/q and occasionally above 1000 amu/q [Coates et al. 2007a; Coates et al. 2010a] that were an extension of lower-mass (1 to 100 amu/q) ion spectra measured by Ion and Neutral Mass Spectrometer (INMS) [Coates 2005; Waite et al. 2005, 2007a]. Analysis of these data, combined with chemical modeling, suggests that the heavy ions are precursors of aerosols and tholins seen much lower in the atmosphere (~few hundreds of km). Estimates suggest that this process results in ~0.1 to ~1.0 metric tons per year of tholins added to the atmosphere. These discoveries, together with modeling of the atmosphere and its chemistry, reveal that Titan has what is easily the most complex atmosphere in the solar system.

Titan's ion wake is the most prominent example of Titan-magnetosphere interactions [Hartle et al. 2006b; Wellbrock et al. 2012]. It consists primarily of heavy (m/q ~16 and 28) and light (m/q = 1–2) ions stripped off by the co-rotating flow at a rate estimated to be ~0.3 to 4.0×10^{28} amu/q/s down Titan's wake (or tail as some prefer).

Extensive measurements of the distribution of ion density, temperature and flow velocity made over a period of 4.5 years have revealed the major structures and flow patterns in the magnetosphere [Thomsen et al. 2010]. From Voyager data it was expected that N^+ originating at Titan would be a major plasma component; however, Thomsen et al. [2010] established that water group ions (O^+, OH^+, H_2O^+ and H_3O^+ collectively referred to as W^+) are the dominant species, coming primarily from ion pickup near the orbit of Enceladus. Titan is a relatively weak source with most magnetospheric N^+ originating at Enceladus—yet another surprising feature of the chemical composition of Saturn's magnetosphere [Smith et al. 2008]. CAPS also found that the plumes of Enceladus contain large amounts of negative ions and heavy positive ions with a mass continuum that extends up into the tens of thousands of amu/q reaching into the realm of nano-grains at densities up to 10^3 particles/cm^3 [Hill et al. 2012]. It is thought that as plume gases are ionized they load and deflect the passing co-rotating magnetic flux tubes, leading to the addition of approximately 100 kg/s of fresh Enceladus plasma. This amount of mass loading was confirmed by an analysis of stresses in the distended magnetodisk located in the equatorial plane [Sergis et al. 2010]. Calculation of stress balance in the magnetodisk leads to estimates of a total mass

~10^6 kg for the closed portion of the magnetosphere. Extensive studies of magnetotail dynamics showed that the primary magnetospheric plasma sink is associated with plasmoid generation and subsequent losses down the magnetotail into the solar wind [Hill et al. 2008].

As the number of orbits piled up and their geometric relation to magnetosphere boundaries changed with local time and latitude, the structure of the magnetosphere became apparent. The distribution of plasma is highest near the orbit of Enceladus (3.95 R_S) with an average density ~100 ions/cm^3 and then drops by a factor of ~1000 near ~16 R_S [Thomsen et al. 2010]. Plasma structures in Saturn's magnetosphere do not appear to have strong long-term annual or seasonal variability although on scales of hours to days plasma structures created by interchange instabilities create marked variation in plasma properties [Hill et al. 2005].

From the very first orbits passing through the high-altitude magnetosphere, it was apparent that the magnetosphere is far more dynamic than previously thought. Hundreds of plasma injection events were observed in which hotter plasma from beyond ~10 R_S invaded cold plasma deeper in the magnetosphere. Detailed analysis revealed that the injections were the result of a centrifugal instability set up by forces generated by the co-rotating inner magnetosphere [Hill et al. 2005]. Transport driven by these instabilities is largely responsible for moving the hundreds of kilograms of plasma produced by Enceladus into the outer magnetosphere.

Many plasma observations and analyses featured data collected simultaneously by most if not all of the particles and fields instruments. Prior to the mission it was understood that collaboration by the entire Magnetospheres and Plasma Science (MAPS) suite (CAPS, INMS, MAG, MIMI, and RPWS) was essential to the success of Cassini, and would lead to synergistic science opportunities on many spatial and temporal scales. A glance at the references included with this report, and the complete CAPS publication list of papers in the refereed literature, shows that the goal was indeed achieved.

The CAPS investigation team met or exceeded all of the objectives of both the Primary and Cassini Solstice Missions.

CAPS operated for the first eight years of the Cassini mission before a power anomaly forced the instrument to be turned off in 2012 [NASA Engineering and Safety Center (NESC)-2013]. Understandably this left behind numerous science questions (see the section below on Top Open Questions). Thus there are many significant issues remaining, one in particular is the processes responsible for creating heavy negative and positive ions in the atmosphere of Titan and the plumes of Enceladus. Other important open questions about the magnetosphere include: how is plasma transported outward, and magnetic flux returned inward, in the region between 12 and ~20 to ~25 R_S? and where and how does the magnetosphere unload tons of cold, dense plasma?

As this cursory summary shows, the CAPS investigation met or exceeded all of the objectives of both the Primary and Cassini Solstice Missions. During the Primary Mission CAPS achieved all of its highest-priority goals and major objectives. Moreover, serendipity at Titan and Enceladus

allowed CAPS ELS to make the completely unanticipated discovery of negative ions in both ionospheres. This, and heavy positive ion measurements by IBS, have led to an entirely new understanding of the chemistry of planetary atmospheres with features that were not anticipated in the initial instrument objectives. CAPS measurements of the global composition of the magnetosphere, the surprisingly wide range of plasma sources and sinks, and the primary drivers of plasma transport all mark major contributions to our understanding of magnetospheric physics. Solstice Mission objectives were to enhance our knowledge of the general workings of the magnetosphere and to increase our understanding of long-term temporal variations in plasma sources and sinks from one solstice to the next.

Top Science Highlights

1. Discovered heavy negative ions with masses up to and greater than 13,800 amu/q, and heavy positive ions with masses up to and greater than 1000 amu/q in Titan's upper atmosphere.

2. Discovered that the newly found massive ions are precursors to the formation of atmospheric aerosols and tholins that form the haze components of Titan's upper atmosphere, and that may eventually settle to its surface.

3. Discovered that the plumes of Enceladus contain heavy negatively and positively charged water cluster ions and ice grains with masses extending well above 10,000 amu/q.

4. Discovered that the Enceladus plume emits ~100 kg/s of water-based ions (O^+, OH^+, H_2O^+ and H_3O^+) that become the dominant source of plasma in the magnetosphere.

5. Discovered that Enceladus, not Titan, is the primary source of nitrogen ions in the magnetosphere as was previously thought from Voyager data.

6. Discovered that the main rings of Saturn have an atmosphere consisting of molecular oxygen and water ion products.

7. Discovered that plasma found outside the edge of the A-ring is quenched by nanograins from the rings.

8. Discovered that the ring atmosphere changes with season because of changes in illumination by solar UV.

9. Discovered molecular oxygen exospheres around Dione and Rhea and a dust ring or halo at Rhea.

10. Discovered hydrogen ion outflows leaving Saturn's high latitude atmosphere along magnetic field lines.

11. Discovered hundreds of hot plasma injections in the middle magnetosphere. These result from centrifugal interchange instabilities that drive the radial transport of plasma out of the inner magnetosphere.

12. Discovered a massive heavy-ion co-rotating magnetodisk in the middle magnetosphere weighing ~1000 tons.

13. Discovered an unknown and unexplained plasma convection pattern in the inner magnetosphere that displaces plasma inward near local midnight and outward near noon.

14. Discovered plasmoids carrying water ions down the magnetotail at distances greater than 3 million km at a rate consistent with removal of plasma originating from Enceladus.

15. Discovered that both Dungey-style and Vasyliunas-style reconnection events, which propel plasma down the magnetotail, may occur depending on solar wind conditions.

16. Discovered heliospheric pickup ions (H^+, He^+, He^{++}, and O^+) beyond the orbit of Jupiter. This is the first evidence for interstellar helium atoms and is only the second observation of the Sun's hydrogen shadow.

17. Discovered that Jupiter's bow shock and magnetosheath extend as far as 700 Jupiter radii downstream from the planet.

Top Open Questions

1. What are the chemical and physical mechanisms that create and destroy large negative and positive ions at Titan, and what are their lifetimes?

2. Sunlight clearly plays a key role in determining the maximum negative ion masses found in Titan's atmosphere, but does it control production, loss, or the balance between the two?

3. What is the mechanism causing heavy ions in Titan's atmosphere to form aerosols? And do the aerosols then grow to form tholins? Or are they all the same thing?

4. Are heavy ions (above ~100 amu/q) at Titan picked up by co-rotating plasma, and negative ions picked up in a way that is analogous to positive ions? If so then what is their fate? Are they ejected or destroyed?

5. The loss mechanisms for some species such as N_2 and CH_4 are critical to understanding Titan's atmosphere. Can the daughter ion species be detected in the magnetosphere and the loss rates estimated?

6. What are the chemical and physical mechanisms that create and destroy large negative and positive water ions and neutrals in the Enceladus plume?

7. How are the nano-grain ice-particles in the Enceladus plume formed?

8. How is cold heavy plasma transported outward from the middle magnetosphere (~12 R_S) and magnetic flux returned from the outer magnetosphere (~25 R_S)?

9. Where and how does the magnetosphere unload its cold, dense plasma?

10. How do the sources of magnetospheric plasma (Enceladus plumes, Titan's ionosphere, Saturn, solar wind) match up with the sinks removing plasma (solid surface adsorption, reconnection and plasmoids) to keep the mass budget of the magnetosphere in equilibrium? Does this change with season?

11. What role does the ring atmosphere play in determining the composition of Saturn's upper atmosphere?

12. What causes the inner magnetosphere's dawn-ward convection that drives the noon-midnight asymmetry in plasma temperature, plasma density, energetic particle intensity, etc.?

13. What determines the scale size and inflow speed of interchange injections, and what determines the apparently variable rate and depth of such injections?

14. What is the relationship between large-scale, tail-reconnection-driven plasma injections and small-scale interchange injections?

15. Jupiter's magnetosheath was observed as far as 700 R_J downstream—how far does it extend?

Instrument Summary

The CAPS instrument was a novel design comprising three high-performance sensors that together measured the velocity distributions of electrons and ions from approximately one electron volt (eV) to several tens of kiloelectron volts (keVs) [Young et al. 2004]. The CAPS sensors exceeded their design goals, leading to discoveries of new charged particle populations that reveal the magnetosphere and Saturn's satellites to be a far richer and more complex environment than earlier Voyager data and scientific modeling would have led us to believe. In particular, the discovery at Titan of heavy and ultra-heavy negatively and positively charged ions will lead the way to an understanding of the origin and growth of tholins in Titan's atmosphere. The discovery at Enceladus of a broad range of charged particles including heavy and ultra-heavy negatively and positively charged ions, charged water cluster ions, and charged nano-grains, has helped establish the unique characteristics of the plumes as well as chemical and ionization processes in dusty plasmas.

The photograph in Figure CAPS-1 shows the location and orientation of the three sensors (arrows point to their apertures), and the data processing unit (DPU) which contains command and control electronics, data processors, spacecraft interfaces, and most of the low- and high-voltage power supplies. The entire instrument including the DPU is mounted on an actuator capable of rotating the CAPS sensors through a range of 160º parallel to the spacecraft z-axis at a nominal rate of 1°/s. This compensates in part for the three-axis stabilization of the Cassini spacecraft. Figure CAPS-2 is a cross-section of the optical design of the three sensors in simplified form.

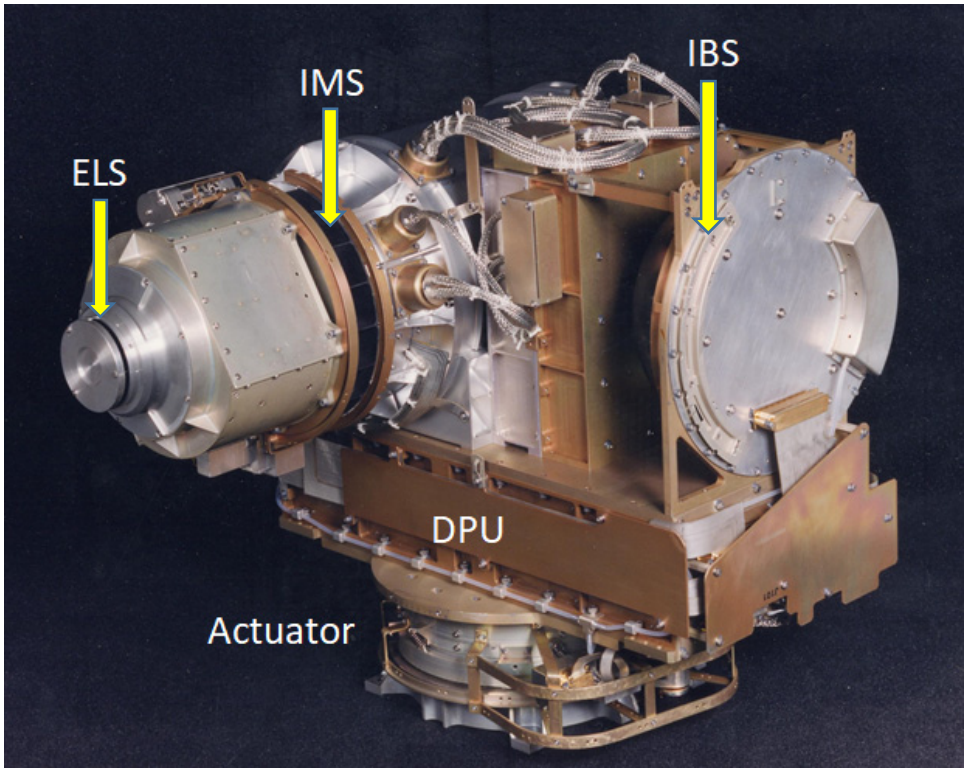

Figure CAPS-1. The CAPS flight unit prior to integration on the Cassini spacecraft late in 1997.

The ELS is an electrostatic energy-angle analyzer that measures electron velocity distributions with medium energy resolution ($\Delta E/E = 0.17$) and azimuthal resolution $\Delta\alpha = 5.2º$ (the angle α is in the plane of the drawing). ELS covers an elevation range of 160° in elevation with a resolution of $\Delta\beta = 20°$ corresponding to eight sectors on the microchannel plate detector. (These response characteristics were chosen to match those of the IMS.) As for all three CAPS sensors the azimuthal range of coverage when the instrument is scanned is ~160° corresponding to the actuator rotation range (the actuator axis of rotation is perpendicular to the plane of the paper). The energy range of 1 eV to 28 keV is sufficient to cover thermal energy electrons found near the icy satellites and rings and all but the most energetic trapped populations found in the outer magnetosphere. A scan over the energy range requires 2.0 s.

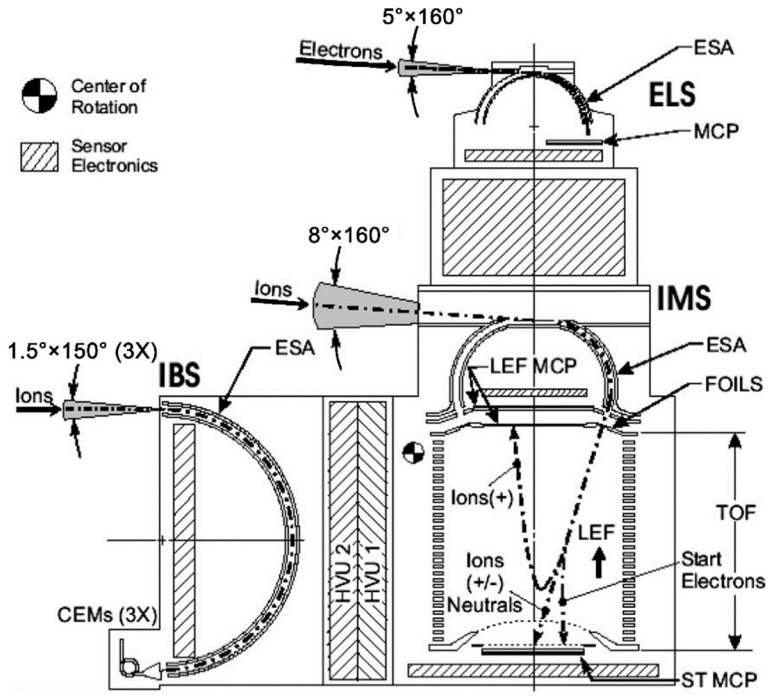

Figure CAPS-2. Cross-section of the three CAPS sensors showing schematic optical paths.

An important feature of the ELS that was not anticipated prior to arrival at Saturn was its ability to measure negative ions as well as electrons. Some scientists miss the point that an energy/charge analyzer is insensitive to the mass/charge of particles passing through its electric field and reaching the detector. It is easy to see why this is the case. The centrifugal force on a charged particle is $F = mv^2/qR_0$, where R_0 is the central radius of the analyzer and the velocity squared of the same particle is $v^2 = (2\ E/q)/(m/q)$, E/q is ion energy/charge, and m/q is its mass/charge. If we substitute the second equation into the first, then m/q cancels out and the force bending the particle through the analyzer is dependent only on energy per charge: $F = 2\ E/qR_0$. The ELS energy distribution can then be converted from E/q to $m/q = 2\ E/qV_{SC}^2$ where V_{SC} is the spacecraft ram velocity (this equation is conceptual—the actual conversion from ion energy to mass/charge must account for both the ELS passbands and the thermal velocity of the measured distribution).

ELS sensitivity, like those of the other two CAPS sensors, is proportional to its geometric factor G, which is defined such that:

$$C = J\ G\ \Delta t,$$

where C is the detector counting rate in counts/s, J is the differential particle energy flux in eV/cm^2 s sr eV, and Δt is the sampling interval in seconds. The geometric factor is made up of several elements and in its approximate (conceptual) form is given by:

$$G \sim A\ \varepsilon\ \tau\ \Delta\alpha\ \Delta\beta\ \Delta E/E,$$

where A is the effective analyzer sensitive area in cm^2, ε is the detector efficiency in counts/ion, τ is the transmission of any grids in the optical path (dimensionless), Δα and Δβ (radians) are the angle passbands introduced above, and ΔE/E is the energy passband (in units of eV/eV). The geometric factor of ELS is calibrated to be $G = 1.4 \times 10^{-2}$ cm^2 sr eV/eV.

The IBS is also an electrostatic energy-angle analyzer, but with the very high resolution required to resolve high Mach number ion flows (~10 or greater) found in the solar wind in the outer solar system, and during flybys through the cold ionospheres of Titan and Enceladus. An advantage of this design that turned out to be far more important than anticipated, is that the high spacecraft flyby velocities (~7 km/s at Titan) and low ion thermal speeds (<100 m/s) yielded very high Mach number flows in the spacecraft frame of reference that allowed IBS to effectively resolve ion velocity distributions into mass spectra.

IBS energy resolution is ΔE/E = 0.014 with an angle resolution in azimuth x elevation of Δα × Δβ = 1.4° × 1.5°. Although the range in azimuth is very limited by its high resolution, IBS has an unresolved elevation response of 160° for a single detector (out of three). IBS energy range is 1 eV to 50 keV which is covered in 2.0 s. The very high resolution makes the IBS sensitivity of 4.7×10^{-5} about two orders of magnitude smaller than that of the other two sensors.

The IMS is a time-of-flight (TOF) ion mass spectrometer that has certain advantages in terms of sensitivity, energy range and mass resolution in comparison to other types of mass spectrometers flown on space missions [Young et al. 2004]. Figure CAPS-2 shows a cross-section schematic of the IMS optics.

The IMS measures ion energy and angle distributions with a resolution similar to ELS (ΔE/E = 0.17 and Δα = 8.3°). Its elevation range, and resolution is the same as ELS: Δβ = 20° in eight sectors covering 160°. The IMS energy range is 1 to 50,000 eV which is covered in 4.0 seconds.

Ions enter the IMS via an electrostatic energy analyzer (ESA) operating on the same principle as the ELS and IBS sensors. After leaving the ESA ions are accelerated by 15 kV before striking one of eight ultra-thin carbon foils (~1 $\mu g/cm^2$) and entering the TOF analyzer. As ions leave the foils they emit secondary electrons that strike the Straight Through (ST) microchannel plate (MCP) detector, initiating timing electronics. When ions (which may be positive, negative, or neutral) strike either the ST or LEF detectors (Figure CAPS-2) the event stops the timing and the ion TOF is recorded together with ion energy and angle of arrival.

IMS makes two independent TOF measurements, medium and high resolution. Medium resolution measurements are made with ST optics (Figure CAPS-2) at M/ΔM ~8 with a range M/q 1 to ~400 amu/q. The sensitivity in this mode is typically ~5×10^{-3} cm^2 sr eV/eV depending on ion species and energy. High resolution measurements are made with time-focusing linear electric field (LEF) reflectron optics at resolutions M/ΔM ~60 depending on ion energy and species. The mass range in this mode is 1 to ~100 amu/q.

Ion mass/charge is given approximately by the simple equation $M/q \approx 2E/q\ (T/L)^2$ where E/q is ion energy/charge, T is the time-of-flight, and L is the effective distance the ion travels from carbon foil to detector about 18 cm. However, this equation is only approximate because energy lost in the foils and optics has to be considered and the flight distance depends on the angle at which the ion leaves the foil.

This abbreviated description of the IMS optics makes clear that there are several factors dependent on averages over random processes that affect TOF measurements. The width of the TOF peaks, and therefore mass resolution, are affected by ESA energy resolution, by scattering in the carbon foils and the effect that that has on trajectories. Sensitivity depends on ion species, transmission through the foils, and the secondary electron yield of the foils and the two detectors. In addition, "ghost" peaks caused by scattering may appear, further complicating TOF spectra. The complexity of IMS optics and electronics, and its dependence on random atomic processes that are essential to its functioning, were addressed by extensive pre-flight calibration as well as post-flight calibration of a high-precision ion optical model, and extensive numerical simulations. In the end these post-flight efforts allowed accurate determinations of even minor ion species. Prominent examples are measurements of very small amounts of nitrogen and nitrogen-bearing compounds in the outer magnetosphere [Smith et al. 2005, 2007, 2008].

> The complexity of IMS optics and the multiple random processes that contribute to CAPS measurements of mass spectra were addressed by extensive post-flight calibration of a high precision model of the optics, and literally years of numerical simulations.

CAPS collects data based on two measurement cycles. During the shorter A-Cycle (32 seconds) CAPS acquires ion and electron count rate distributions consisting of energy × eight elevation-angle "pixels" × TOF (in the case of IMS). The longer B-Cycle (256 seconds) consists of 8 A-Cycles and corresponds very roughly to the amount of time needed for the CAPS turntable, which moves approximately 1°/s, to rotate through an azimuth range of ~160°. Data are acquired and buffered for one B-Cycle in one side of a ping-pong memory while a second B-Cycle is acquired in the other side. The first side is then read out to telemetry and the next cycle of data acquired.

A critically important aspect of the CAPS instrument that greatly affected scientific aspects of the investigation was that because CAPS was mounted on the Particles and Fields Pallet, which is fixed to the spacecraft (Figure CAPS-3), it was not possible to view the full sky (4π sr) at any one time. Being able to scan the entire sky is critical to plasma observations because plasma distributions are seldom isotropic and are typically distorted in many ways (e.g., field-aligned, pancaked, rammed), all of which are key to understanding the phenomena causing the anisotropy in the first place.

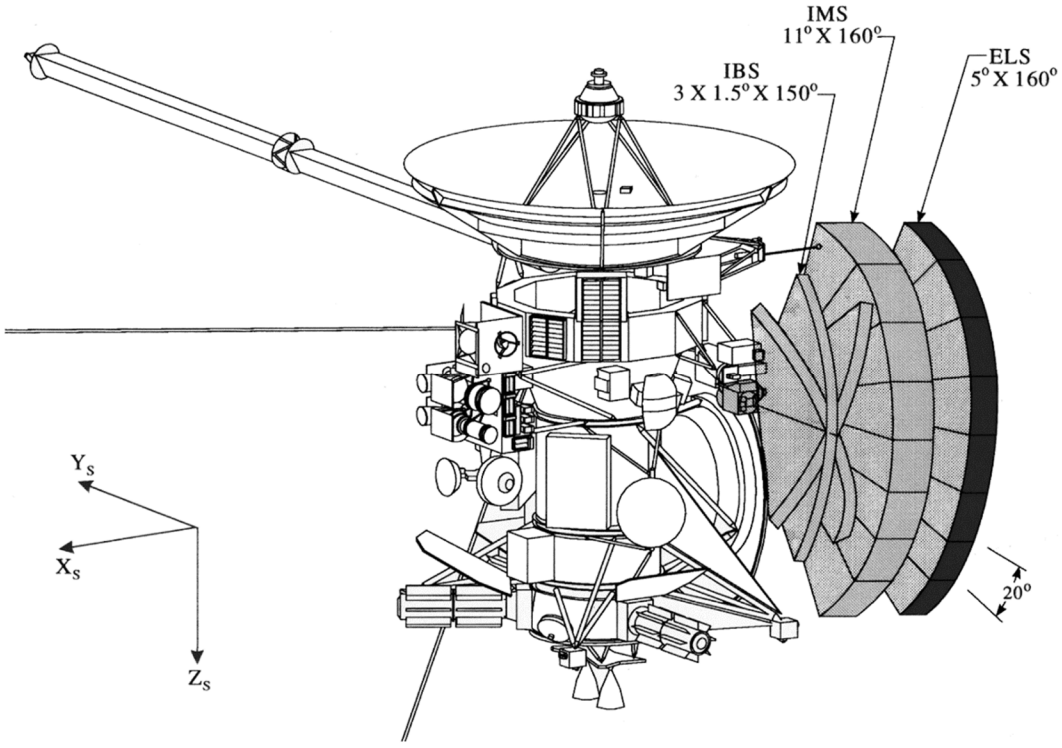

Figure CAPS-3. Location of CAPS on the Fields and Particles Platform showing the sense of CAPS rotation and location of the fields-of-view.

To address the problem of a limited field-of-view (FOV) the design team began by mounting the entire complement of CAPS sensors and the DPU on an actuator (ACT) capable of scanning the sensor FOVs around an axis parallel to the spacecraft Z-axis over a range of ±104° centered on the spacecraft −Y axis. After launch there was an indication that CAPS rotation caused it to snag on a piece of multi-layer insulation (MLI) thermal protection blanket. Out of caution that CAPS might get stuck in one position for the remainder of the mission the ACT scan was limited to +104° (the direction along the spacecraft +X axis) and −80°.

Limited to a scan range of 184° about the Z-axis, the ACT solved only part of the FOV access problem and only in the azimuthal direction. When combined with the elevation acceptance angle of 160° and protrusions of portions of the spacecraft into the FOV (i.e., the high gain antenna, Radioisotope Thermoelectric Generator (RTG) shielding, and other instruments on the pallet—see Young et al. [2004] and Figure CAPS-5) the solid angle commanded by CAPS was limited to approximately 5.8 sr or about 45% of the full sky.

The solution to these limitations was to rotate or otherwise re-orient the spacecraft to enable CAPS (as well as other MAPS particle instruments) to observe a region of the sky closer to 4π sr, albeit slowly. This made operations more difficult for CAPS, MAPS, remote sensing instruments, and indeed the entire spacecraft operations team (see Cassini Final Mission Report Volume 5: Mission Operations System Performance Assessment).

Calibration of ELS and IBS, which are conventional plasma energy-angle analyzers, was relatively straightforward. Calibration of IMS was an entirely different, and far more complex, matter. Figure CAPS-4 shows an example of IMS calibration data taken in an ion beam of m/q = 16 ions. The mass separation optics used to form the calibration ion beam did not have resolution sufficient to separate ion species with virtually the same m/q, it was possible to form beam containing O^+, NH_2^+ and CH_4^+ simultaneously and use it to probe the ability of IMS to separate these species using TOF.

Figure CAPS-4 shows a sample of IMS straight-through (ST) and LEF calibration data from a beam containing O^+, NH_2^+ and CH_4^+at 1024 eV, one of the standard IMS calibration energies. The LEF spectrum shows H^+ and C^+ from the breakup of CH_4^+ in the foils, H^+ and N^+ from the breakup of NH_2^+, and O^+ and O^{++} from oxygen ions in the beam. This spectrum demonstrates the ability of the IMS TOF system to separate three ion species with nearly identical mass/charge ratios that could not otherwise be separated by conventional magnetic or quadrupole spectrometers flown on space missions. The ST spectrum shows H^- ions from the breakup of NH_2^+ and CH_4^+ together with C^- from the latter and O^- from oxygen. All three species in the calibration beam produce neutral atoms that show up as a single peak. There are two ghost peaks centered at 250 and 270 channels caused by electrons leaving structures around the LEF detector and reaching the ST detector. These can be identified and calibrated out.

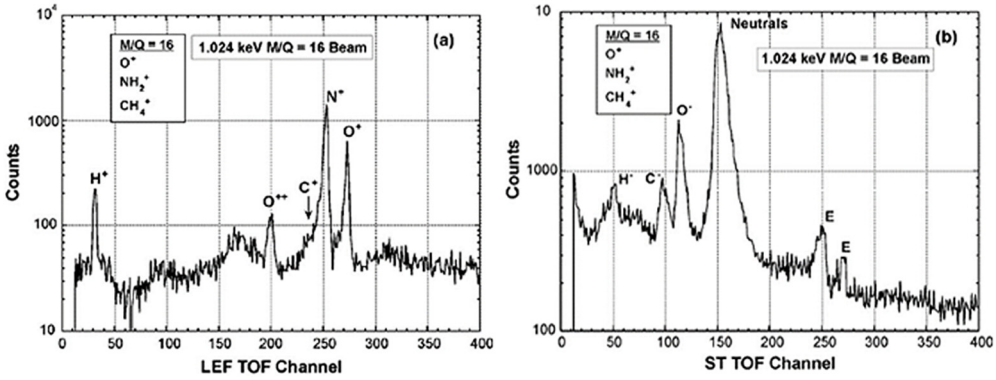

Figure CAPS-4. IMS TOF calibration data for an input beam of M/q = 16$^+$ ions at 1024 eV.

Key Goals and Objectives of the CAPS Investigation

The overarching scientific objectives of the CAPS investigation spelled out in the AO were to perform the highest quality measurements that would allow the CAPS team to understand the physical, compositional, and temporal characteristics of Titan's ionosphere, the icy satellites, the rings, and Saturn and their interactions with Saturn's magnetosphere. A second goal was to achieve those measurements with a quality that was at least ten times better than that of Voyager since their measurements and analysis had been considered the gold standard for studies of Saturn's magnetosphere. In fact, it was data from the Voyager mission that were used to develop the CAPS science objectives, performance guidelines, and sensor requirements. In the following section we briefly summarize the specific objectives of the CAPS investigation.

Note: In the short discussion of AO and CSM objectives given below there are several sections in which we hybridized goals by combining objectives such as Titan-Magnetosphere Interactions, Rings-Magnetosphere Interactions, etc. In those sections we list and discuss objectives from both disciplines, e.g., Titan-Magnetosphere Interactions contains both Titan and Magnetosphere AO and CSM Objectives in order to capture the full breadth of the science objective.

Titan

Because of its mass-resolving capabilities, the CAPS investigation was expected to contribute to measurements of the overall composition and abundances of complex and trace ions in the upper atmosphere (**T_AO1, T_AO2, T_AO5, TN1c**), and explore their vertical and horizontal distributions (**T_AO2**) as well as seasonal dependence (**TC1a**) in order to help determine the evolution of Titan's atmosphere. CAPS contributed also to understanding the magnetosphere as a source of ionization at Titan, and the contribution made by Titan to the outer magnetosphere (**T_AO5**).

Titan AO objectives

- **Titan Atmospheric Formation and Evolution (T_AO1):** Determine abundances of atmospheric constituents (including any noble gases), establish isotope ratios for abundant elements, constrain scenarios of formation and evolution of Titan and its atmosphere.
- **Titan Atmospheric Composition and Distribution (T_AO2):** Observe vertical and horizontal distributions of trace gases, search for more complex organic molecules, investigate energy sources for atmospheric chemistry, model the photochemistry of the stratosphere, study formation and composition of aerosols.
- **Titan Upper Atmosphere (T_AO5):** Investigate the upper atmosphere, its ionization, and its role as a source of neutral and ionized material for the magnetosphere of Saturn.

Titan CSM objectives

- **Titan's Great Seas (TC1a):** Determine seasonal changes in the methane-hydrocarbon hydrological cycle of lakes, clouds, aerosols, and their seasonal transport.
- **Determine intrinsic and/or internal induced magnetic field (TN1b):** Characterize possible inducing magnetic fields by measuring the draping of the magnetic field. Study the decay of ionospheric magnetic fields.
- **Measure aerosol and heavy molecule layers and properties (TN1c).**

Titan-Magnetosphere Interactions

- With sensors that functioned as both energy and mass analyzers CAPS was uniquely positioned to study the interactions between Titan and the magnetosphere (**M_AO4**), and the reverse situation (**M_AO5**), including specifically contributions to the magnetodisk (**TC2a**) which, it turns out, was very little. Measurements of heavy ion layers (**TN1c**) were a continuation of the (**T_AO1**) objective to study atmosphere/ionosphere composition. Plasma flow past Titan drags magnetospheric magnetic field lines across Titan's ionosphere inducing magnetic fields that may affect the ability to observe intrinsic fields (**TN1b**).

Titan-magnetosphere AO objectives

- **Titan Atmospheric Formation and Evolution (T_AO1):** Determine abundances of atmospheric constituents (including any noble gases), establish isotope ratios for abundant elements, constrain scenarios of formation and evolution of Titan and its atmosphere.
- **Magnetosphere and Solar Wind Interactions with Titan (M_AO4):** Study the effect of Titan's interaction with the solar wind and magnetospheric plasma.
- **Plasma Interactions with Titan's Atmosphere and Ionosphere (M_AO5):** Investigate interactions of the surrounding magnetospheric plasma with Titan's atmosphere and exosphere.

Titan-magnetosphere CSM objectives

- **Titan-Magnetosphere Interaction (TC2a):** Observe Titan's plasma interaction as it goes from south to north of Saturn's solar-wind-warped magnetodisk from one solstice to the next.
- **Titan Atmospheric Composition (TN1c):** Measure aerosol and heavy molecule layers and properties.

Enceladus

CAPS was uniquely able to measure both negative and heavy positive ions from Enceladus plumes (**M_AO2**) together with charged nano-grains over a long period of time, thus contributing to our understanding of plume composition and variability (**MC1a**) as well as surface composition from material falling back to the surface (**I_AO3**). Enceladus water-based plasma turned out to completely dominate the composition of the magnetosphere and, through mass loading, much of its dynamics (**I_AO5**).

Icy satellites AO objectives

- **Icy Satellite Surface Composition (I_AO3):** Investigate the composition and distribution of surface materials, particularly dark, organic rich materials and low melting point condensed volatiles.
- **Icy Satellite Magnetosphere and Ring Interactions (I_AO5):** Investigate satellite interactions with the magnetosphere and ring systems and possible satellite gas injections into the magnetosphere.
- **Magnetosphere Charged Particles (M_AO2):** Determine current systems, composition, sources, and sinks of magnetospheric charged particles.

Icy satellites CSM objectives

- **Enceladus Plume Variability (MC1a):** Determine the temporal variability of Enceladus' plumes.

Icy Satellite Science

In addition to contributing in major ways to determining composition and sources and sinks of plasma (**M_AO2**), CAPS was able to identify and measure small amounts of plasma surrounding Dione, Rhea, and Tethys (**IN1c, IN2a, IN2b**), which went on to interact with the magnetosphere (**I_AO5**). Measurements of material returning from the magnetosphere to the satellite could be used to infer origins of surface coatings (**I_AO3**).

Icy satellites AO objectives

- **Icy Satellite Surface Composition (I_AO3):** Investigate the compositions and distributions of surface materials, particularly dark, organic rich materials and low melting point condensed volatiles.
- **Icy Satellite Magnetosphere and Ring Interactions (I_AO5):** Investigate interactions with the magnetosphere and ring systems and possible gas injections into the magnetosphere.
- **Magnetosphere Charged Particles (M_AO2):** Determine current systems, composition, sources, and sinks of magnetospheric charged particles.

Icy satellites CSM objectives

- **Dione (IN1c):** Determine whether Dione exhibits evidence for low-level activity, now or in recent geological time. Investigate Dione's current level of activity.

- **Rhea (IN2a):** Determine whether there is ring material orbiting Rhea, and if so, what its spatial and particle size distribution is. Investigate the interaction of Rhea material with Saturn's magnetosphere.
- **Tethys (IN2b):** Determine whether Tethys contributes to the E-ring and the magnetospheric ion and neutral populations.

Rings

Although CAPS could not participate in the final Cassini orbits over the rings, it did establish that there is an atmosphere and ionosphere formed by UV photolysis hovering over the main rings (**R_AO2**) with the resulting plasma moving along field lines connected to Saturn's ionosphere (**R_AO1, RAO_5**). An unexpected finding is that very clean O_2^+ and O^+ peaks in mass spectra indicate the dearth of contaminants in surface ices of ring particles (**RN1a**). The origin of locally formed negative ions is likely nano-grain particles ejected from the rings themselves (**R_AO4, RN1a**) which likely extend beyond the edge of the A-ring. Observed changes in the plasma composition outside the rings over time are caused by changes in solar UV illumination of the ring particles (**RC1a**).

Rings AO objectives

- **Ring Structure and Dynamics (R_AO1):** Study configuration of the rings and dynamical processes (gravitational, viscous, erosional, and electromagnetic) responsible for ring structure.
- **Ring Particle Composition and Size (R_AO2):** Map composition and size distribution of ring material.
- **Dust and Meteoroid Distribution (R_AO4):** Determine dust and meteoroid distributions both in the vicinity of the rings and in interplanetary space.
- **Ring Magnetosphere-Ionosphere Interactions (R_AO5):** Study interactions between the rings and Saturn's magnetosphere, ionosphere, and atmosphere.

Rings CSM objectives

- **Changing Rings (RC1a):** Determine the seasonal variation of key ring properties and the microscale properties of ring structure, by observing at the seasonally maximum opening angle of the rings near Solstice.
- **Ring Age and Origin (RN1a):** Constrain the origin and age of the rings by direct determination of the ring mass, and of the composition of ring ejecta trapped on field lines.

Rings-Magnetosphere Interactions

Material from the outer rings is found in the inner magnetosphere (**R_AO5**) while the rings are the major supplier of neutral H_2 ionized to form H_2^+ farther out in the magnetosphere and a highly seasonal supplier of neutral O_2 (**M_AO2**).

Rings-magnetosphere AO objectives

- **Ring Magnetosphere-Ionosphere Interactions (R_AO5):** Study interactions between the rings and Saturn's magnetosphere, ionosphere, and atmosphere.
- **Magnetosphere Charged Particles (M_AO2):** Determine current systems, composition, sources, and sinks of magnetospheric charged particles.

Magnetosphere Composition, Sources, Transport, and Losses

CAPS explored the structure of Saturn’s magnetosphere, which shares some features with Earth’s, whereas its composition is dominated by water-group ions produced by the plumes of Enceladus (**M_AO2, SC2a**). Many phenomena exhibit diurnal periodicities associated with the plasma sheet, but little in the way of seasonal variability except near the rings due to changes in UV illumination (**MC1b, SC2a**). Rather surprisingly, N^+ was shown to originate primarily at Enceladus and not Titan (**M_AO2, M_AO4, M_AO5**). Plasma outflows from Saturn’s ionosphere carry tens of kg/s of ions and field-aligned currents connecting Enceladus to its auroral footprint (**MN1b, SC2a**).

MAPS AO objectives

- **Magnetosphere Charged Particles (M_AO2):** Determine current systems, composition, sources, and sinks of magnetosphere charged particles.
- **Magnetosphere and Solar Interactions with Titan (M_AO4):** Study the effect of Titan's interaction with the solar wind and magnetospheric plasma.
- **Plasma Interactions with Titan’s Atmosphere and Ionosphere (M_AO5):** Investigate interactions of Titan's atmosphere and exosphere with the surrounding plasma.

MAPS CSM objectives

- **Seasonal and Solar Cycle Variations (MC1b):** Observe Saturn’s magnetosphere over a solar cycle, from one solar minimum to the next.
- **Saturn’s Ionosphere and Radiation Belts (MN1b):** Investigate the temporal dependence and effects of solar wind coupling on the aurora, ionosphere, and magnetosphere. Probe for UV satellite footprints on Saturn.

- **Aurorae, Chemistry, and Upper Atmosphere (SC2a):** Observe the magnetosphere, ionosphere, and aurora as they change on all time scales—minutes to years—and are affected by seasonal and solar cycle forcing.

Magnetosphere Dynamics

Plasma created in the Enceladus plume at a rate of 100 kg/s deep in Saturn's magnetosphere (**M_AO2**) is transported inward by scattering and outward by the centrifugal interchange instability (**M_AO3**) and eventually, primarily through plasmoid formation, is ejected down the magnetotail (**MN1a**). Dynamical processes (not yet understood) lead to periodicities in plasma characteristics near Saturn's rotation period that are associated with motion of the plasma sheet and possibly a plasma cam structure (**MN1a, MN1c**).

MAPS AO objectives

- **Magnetosphere Charged Particles (M_AO2):** Determine current systems, composition, sources, and sinks of magnetospheric charged particles.
- **Magnetosphere Wave-Particle Interactions (M_AO3):** Investigate wave-particle interactions and dynamics of the dayside magnetosphere and the magnetotail of Saturn and their interactions with the solar wind, the satellites, and the rings.

MAPS CSM objectives

- **Magnetotail (MN1a):** Determine the dynamics of Saturn's magnetotail.
- **Magnetosphere Periodicities (MN1c):** Investigate magnetospheric periodicities, their coupling to the ionosphere, and how the Saturn Kilometric Radiation (SKR) periods are imposed from close to the planet (3–5 R_S) out to the deep tail.

Shock, Magnetopause, Outer Magnetosphere

Cassini crossed Saturn's bow shock on numerous occasions as it and the magnetopause (average standoff 21 to 27 R_S) swept back and forth over the spacecraft (**M_AO3**). The magnetosheath flow carries both solar wind and W^+ ions, but there is little evidence for N^+ from Titan in part because its orbit lies just inside the average magnetopause distance from Saturn (**M_AO4**).

MAPS AO objectives

- **Magnetosphere Wave-Particle Interactions (M_AO3):** Investigate wave-particle interactions and dynamics of the dayside magnetosphere and the magnetotail of Saturn and their interactions with the solar wind, the satellites, and the rings.

- **Magnetosphere and Solar Interactions with Titan (M_AO4):** Study the effect of Titan's interaction with the solar wind and magnetospheric plasma.

Saturn

Both the aurora and SKR are dynamic phenomena controlled to varying degrees by both the solar wind and internal rotation of the magnetosphere. These dynamic phenomena have been observed to vary on all timescales from minutes up to the rotation period (~10 hours). They can be expected to vary on seasonal time scales because of the connection of the magnetosphere with the solar wind, which varies with solar activity (**SC2a**).

Saturn CSM objectives

- **Magnetosphere, Ionosphere and Aurora (SC2a):** Observe the magnetosphere and ionosphere as they change on all time scales—minutes to years—and are affected by seasonal and solar cycle forcing.

Solar Wind

Measurements of the solar wind were carried out at intervals during cruise primarily to study the evolution of solar wind transients propagating through the solar system (**C_AO2**). CAPS also served as an upstream solar wind monitor during studies of Jupiter's magnetosphere (**J_AO3**) and helped show that Saturn's aurora is controlled by solar wind dynamic pressure (**SC2a**).

Cruise AO objectives

- **Cruise Solar Wind Investigations (C_AO2):** Investigate the behavior of the solar wind during solar minimum for comparison with earlier Galileo and Ulysses measurements.
- **Jupiter Magnetospheric Studies (J_AO3):** Explore the dusk side of the magnetosphere and intermediate regions of the magnetotail unvisited by previous spacecraft.

Venus

CAPS was not operating during the two Venus encounters.

Earth's Magnetosphere

Earth's magnetosphere was a target-of-opportunity with no specific objectives. CAPS operated for 10 hours upstream of Earth in the solar wind and then spent nine hours as Cassini flew through

virtually every major plasma structure in the magnetosphere. This gave an unusual cross-section freeze-frame snapshot including two substorms that took place during the fly-through.

Jupiter's Magnetosphere

Cassini flew down the Jovian magnetosheath in early 2001. The shock and sheath passed over the spacecraft about 40 times allowing observations that were shown to be consistent with a slow mode shock (**J_AO3**).

Jupiter flyby AO objectives

- **Jupiter Magnetospheric Studies (J_AO3):** Explore the dusk side of the magnetosphere and intermediate regions of the magnetotail unvisited by previous spacecraft.

Heliosphere

During cruise phase between Jupiter and Saturn, CAPS made the first observations of interstellar hydrogen, helium and oxygen as pickup ions (**C_AO1**). Modeling of the data also showed that Cassini was in the interstellar hydrogen shadow.

Cruise AO objectives

- **Interstellar Ion Composition (C_AO1):** Extend the sensitivity of composition measurements of interstellar ions by approximately three orders of magnitude.

CAPS Science Assessment

Table CAPS-1 shows the CAPS, AO, and Traceability Matrix (TM)/CSM Science objectives and the CAPS assessment.

Table CAPS-1 CAPS Science Assessment.

CAPS Objectives	AO and TM/CSM Science Objectives	CAPS Assessment
TITAN		
Atmospheric and ionosphere composition	T_AO1, TC1a, TN1c	
Ionospheric structure	T_AO2	
Magnetosphere interactions	T_AO5, T_AO6, M_AO5, TC2a, TN1b	
Seasonal variations	MC2a, TC1a	
MAGNETOSPHERE-TITAN INTERACTIONS		
Interactions with magnetosphere, solar wind	M_AO4, TC2a	
Interactions with plasma	M_AO5, TN1b	

Table CAPS-1 CAPS Science Assessment.

CAPS Objectives	AO and TM/CSM Science Objectives	CAPS Assessment
ENCELADUS		
Plume variability	MC1a	
Plume gas composition	IC1a	
Plume dust and ice composition	IN1a	
ICY SATELLITES		
Dione activity and interactions	IN1c	
Rhea activity, ring, interactions	IN2a	
Tethys contributions to E-ring, magnetosphere	IN2b	
Hyperion plasma environment	IN2e	
MAGNETOSPHERE - ICY SATELLITE INTERACTIONS		
Magnetosphere	I_AO5	
RINGS		
Composition of ring material	R_AO2	
Ejecta composition	RN1a	
MAGNETOSPHERE-RING INTERACTIONS		
Magnetosphere-ring interactions	R_AO5, I_AO5	
Ring coupling	MN2a	
GENERAL MAGNETOSPHERE		
Magnetosphere solar cycle variation	MC1b, SC2a	
Radiation belt	MN1b	
MAGNETOSPHERE DYNAMICS		
Wave-particle interactions	M_AO3	
Magnetotail dynamics	MN1a	
Aurora and ionosphere	MN1b	CAPS was off at low altitudes
Periodicities and SKR	MN1c	
SHOCK AND MAGNETOPAUSE		
Dayside magnetosphere	M_AO3	
SATURN		
Aurora, magnetosphere, ionosphere	SC2a	
CRUISE		
Solar wind	C_AO2	
VENUS		CAPS did not operate at Venus
EARTH		
Dusk side magnetosphere	Same as J_AO3	
JUPITER		
Magnetosphere	J_AO3	

Table CAPS-1 CAPS Science Assessment.

CAPS Objectives	AO and TM/CSM Science Objectives	CAPS Assessment
HELIOSPHERE		
Interstellar composition	C_AO1	

Detailed Magnetospheric Science Results

Composition of Titan's Atmosphere and Ionosphere

Discovery of heavy positive and negative ions

Before proceeding with this section, it should be understood that ELS and IBS, which are electrostatic energy/charge analyzers, have no intrinsic capabilities as mass spectrometers. Rather the detection of negative ions and very heavy positive ions, discovered by CAPS and discussed in detail below, is made possible because the ram velocity of the spacecraft in the Titan rest frame is far higher (at 6 to 6.4 km/s) than ion thermal speeds of at most a few hundred meters/s. Using the relationship $m/q = 2E/qV_{ram}^2$, where E is the ion energy and V_{ram} is the spacecraft velocity, the energy spectra of ions entering ELS or IBS (or for that matter IMS) can be treated as mass spectra albeit with relatively low mass resolution. Since ELS is designed to detect electrons, its measurements can be interpreted as negative ion mass spectra.

Measurements made by CAPS sensors between altitudes of 950 to 1400 km were responsible, along with those of INMS, for one of the major surprises of the Cassini mission—the high level of chemical complexity observed in Titan's ionosphere. From the earliest close encounters ELS detected heavy negatively charged ions with mass/charge up to 13,800 amu/q (Figure CAPS-5 and Fgiure CAPS-6). In addition, heavy positive ions up to ~350 amu/q [Crary et al. 2009] and as high as 1000 amu/q [Coates et al. 2010a] were detected by IBS. An unexpected level of chemical complexity was seen in the neutrals as well [Waite et al. 2007]. Before Cassini, models of Titan's chemistry had shown some complexity in the interaction of the neutral atmosphere with positive ions [Wilson and Atreya 2004]. The observations from Cassini necessitated more sophisticated modelling of the positive ion composition [Cravens et al. 2006, 2009]. The negative ion observations by ELS were completely unexpected at the altitudes sampled by Cassini, opening a whole new field for modeling and understanding the complex chemistry of Titan's atmosphere.

With these discoveries, Titan's ionosphere is now known to be the most chemically complex in the solar system. This complexity extends to altitudes sampled by Cassini and, based on models, even deeper in the atmosphere. Much of this complexity relative to other terrestrial planets, including Earth, is due to the cold, dense nitrogen-methane atmosphere and Titan's relatively low gravity compared to the other planets. CAPS pioneering discovery of large negative ions has been followed up by further studies of the spatial distribution and density of these ions on altitude and solar zenith angle [Ali et al. 2013; Wellbrock et al. 2013; Desai et al. 2017].

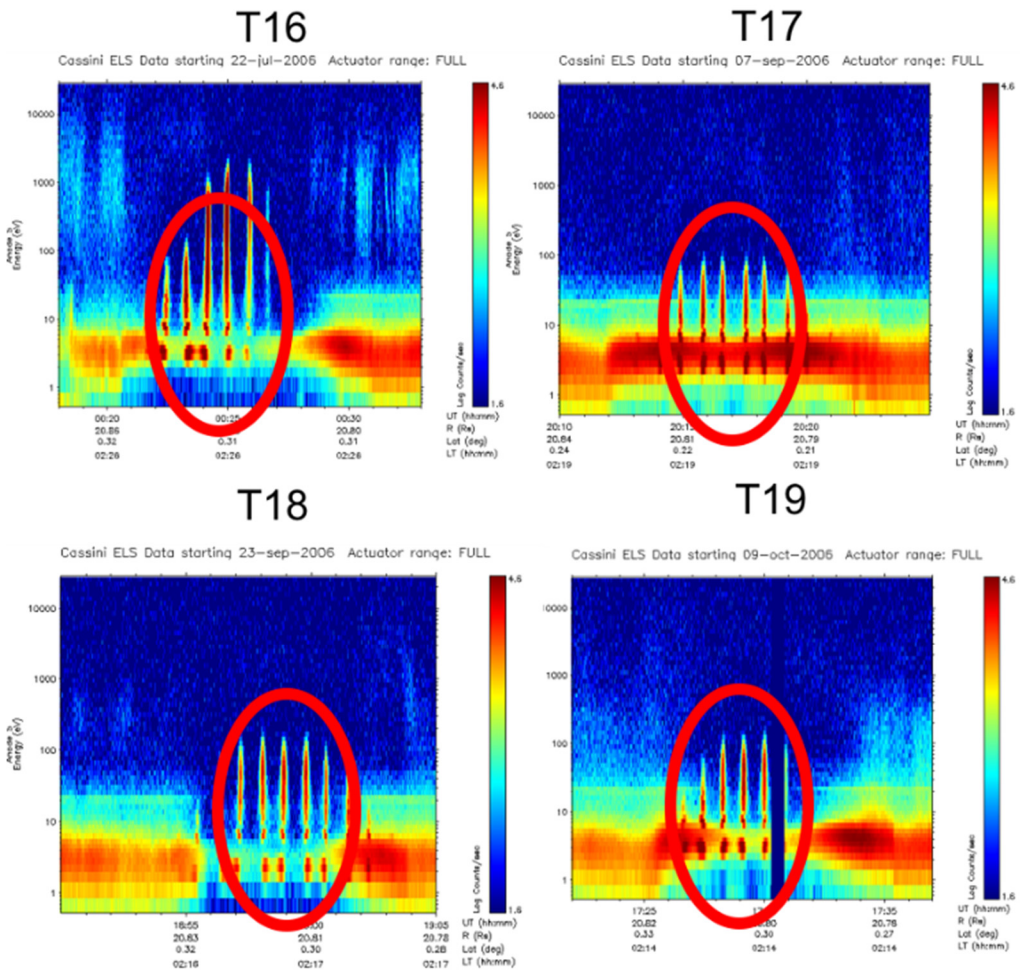

Figure CAPS-5. Energy-time spectrograms of negative ions taken over 15-minute intervals by CAPS ELS during successive Titan encounters T16, T17, T18, and T19. The sharp spikes encircled in red are compressed spectra measured each time the CAPS turntable swept the ELS field-of-view across the ram direction. Figure from Coates et al. [2007a].

Wellbrock et al. [2013] have shown that the highest densities of negative ions are found at lower altitudes. Moreover, the average altitudes where peak ion densities occur decrease with increasing ion mass. In addition, the maximum altitudes at which ions from a specific mass group are observed (the reference altitude) decrease with increasing mass group. This study provides the first step in investigating conditions which affect the densities of different negative ion mass groups.

The highest mass negative ions were observed during the T16 encounter (Figure CAPS-6). A recent analysis of this data shows that polar winter is where the heaviest negative ions are seen [Wellbrock et al. 2018]. This helps to constrain the chemical processes that produce these large ions.

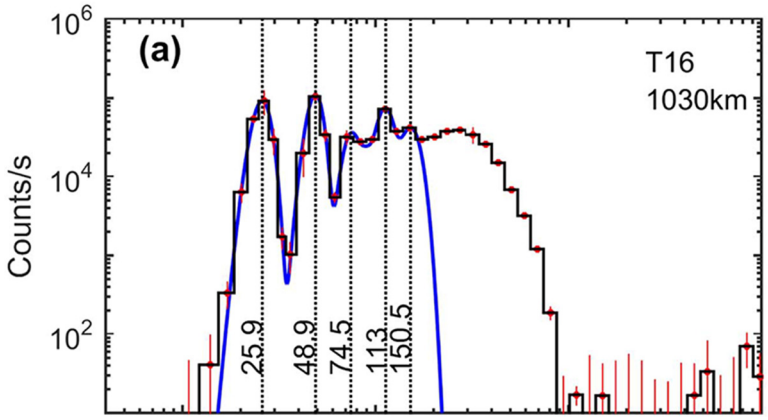

Figure CAPS-6. Fitting negative ion spectra using the instrument response function reveals that intermediate mass negative ions provide a steppingstone in producing the spectacularly heavy ions up to 13,800 amu/q [Desai et al. 2017]. The existence of negative ions was confirmed using RPWS Langmuir probe data, initially using observations at the lowest altitude encounter T70 [Ågren et al. 2012], where CAPS was not oriented in the ram direction for safety reasons, and subsequently at other encounters [Shebanits et al. 2016].

Chemical source of heavy ions

The relatively low-mass negative ions were identified as CN^-, C_3N^- and C_5N^- in the first chemical models used to describe the negative ions seen at these altitudes [Vuitton et al. 2009]. Considering several processes and estimating chemical reaction rates, they suggested that the most likely production process is dissociative electron attachment. They also suggested the most likely loss processes to be associative detachment supplemented by photo-detachment.

While some progress has been made on formation of higher mass ions, this topic is still under study. The geometric configuration of heavy ions is relatively unconstrained, and chains, rings or even fullerenes may be possible. Sittler et al. [2009a] have suggested that the latter may trap and transport oxygen [de Kok et al. 2007] to the surface although there are no observations that confirm this hypothesis. Agglomeration of large molecules caused by charging [Michael et al. 2011] or chemical processes [Lavvas et al. 2013] have been suggested as potential mechanisms to produce the large negative ions. However recent work by Desai et al. [2017] shows that chains of negative ions at intermediate masses may provide another pathway for heavy ion formation (Figure CAPS-7). Heavy negative and positive ions may also link up to form embryo aerosols of both negative and positive charge [Coates et al. 2007a; Crary et al. 2009].

Desai et al. [2017] use observations of negative ions by CAPS/ELS to show mass peaks where unsaturated carbon-chain negative ions such as CN^-/C_2H^-, C_3N^-/C_4H^-, C_5N^-/C_6H^-, etc., might exist (see also the comprehensive review by Millar et al. [2017]). Higher mass ions ~117 ±3 amu/q and 154 ±8 amu/q could be longer negatively charged carbon chains with 10 or 12 or more carbon atoms in saturated aromatic versions. Thus, negative ions exist at masses where INMS cannot measure positive ions. This makes the two instruments not only complementary in their measurements but also makes them highly dependent on each other if we are going to achieve

deeper insights into the composition of Titan's ionosphere. A second example of INMS/CAPS interdependence are IBS observations of heavy positive ions above 1000 amu/q [Crary et al. 2009] which complements INMS measurements that are limited to m/q ≤ 100 amu/q (Figure CAPS-7).

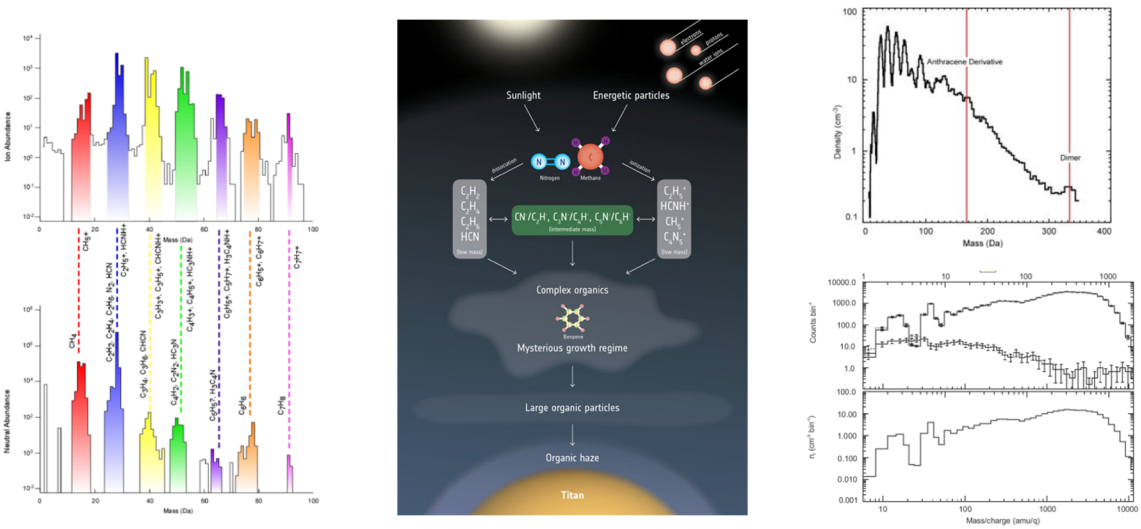

Figure CAPS-7. Observations of negative ions by CAPS/ELS show mass peaks where unsaturated carbon-chain negative ions might exist. The combination of the *Left panel:* INMS neutrals [Waite et al. 2007], *Middle panel:* IBS positive ions [Crary et al. 2009], and *Right panel:* ELS negative ions [Coates. et al. 2007] with a schematic illustrating the process of large ion formation. Figure from Desai et al. [2017].

Tholin formation

The maximum mass of negative ions increases with decreasing altitude [Coates et al. 2009]. Additionally, the number density of the higher mass group increases there [Wellbrock et al. 2013]. Furthermore, a depletion of the low mass (<150 amu/q) negative ions at a rate proportional to the increase of higher mass ions has been observed at the lowest altitudes (950 km) sampled by CAPS [Desai et al. 2017]. Additionally, non-mass-resolved negative ions were inferred from Langmuir probe data at 870 km [Ågren et al. 2012]. Taken together, the CAPS data provide evidence that the space plasma environment in the ionosphere produces these larger ions, while the RPWS data provide in situ evidence that they reach the lowest altitudes ever sampled by Cassini. The large ions then provide the source for aerosols and tholins that float down through Titan's atmosphere, forming the well-known haze layers. This idea is supported by UV occultation measurements—for example, Liang et al. [2007], which show that the density of tholins is measurable at 950 km and increases in density at lower altitudes, possibly all the way to the surface. Based on a combination of RPWS and CAPS data it is estimated that 10^5 to 10^6 metric tons per year of heavy organic aerosol compounds are added to the atmosphere from the ionosphere.

At the surface, the heaviest constituents of the haze could contribute hydrocarbons and nitriles to the dunes seen by the radar and could also provide material that would sink to the bottom of Titan's lakes. However, this process has not been observed directly in situ which leaves several

open questions for future Titan exploration [Tobie et al. 2014]. Several mission concepts have been proposed which could follow this process. These include the ESA-NASA TANDEM mission [Coustenis et al. 2009] and the NASA Dragonfly rotorcraft lander mission [Turtle et al. 2017].

Titan – Magnetosphere Interactions

The main themes of CAPS studies of the Titan-magnetosphere interaction are summarized in Figure CAPS-8. The particular goals were to: 1) measure the kinetic interaction between Titan's upper atmosphere and ionosphere with Saturn's magnetosphere where ion gyro-radii can be larger than Titan itself; 2) measure the composition of the plasma environment around Titan including its exosphere and ionosphere; 3) contribute to our understanding of the surface composition and its organic chemistry; and 4) contribute to our understanding of atmospheric loss and the required

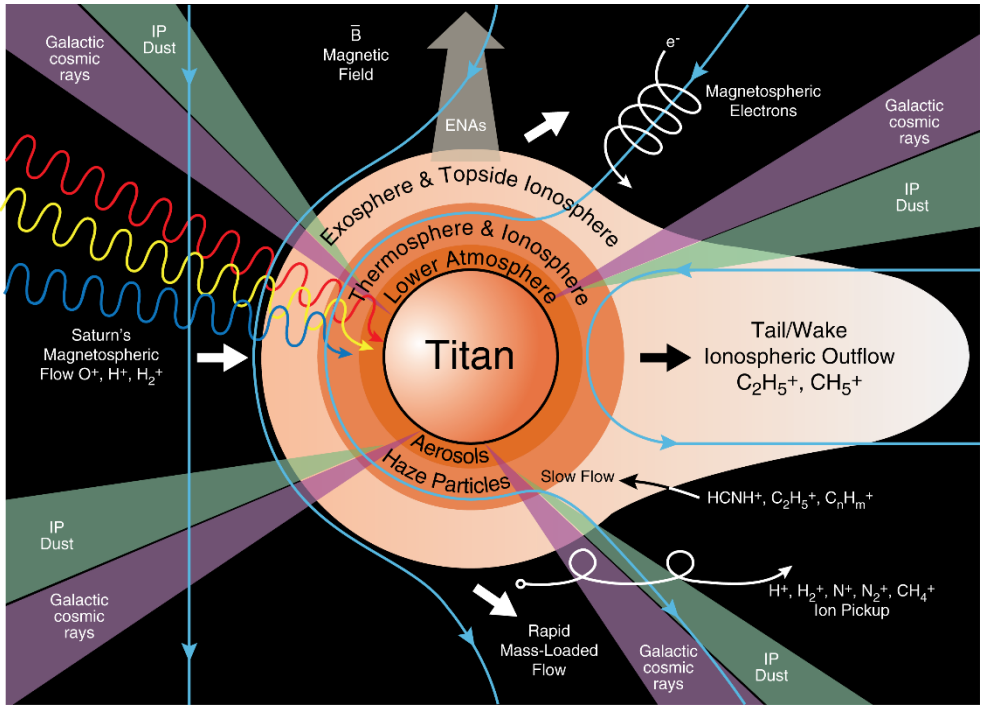

Figure CAPS-8. The main themes of CAPS studies of the Titan-magnetosphere interaction. Colorized figure of Titan includes: various atmospheric layers; surface and incoming photons, plasma, dust, energetic neutral atoms; and energetic charged particles, as well as other processes related to the interaction with the magnetosphere.

replacement timescales from the sub-surface of Titan for the content of methane within Titan's atmosphere, lakes, and surfaces. Lunine et al. [2009] have estimated the lifetime of methane due to photochemical reactions alone to be < 10 million years. Ultimately CAPS may contribute to the larger theme of understanding Titan's origins and the nebula from which the Saturn system was born—see Lunine [2009] and references within.

Kinetic interactions

CAPS discovered pickup ions in the form of beams of CH_4^+ and N_2^+ that can be explained theoretically as the result of kinetic interactions between Titan and the magnetosphere [Hartle and Killen 2006; Hartle and Sittler 2007; Hartle et al. 2011]. It is no surprise that beam composition is consistent with the composition of Titan's exosphere and atmosphere which are dominated by N_2 (98.4%) and CH_4 (1.4%)—cf. Waite et al. [2005].

Sittler et al. [2010] observed nearly field-aligned outflows from the topside ionosphere during the T9 flyby and estimated the loss of methane ions due to pick up from the exosphere at ~5 × 10^{22} molecules/s [Sittler et al. 2009b]. The outflows serve ultimately as a sink from Titan's atmosphere of roughly ~5 × 10^{24} molecules/s. Later, Coates et al. [2007b, 2012] observed similar amounts of ionospheric outflows during the T9, T63 and T75 flybys. The theoretical cause of these outflows was originally discussed in Hartle et al. [2008]. They are produced by a field-aligned polarization electric field $E_{pol} \sim -1/ne\nabla_{||}P_e$ so that above the ionospheric density peak the outward acceleration is > 10 times the force of gravity for m/q ~28 amu/q ions (note that the ionospheric electron temperature T_e ~1000° K is much greater than the ionospheric ion temperature T_{ION} < 180° K, which gives rise to charge separation and hence the dipolar electric field). Sittler et al. [2010] found that the resulting ion outflow speeds were ~7 km/s with T_{ION} ~50,000° K. Therefore, both significant acceleration and heating must have occurred at altitudes above 5000 km. Later, using electron observations, Coates et al. [2007b; 2015] measured the total potential drop of this electric field to be ~0.2 μV/m up to heights ~15,000 km, which is sufficient to accelerate methane ions to the observed speeds ~5–6 km/s. Future 3-D hybrid simulations similar to that done by Lipatov et al. [2011, 2012, 2014] will be required to understand the heating (e.g., due to wave-particle interactions) of ions to the observed high temperatures. In addition to the outflows, Sittler et al. [2010] also found evidence of Alfven waves during the T9 flyby with transverse velocity and magnetic field fluctuations that were anti-correlated with time and thus consistent with field-aligned propagation.

One other surprising observation that affects Titan atmospheric chemistry was CAPS discovery of kilovolt oxygen ions with inflows arriving from the magnetosphere at the exobase of Titan's atmosphere ranging up to ~10^{23} O^+/s [Hartle et al. 2006a, 2006b]. Its likely origins are Enceladus and the rings—see Johnson et al. [2005]; Cassidy and Johnson [2010]. Oxygen combined with the complex chemical makeup of the ionosphere is most likely the source of CO in the atmosphere [Hörst et al. 2008; Krasnopolsky 2012]. The influx of O^+ into the atmosphere, where it undoubtedly affects Titan's already complex chemistry, is one more unusual and interesting aspect of Saturn's magnetosphere in which it acts as a conduit for the chemistry of one moon (Enceladus plumes) to affect the chemistry of another.

Aerosol formation and surface composition

Heavy negative ions with m/q > 10,000 amu/q [Coates et al. 2007a; Wahlund et al. 2009], and positive ions with m/q > 1000 amu/q [Crary et al. 2009], can combine to form embryo aerosol particles which can then settle to lower altitudes [Waite et al. 2008]. As they drift down, they grow

to larger sizes to form tholins that make up the well-known smog haze layers extending down to ~400 km altitude. Eventually the particles settle to the surface [Lavvas et al. 2008; Sittler et al. 2009a, 2009b). In the Lavvas et al. [2008] model, more saturated versions of hydrocarbons and nitriles are assumed to form the aerosols, while Sittler et al. [2009a, 2009b] argue for the formation of large negatively charged carbon chains that eventually fold into fullerenes [Kroto et al. 1985; Kroto et al. 1991]. In an interesting connection to Titan chemistry, fullerenes are also thought to exist in interstellar molecular clouds and planetary nebula [Herbst 1981; McCarthy et al. 2006; Millar et al. 2007; Brünken et al. 2007; Remijan et al. 2007; Sakai et al. 2007, 2008; Thaddeus et al. 2008; Herbst and Osamura 2008].

Desai et al. [2017] present clear observational evidence that long-chain negative carbon ions can form and eventually grow into larger embryo aerosols. Vuitton et al. [2007, 2009], reporting on negative ion chemistry at Titan, also argue in favor of negative ion carbon chains, but with nitrogen appendages such as CN^-, C_3N^- and C_5N^-. Desai et al. [2017] also noted that stable multiply-charged heavier fullerenes might also be present within the ELS mass spectrum at m/q ~360 amu/q for C_{60}^{-2} or 420 amu/q for C_{70}^{-2} (see spectra in Figure CAPS-2 and Figure CAPS-3). When heavier negative ions above 150 amu/q are present at altitudes below the main ionospheric peak, broad mass peaks between 300 amu/q to 800 amu/q are present. This suggests that multiple charge state negatively charged fullerenes may exist in Titan's ionosphere—see Wang et al. [2009]; Shebanits et al. [2016]. Sittler et al. [2009a, 2009b] made the argument that the keV O^+ ions reported by Hartle et al. [2006a, 2006b] can penetrate to lower altitudes [Cravens et al. 2008], and become trapped inside the fullerenes—a condition known to occur with noble gasses such as ^{40}Ar, and nitrogen atoms [Pietzak et al. 1997]. Once trapped inside the fullerenes, the latter can condense into embryonic aerosols within the ionosphere. This process isolates the oxygen atom from reactions with Titan's reducing atmosphere. The oxygen ions will then ultimately end up on the surface of Titan where further chemical processing, driven by highly energetic galactic cosmic rays that penetrate to the surface, could lead to still more complex exobiological molecules [Sittler et al. 2009a, 2009b].

Atmospheric loss

Both CAPS and the INMS have provided crucial data for estimating processes that contribute to atmospheric loss. The review article by Johnson et al. [2009] highlights mechanisms and estimates of loss. They are primarily H_2 thermal (Jeans) escape, CH_4 destruction/precipitation, N_2/CH_4 sputtering, and ion pickup causing ionospheric outflows. Loss of CH_4 by hydrodynamic outflow [Yelle et al. 2008; Strobel 2008] thought to also contribute, was later shown not to be the case.

Waite et al. [2005] presented the first observations of H_2, CH_4 and N_2 altitude profiles extending above the exobase to ~1400 km. There is a break in the altitude profiles above the exobase that is consistent with atmospheric escape. Cui et al. [2008] and Bell et al. [2009] estimated H_2 escape to be ~10^{10} amu/q/cm^2/s locally, and ~1.6×10^{28} amu/q/s globally (integrated over the surface area of the atmosphere). Sittler et al. [2010] reported that during the T9 and T18 flybys H^+ and H_2^+ ions were present in the flow of plasma moving towards Titan. The ions also

happened to be moving perpendicular to the local magnetic field, leading Sittler et al. [2010] to conclude that they were seeing pickup ions from Titan's hydrogen corona which can extend to ~20 Titan radii (i.e., out to the Hill sphere).

Primary chemical losses occur when methane is dissociated and ionized by photochemical reactions initiated by solar UV and particle impact. Further reactions with neutrals and ions then make heavier hydrocarbons and nitriles, which can eventually grow into aerosols that precipitate to Titan's surface. Sittler et al. [2009a], using an analogy to molecular clouds and planetary nebulas, suggested that negative chains of carbon atoms form and eventually fold into fullerenes, implying that the same might be going on at Titan. They estimated precipitation to the surface to be ~2.7 × 10^{-14} kg/m^2/s at 950 km altitude and a global rate of ~4 × 10^{27} amu/q/s. This mass loss rate appears to dominate all other present-day atmospheric loss mechanisms—for example, Johnson et al. [2009]. Because the rate is large, in order to maintain a steady state methane concentration an upward diffusion of methane would be required, presumably from a source of methane on Titan's surface.

Sittler et al. [2009b] estimated the loss rate due to pick up ions to be between ~5 × 10^{22} ions/s and ~10^{24} amu/q/s, which is much smaller than the lower bound given by Johnson et al. [2009] of ~10^{26} amu/q/s, possibly due to the inclusion of scavenging down Titan's ion tail—see Sillanpaa et al. [2006]; Hartle et al. [2006b]. Woodson et al. [2015] showed the ion outflow detected between ~1 and 5 Titan radii consisted of H^+, H_2^+ and H_3^+ as well as two hydrocarbon groups with mass ranges between 12–19 amu and 24–32 amu. The net escape caused by ionospheric outflows is ~5 × 10^{24} mol/s or ~10^{26} amu/q/s [Sittler et al. 2010; Coates et al. 2012] which should be included in the Johnson et al. [2009] estimate. The escape fluxes caused by sputtering, hot atomic recoils and charge transfer by energetic neutral atoms also cause heating of the thermosphere and corona [De La Haye et al. 2007a, 2007b]. Adding all these terms Johnson et al. [2009] find a total escape rate of ~0.32 to ~3.8 x 10^{28} amu/q/s.

Recent work highlights the need to reanalyze INMS data … in order to understand the energy distribution of neutral molecules in the exosphere region.

Recent work highlights the need to reanalyze INMS data using detailed models of sputtering and energy deposition in the upper atmosphere in order to understand the energy distribution of neutral molecules in the exosphere region. Snowden and Yelle [2014] used Fourier's Law to extract energy deposition rates in the upper atmosphere from INMS data. They suggested that precipitation of magnetospheric ions observed by CAPS is likely too small to explain the observed temperature variations [Snowden et al. 2013] and escape rates. They also suggest that gravity waves produced in the lower atmosphere could cause the variability, but a source for the waves has not been identified, and it has recently been shown that the means of estimating the local temperature in an atmosphere with significant density structure might be problematic.

Tucker et al. [2016] showed that using the Louisville Theorem approach, with a non-thermal energy distribution at the exobase, can lead to incorrect estimations of the upper atmospheric thermal structure and, consequently, escape rates due to collisions in the transitional region. Furthermore, such corona fits obtain different exobase energy distributions for N_2 and CH_4 density distributions, which is suggestive of different heating mechanisms occurring between species. Therefore, ion/pickup fluxes and spectra extracted from CAPS data and model development of gas-kinetic models are needed for detailed simulations of the ion-neutral interaction. Such models can consider the ion-neutral interaction at the microscopic level and include the production of hot recoil molecules. This has led to a re-evaluation of an earlier Titan atmosphere model investigated by Johnson et al. [2016].

The final topic is hydrodynamic loss proposed by Yelle et al. [2008] and Strobel [2008]. By using CH_4 and N_2 ingress altitude profiles with methane diffusing through atmospheric N_2, and then using the ^{40}Ar density profiles, they were able to separate the molecular and eddy diffusivities, which then required an upward methane flux ~4–5 × 10^{10} amu/q/cm^2/s and globally ~4.5 × 10^{28} amu/q/s. This estimate is close to the chemical destruction/precipitation of methane to heavier molecules and aerosols. The model by Strobel [2008] called slow wind ague that solar UV penetrates below the ionosphere where it is deposited. This excess heat is then conducted upward to higher altitudes to drive the hydrodynamic slow wind. But, in order to meet the upward flux required by Yelle et al. [2008] this heat must be transported above the exobase where there are no collisions to conduct the heat, which is its major weakness. Direct Simulation Monte Carlo (DSMC) simulations by Tucker and Johnson [2009] did not show any enhancement of the methane escape rate significantly greater than the Jeans escape rate ~3 × 10^{22} amu/q/s. Therefore, it is highly unlikely that hydrodynamic escape of $CH_4$is currently occurring at Titan. Tucker et al. [2013] showed that H_2 escape cools the background gas resulting in non-isothermal density profiles without requiring a significant escape rate. Volkov et al. [2011] examined the hydrodynamic escape problem in detail using DSMC simulations. They found that above a Jeans parameter of 6 at the exobase the thermal escape rate is enhanced towards the analytical Jeans rate only by a factor of 1.4–1.7. This contrasts with Strobel [2008] who predicts a CH_4 escape rate orders of magnitude larger than the Jeans rates, possibly due to an overestimation of heat conduction in the transitional region.

Enceladus

In 2005, and far from Enceladus, IMS measured pick-up water group ions (O^+, OH^+, H_2O^+ and H_3O^+ or, collectively, W^+) throughout Saturn's inner magnetosphere [Young et al. 2005; Sittler et al. 2005; 2006; Tokar et al. 2008]. The source of these ions is charge-exchange collisions that scatter water group neutrals, replacing a fraction of the co-rotating core distribution with a new and slower-moving ion population without changing the total ion content. The newly created ions are moving near the local Keplerian speed, which is slower than the co-rotation speed, and hence are picked-up by Saturn's magnetic field. IMS detected these water-group ions within their source region, the Enceladus torus, thus providing the first measurements of W^+ ions throughout their toroidal source region and far from Enceladus. High ion count rates in IMS were observed at the

ion pick-up energies as shown in Figure CAPS-9 with largest signals near the Enceladus and Dione orbits. Another surprising measurement was the discovery of negative ions in the Enceladus plume, a result as surprising for Enceladus as it was for Titan [Coates et al. 2010a, 2010b].

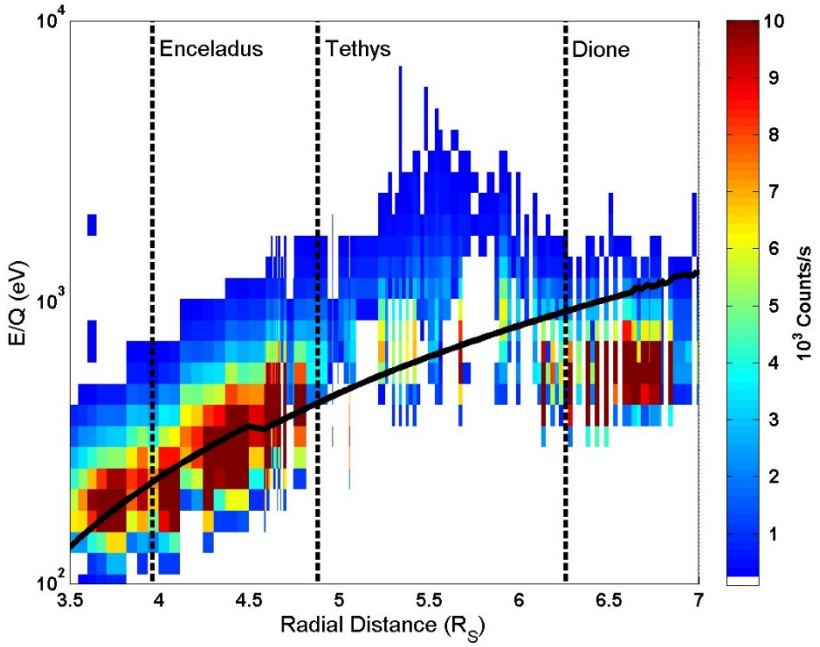

Figure CAPS-9. Energy charge of detected ions versus radial distance from Saturn in Saturn radii (1Rs = 6.03x10^5 km). Figure from Tokar et al. [2008].

Striking observations were also obtained with IMS during the close encounters of Cassini with Enceladus. Early in the Cassini mission, on July 14, 2005, the spacecraft flew within 175 km of Enceladus, passing through its surrounding cloud of neutrals and plasma. Although encounters with Enceladus later in the mission would be at much closer distances, CAPS was still able to detect indications of a strong interaction between Enceladus and magnetospheric plasma [Tokar et al. 2006]. Originally detected by the Hubble space telescope, Enceladus was known to sit in a cloud of neutral OH forming a torus around Saturn. The cloud detected by CAPS extends from about 3 to 8 R_S with maximum concentration of ~10^3 cm^{-3} inferred to exist near the orbit of Enceladus (3.95 R_S). The OH cloud is produced by dissociation of H_2O, and although the peak concentration suggested that the largest source of water molecules was in the region near the orbit of Enceladus, the nature of this source was unknown. IMS measurements during the 2005 encounter established a strong perturbation of the plasma flow caused by Enceladus, and perhaps most importantly, the presence of W^+ ions (Figure CAPS-10). This population had been detected earlier during Saturn orbit insertion [Young et al. 2005].

Later in the mission, during closer encounters with Enceladus, CAPS obtained in situ measurements of W^+ ions freshly produced in the dense Enceladus plume. The dominant species there are light ions (H^+, H_2^+), W^+ ions, and single water cluster ions, ($H_2O^*H_2O^+$). All were observed close to, and nearly due south, of Enceladus. The ions have kinetic energies in the IMS frame

roughly equal to ions that are at rest with respect to Enceladus and rammed into the CAPS sensors at the spacecraft speed. This is the signature of freshly produced ions in the plume due, e.g., to charge exchange interactions of incoming magnetospheric ions with neutral plume gas. Figure CAPS-11 shows an example of these ions detected by IMS during the E3 encounter only 52 km from Enceladus. The high counting rates close to the ion ram energies (denoted by vertical arrows) are clearly visible. Further details of these data are discussed in Tokar et al. [2009].

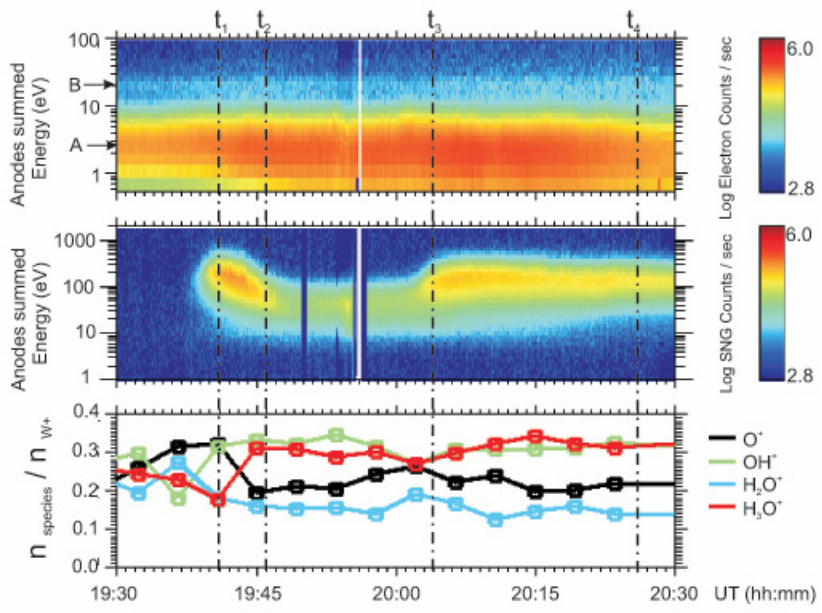

Figure CAPS-10. Data from CAPS on July 14, 2005. *Upper panel:* ELS electron counting rates summed over all direction anodes. Cold and hot electron components were detected with peak counts near A and B. *Middle panel:* Ion counting rates from IMS, with the slowing of the of the ion flow evident between t_1 and t_2. *Bottom panel:* Individual water group (W^+) ion densities divided by the total water group ion density, obtained from IMS time-of-flight measurements. Reduced χ^2 fits for mass spectra give high confidence for identification of the ions. Figure from Tokar et al. [2006].

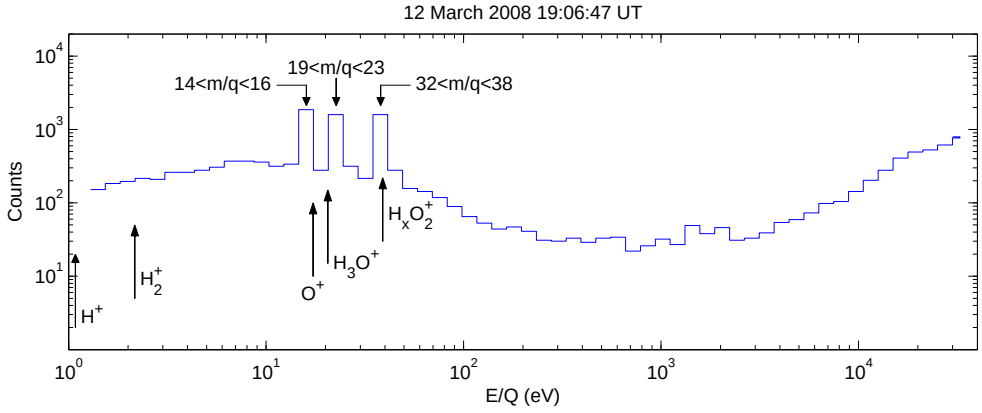

Figure CAPS-11. Individual ion counting rates versus energy per charge measured by IMS anode 5 within the plume during the March 12, 2008 (E3) flyby of Enceladus. Figure from Tokar et al. [2009].

The E7 encounter on November 2, 2009 provided additional observations of the plume stagnation region as Cassini passed directly through the Enceladus plume. The IMS detector sensitive to rammed ions observed stagnation and fresh ions at the ion ram energies (Figure CAPS-12). The strong interaction region within the plume is clearly visible in the CAPS IMS data as are the water group ions near 10 eV that are at rest in the Enceladus frame.

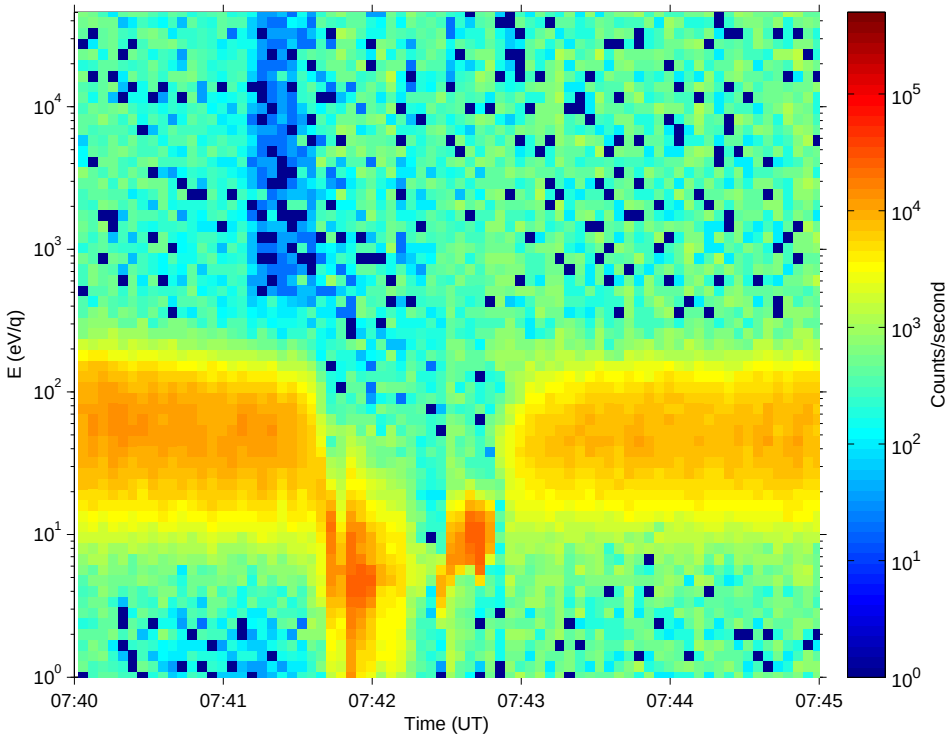

Figure CAPS-12. CAPS energy-time spectrogram from the E7 encounter. Figure from Smith et al. [2017].

Data from the E7 encounter also exhibited the close correspondence between IMS observations of ion slowing and the observed entry into the dense water vapor plume measured by INMS. This is depicted in Figure CAPS-13, which shows the IMS ion flow speed and the INMS mass 44 counts, a proxy for plume water vapor concentration. The E7 closest approach (C/A) is at ~07:41:58 universal time (UT) when IMS observed a rapid decrease in the ion flow speed ~20 sec before C/A. Similarly, INMS observed an increase from 29 to 399 counts at m/q = 44 from 17.5s to 11.3s before C/A. The data suggest that magnetospheric plasma enters the dense plume leading to charge exchange with plume water vapor followed by subsequent pick-up into the co-rotating flow. The signature of this process is very sharp on the Saturn-ward side of the plume as the new ions are picked-up and gyrate away from Saturn. The transition out of the plume opposite Saturn for E7 is more extended due to several factors, e.g., ion drift velocity and variable ion gyroradius for the various masses created. Note in the figure that the observed ion flow speed obtained from count distributions in the ram direction imply speeds as low as a few km/s in the Enceladus frame.

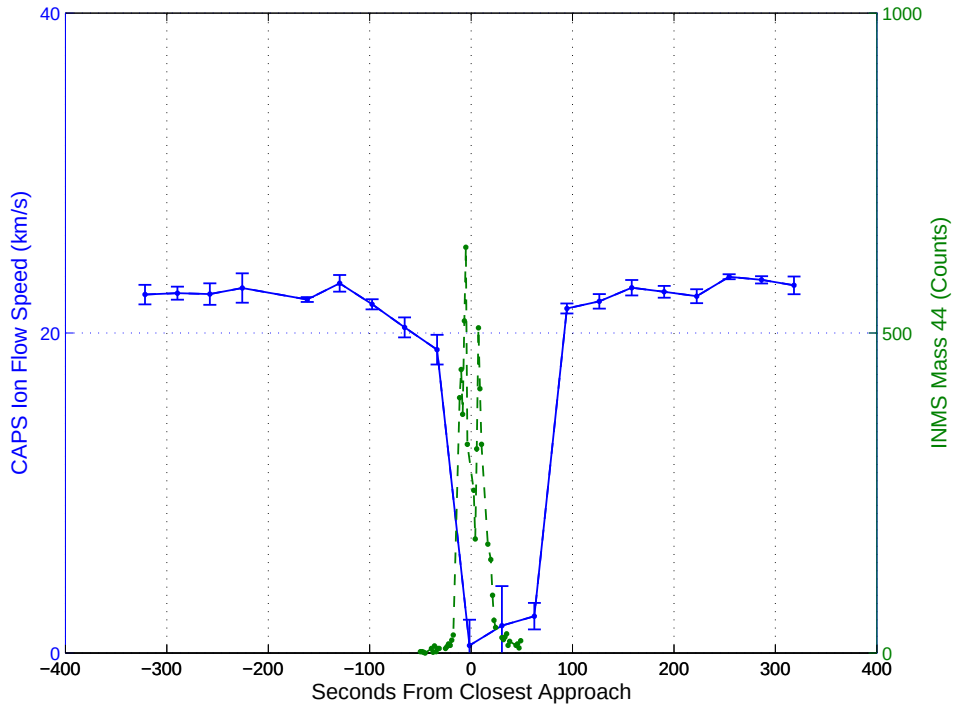

Figure CAPS-13. The CAPS IMS ion flow speed and the INMS mass 44 counts which serve as a proxy for plume water vapor concentration. The E7 closest approach was at ~07:41:58 UT on November 2, 2009.

In addition to the dense neutral water vapor measured by INMS and the resulting cold plasma measured by CAPS and RPWS Langmuir Probe, the south-polar plume of Enceladus was also found by CAPS to carry singly charged nanometer-size water-ice grains [Coates et al. 2009; Jones et al. 2009; Hill et al. 2012; Meier et al. 2014; Dong et al. 2015; Meier et al. 2015]. Such nano-grains had been inferred to exist in various cold, tenuous geophysical and astrophysical environments, but the close Enceladus plume encounters by Cassini offered the first opportunity to measure and characterize nano-grains in situ. Before the CAPS shutdown in June 2012 there were three close Enceladus encounters that provided the ram pointing required to measure these high mass-per-charge particles—E3 on 12 Mar 2008, E5 on 9 Oct 2008, and E7 on 2 Nov 2009. The detailed analysis was reported by Hill et al. [2012].

Hill's analysis confirms that the nano-grains are largely uncharged when they emerge from the surface vents and become increasingly (mostly negatively) charged as they approach Cassini a few tenths of Enceladus radii away. The charged nano-grain density versus distance from the surface source is shown in Figure CAPS-14, from Hill et al. [2012]. The dashed line shows the r^{-2} dependence that would be expected if the grains were already charged when they emerged from the source. The most plausible charging mechanism is electron attachment from the dense plume plasma. The non-neutrality of the nano-grains observed by CAPS, n(−) >> n(+), plausibly cancels the opposite non-neutrality of the plume plasma observed by RPWS-Langmuir Probe (LP). Most of the electrons missing from the plume plasma reside on the nano-grains.

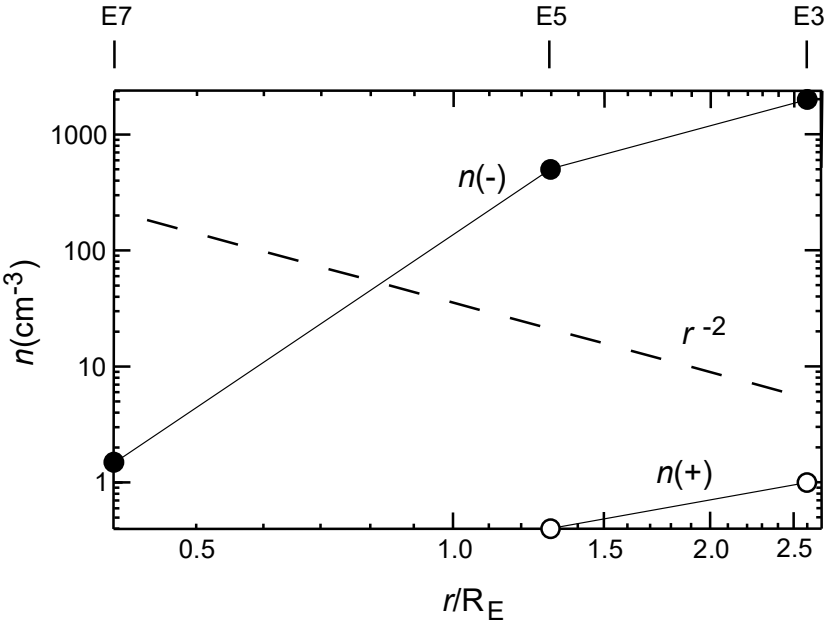

Figure CAPS-14. Total charged nano-grain number density within the CAPS E/q range versus distance from the south-pole source vent.

The link between Jupiter's aurora and its inner large moons was well known, which raised the question of whether a similar relationship might exist between Enceladus and Saturn's aurora. The necessary electrodynamic coupling was established by combining ELS data showing strong field-aligned electron beams, with magnetic field measurements indicating field-aligned currents. Pryor et al. [2011] then used the Cassini UVIS camera to take UV images of the region around Saturn's north pole about two weeks later. The Enceladus footprint was seen as predicted by field line tracing at 64.5° N latitude and the correct longitude.

Icy Satellites

In addition to Enceladus, IMS also detected signatures of magnetosphere-moon interactions at both Dione and Rhea. Dione is in an approximately circular orbit at a radial distance from Saturn of about 6.3 R_S, which is outside Enceladus (R = 3.9 R_S) and Tethys (R = 4.9 R_S) and inside Rhea (R = 8.7 R_S) orbits. Early in the mission IMS observations suggested the presence of an exosphere around Rhea—for example, Martens et al. [2008]—that was produced by radiolysis and sputtering of the surfaces by magnetospheric particles [Johnson et al. 2008]. Subsequent data from CAPS and INMS led to confirmation of very tenuous exospheres around both Dione and Rhea—for example, Tokar et al. [2012] and Teolis et al. [2010]—that have similar density and chemical composition consisting primarily of carbon dioxide and molecular oxygen. During Cassini's April 7, 2010, flyby of Dione (D2), at an altitude of about 500 km, IMS detected O_2^+ pick-up ions that likely originated from a neutral O_2 exosphere. The interaction is depicted in Figure CAPS-15.

Figure CAPS-16 shows IMS and ELS observations of pickup ions. The positive ions are from Rhea's exosphere (denoted by blue trajectories) and are identified as O_2^+ in the IMS data. The distribution of ion arrival directions in the vicinity of Rhea also indicate the presence of a tenuous dust ring or halo [Jones et al. 2008]. Note that negative ions are also visible in the ELS spectrogram.

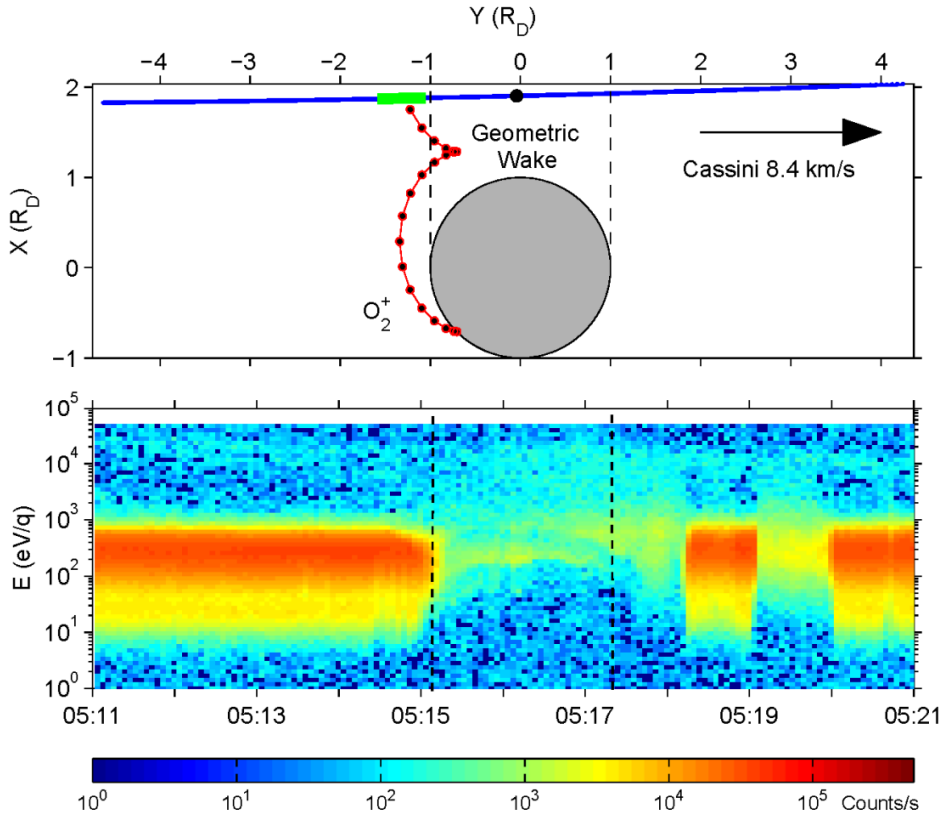

Figure CAPS-15. Depiction of the orbit of O_2^+ at Dione showing the mapping of O_2^+ ions from the observation point of CAPS (green line along trajectory) back to the moon. Figure from Tokar et al. [2012].

The observation of the so-called Pac-Man thermal feature on Mimas by the Independent Review (IR) Team came to be interpreted and modeled by the CAPS team. Schaible et al. [2017] developed a quantitative description of the effect of highly penetrating energetic electrons observed by CAPS causing sintering of the ice grains which increased the thermal inertia of the icy regolith causing the Pac-Man feature.

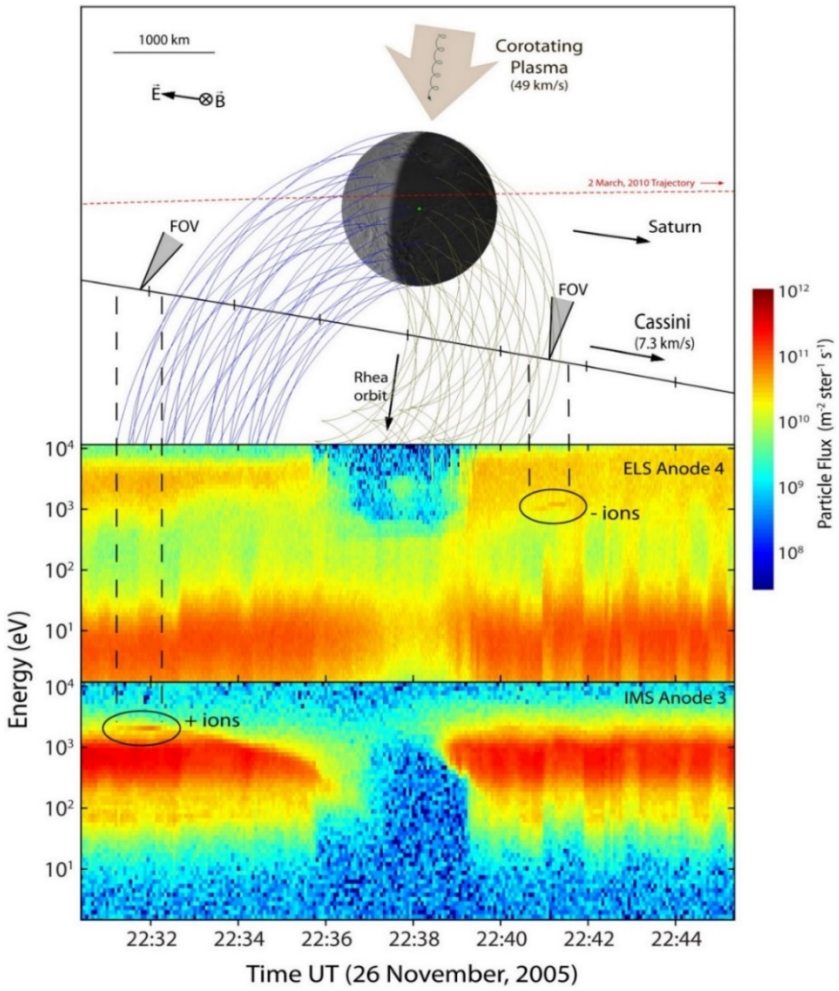

Figure CAPS-16. IMS and ELS observations of pickup ions. Energy spectrograms of ELS (top panel) and IMS (bottom panel) data for the March 10, 2010 shows the encounter with Rhea. Figure from Teolis et al. [2010].

Rings

IMS observed an enhanced ion flux (compared to background outside the rings) outside of the main rings and in the vicinity of the F-ring and G-ring as Cassini crossed the ring plane during orbit insertion on July 1, 2004. Near the edge of the main rings the ion flux as a function of energy per charge provided strong evidence for the presence of O_2^+. Analysis led to the conclusion that the enhanced ion flux between the F-ring and G-ring consisted of the water group ions O^+, OH^+, and H_2O^+ (the other water group ion H_3O^+ could not be identified) coming from Enceladus with an admixture of O_2^+, predominantly from the extended ring O_2 atmosphere. The O_2^+ component appeared to be dominant at Saturn Orbit Insertion (SOI) and was later found to vary with season [Elrod et al. 2012; 2014] due to the changing orientation of the ring plane relative to the solar UV flux (Figure CAPS-17).

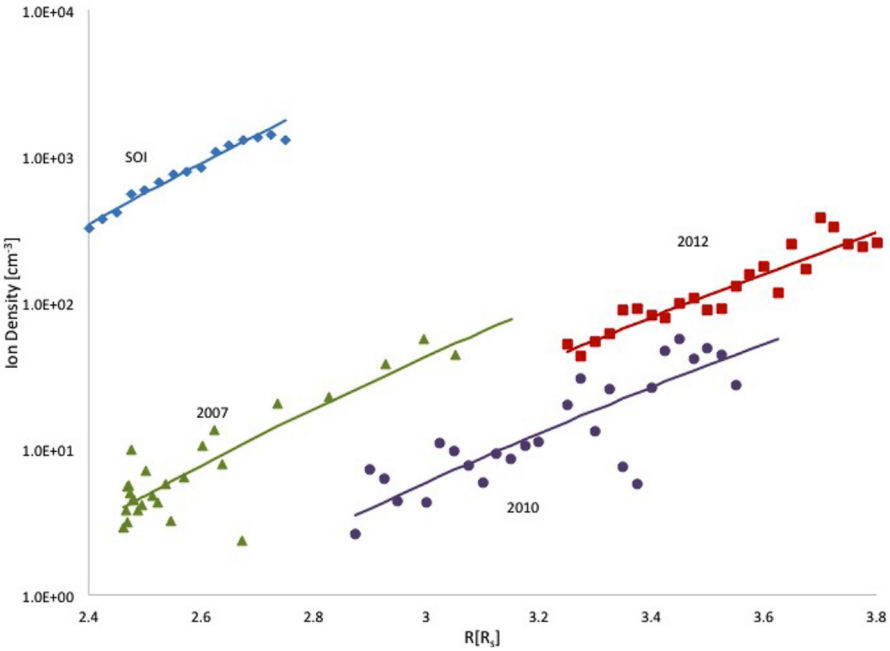

Figure CAPS-17. Ion densities extracted from IMS data at SOI in 2004, and inferred for subsequent years by modelling. The modeling indicates the seasonal dependence of ring plasma. This region contains ions formed from neutrals scattered out of the ring atmosphere as well as ions formed from neutrals in the Enceladus torus. SOI observations were dominated by O_2^+ and in the later years by water group ions. Figure from Elrod et al. [2014].

The seasonal dependence observed and modeled using CAPS data (Figure CAPS-16) confirmed that the O_2^+ ionization source was indeed solar UV acting on oxygen in the ring atmosphere as predicted by Tseng et al. [2010]. Seasonally varying oxygen was subsequently observed at much larger radii by the MIMI instrument, confirming that oxygen originating in the rings can be scattered throughout the inner magnetosphere and, consequently, also into Saturn's atmosphere. This likely accounts for oxygen observed in Saturn's thermosphere. Subsequent modeling [Tseng et al. 2013a] shows that model calculations based on the CAPS data were in reasonable agreement with that data.

Laboratory data showed that radiation decomposition of ice would lead to the production of roughly twice as much H_2 as O_2, thereby maintaining the near stoichiometry of irradiated ice grains —for example, Brown et al. [1982]. Indeed, CAPS measurements have shown that the Saturnian magnetosphere is permeated with H_2^+ and H^+ from a variety of sources (Titan, the Enceladus torus, and Saturn's atmosphere as discussed above), including the ring atmosphere [Tseng et al. 2011; 2013b]. Since H_2 is much lighter than O_2 it has a proportionately larger neutral scale height and can also be easily scattered throughout the magnetosphere by the heavier molecules. Ionization of the H_2 component of the extended ring atmosphere, and the pick-up of H_2^+ formed by this process, was shown by Tseng et al. [2011] to be an important component of magnetospheric H_2^+ detected by CAPS [Thomsen et al. 2010].

Possibly even more important, the very clean mass spectrum seen by CAPS over the rings (Figure CAPS-18) is indicative of the absence of significant levels of contaminants in the ring's ice particles [Cuzzi et al. 2009). In other words, irradiation of samples containing, for instance, carbon, would have produced CO molecules as well as other volatiles, all of which would subsequently have been scattered into the outer magnetosphere, forming pick-up ions that would be detected by CAPS. Although Cassini never flew over the main rings again, INMS data taken during the proximal orbits (when CAPS was off) did suggest that carbon species were indeed coming from the main rings.

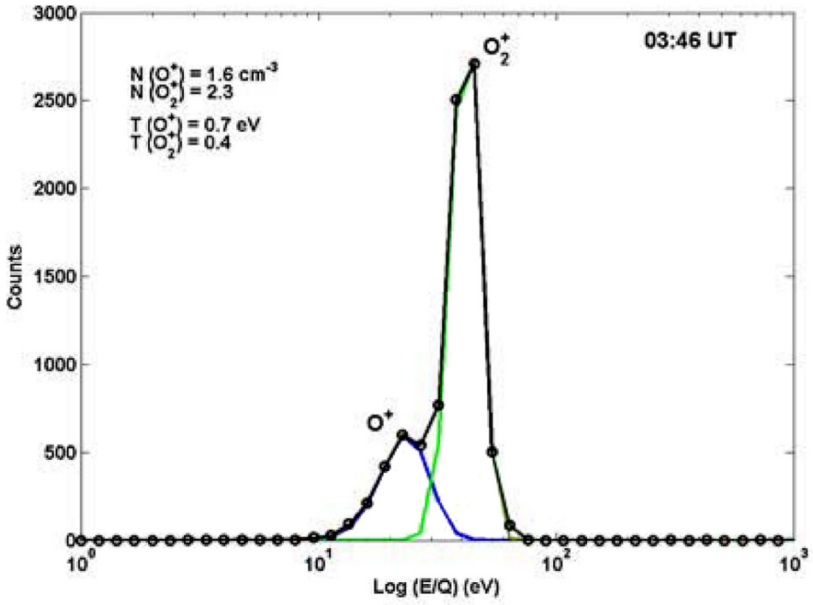

Figure CAPS-18. IMS mass spectrum over the rings taken during SOI at an altitude of ~0.2 R_S above the magnetic equator. Figure from Tokar et al. [2005].

It is worth noting that the INMS team is of the opinion that mass 28 signals seen during the Grand-Finale mission were mostly made by impact dissociation of CO_2 inside the INMS spectrometer ionization chamber. It is, therefore, unclear which molecule would be easier to produce from radiolysis of carbon-contaminated water ice. Both CO_2 and CO are possibilities. The INMS team detected only O_2 and CO_2 in Rhea and Dione exospheres.

Surprisingly, the ion densities observed by IMS between the outer edge of the main rings and Mimas (Figure CAPS-18) are derived from ionization of neutrals from the ring atmosphere and the Enceladus torus and exhibited an unexpected radial dependence [Elrod et al. 2012; 2014]. Not only did the plasma detected by CAPS in this region exhibit a seasonal dependence, with the O_2^+ component dominated by the water products from the Enceladus torus at Equinox, but the observed radial dependence suggested that an ion loss process other than electron-ion recombination, charge exchange or diffusion was acting [Elrod et al. 2014; Tseng et al. 2013a]. Since the CAPS ion densities and the RPWS electron densities differed, particularly at SOI, the observed radial dependence of the CAPS ion data was subsequently determined to be due to quenching of the

ions on nano-grains. These grains, a fraction of which were negatively charged, were presumed to be emitted from the edge of the main rings and present in the tenuous F-ring and G-ring, acted as ion sinks [Johnson et al. 2017]. That this process was occurring in this region of the magnetosphere was subsequently confirmed by the RPWS instrument during the F-ring orbits when, unfortunately, the CAPS instrument was turned off.

Rings-Magnetosphere Interactions

During SOI on July 1, 2004, the spacecraft passed over the B-ring, A-ring, and F-ring and the Cassini division before descending, inside the G-ring, through the ring plane. The trajectory provided the first in situ plasma measurements over Saturn's main rings, complementing data obtained by the Voyager 2 plasma science instrument outside the main rings. During SOI, IMS observed ion fluxes over the main rings consistent with the presence of atomic and molecular oxygen ions [Young et al. 2005]. IMS observations over the main rings detected both O^+ and O_2^+ at densities of a few per cm^3 using the IMS TOF sensor (Figure CAPS-19) [Tokar et al. 2005; Elrod et al. 2012]. Further analysis by Elrod et al. [2012] shows much higher densities of O^+ when CAPS was over the outer edge of the B-ring and again when CAPS was over the inner edge of the A-ring.

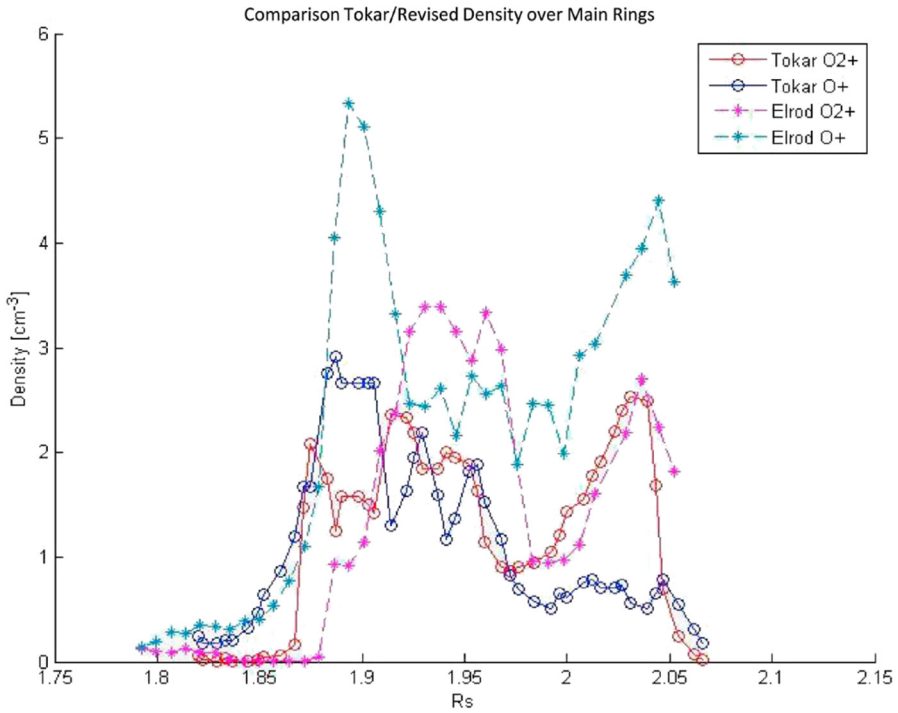

Figure CAPS-19. Densities of O^+ and O_2^+ obtained from IMS data over the main rings as a function of radial distance from Saturn in R_S. Data from Tokar et al. [2005] and re-analyzed by Elrod et al. [2012].

The IMS data suggested the presence of a ring atmosphere that was predominantly O_2 rather than H_2O and much more robust than predicted. Since the energetic ion density in this region is highly depleted due to absorption by ring particles—for example, Cooper et al. [2015], the CAPS

team proposed that the atmosphere was produced by UV-induced decomposition of ice on the ring particles [Johnson et al. 2006b]. Such a neutral atmosphere would have a scale height confining it close to the ring plane. Because ions were detected well above the ring plane, this also led to the prediction that ion-neutral scattering would produce both a ring ionosphere with a much larger scale height, and a neutral oxygen cloud that permeated Saturn's magnetosphere [Johnson et al. 2006b; Luhman et al. 2006; Bouhram et al. 2006]. Following ionization, pick-up and scattering of the neutrals from this atmosphere was shown to populate the magnetosphere with oxygen atoms and molecules which are eventually ionized far from the main rings [Johnson et al. 2006b]. Molecular oxygen ions were eventually discovered in the inner magnetosphere as well [Martens et al. 2008]. This has been subsequently confirmed by additional data and modeling as discussed in the section entitled Rings and Satellites.

Magnetosphere Composition, Sources, Transport, and Losses

The Cassini mission enabled an extensive exploration of Saturn's magnetosphere: its structure, plasma sources, transport, dynamics, loss mechanisms, and interaction with satellites, rings, and other neutral material. In this section we address CAPS findings regarding magnetosphere structure, plasma sources, transport, variability, and loss. More extensive discussions of the magnetospheric dynamics, the interaction with satellites and rings, and the interaction with the solar wind at the bow shock and magnetopause are presented in the separate section entitled Magnetosphere Dynamics. Thomsen [2013] has given a short but very useful overview of magnetosphere dynamics.

Structure

Global Structure. The orbital coverage of Cassini allowed a good determination of the global structure of Saturn's magnetosphere. Based on multiple-instrument observations, summary descriptions of the global structure have been published [Gombosi et al. 2009; Arridge et al. 2011b; Krupp et al. 2018]. As suspected from previous fly-by missions, Saturn's magnetosphere is similar in some respects to the Earth's: Its strong intrinsic magnetic field creates a bubble standing in the incident supersonic solar wind, separated from it by a magnetopause, magnetosheath, and bow shock. The magnetospheric bubble is bullet-shaped, compressed by solar wind dynamic pressure on the dayside and stretching out into a long magnetotail on the night side. The distinguishing factors that determine the structure and dynamics of Saturn's magnetosphere are its strong magnetic field, rapid rotation, and dominant source of magnetospheric plasma deep within the magnetosphere (i. e., neutral water molecules from Enceladus).

Radial Variation. The primary spatial dependence of magnetospheric properties is in the radial direction. From the first pass through the magnetosphere during SOI [Young et al. 2005], several distinct magnetospheric regions could be identified: an outer region (inside the magnetopause) with extremely low density, later understood as magnetospheric lobe; then a significantly denser region with variable density dominated by H^+, later understood as the higher-latitude manifestation of the plasma sheet/ring current; and finally, a much denser inner

plasmasphere dominated by W^+. Subsequent analyses of the SOI data [Rymer et al. 2005; Sittler et al. 2005, 2006a, 2008] provided quantitative estimates of the H^+, W^+, and electron plasma parameters in the inner magnetosphere and demonstrated that the plasma flow velocity is near co-rotation throughout the region (co-rotation is the azimuthal flow that results from essentially rigid rotation with the planet; it is enforced by currents flowing along the magnetic field lines between the upper atmosphere and the magnetospheric plasma). The proton and water-group temperatures were consistent with local ionization and pick-up into the co-rotating flow. The electrons in the inner magnetosphere consist of two populations: 1) a cool component whose temperature tracks the proton temperature; and 2) a hotter population that increases in energy with decreasing radial distance [Young et al. 2005; Sittler et al. 2006b; Schippers et al. 2008]. Later work [Rymer et al. 2007; Rymer 2010; Schippers et al. 2009] showed that the cold electron component was consistent with a local pick-up source and subsequent heating via Coulomb collisions with the protons. The hot component was consistent with adiabatic transport inwards from a source in the plasma sheet/ring current region.

Calculation of the ion plasma moments (density, temperature, flow velocity) from CAPS data is complicated by incomplete and variable viewing directions. Nonetheless, application of a numerical computational scheme to the full data set through March 2009 enabled a survey of the properties of H^+, W^+, and H_2^+ (the third most common ion species in the magnetosphere, as revealed by CAPS time-of-flight measurements) throughout the magnetosphere (Figure CAPS-20)

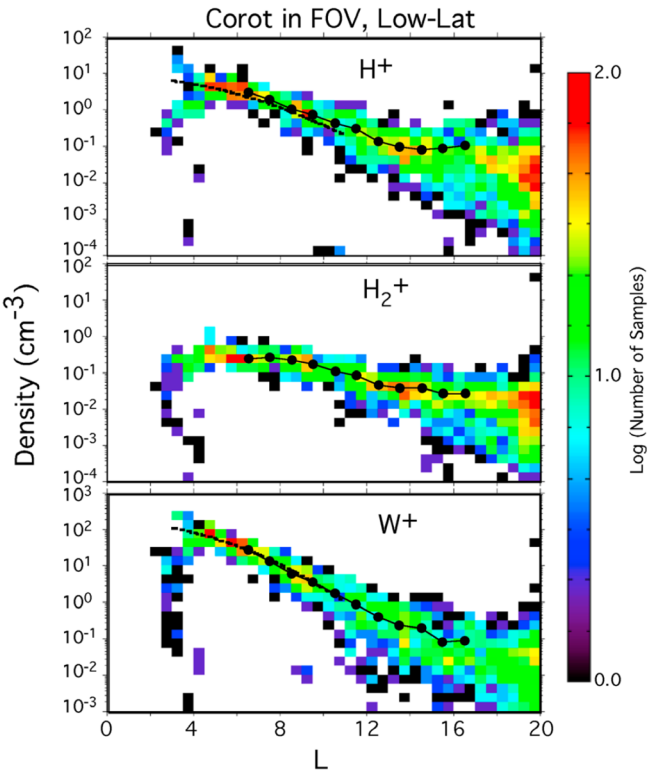

Figure CAPS-20. Radial dependence of low-latitude plasma density when co-rotation was in the CAPS field of view. Figure from Thomsen et al. [2010].

[Thomsen et al. 2010]. The survey confirmed that densities decrease, and temperatures increase, with radial distance inside ~20 R_S, and the W^+ density declines more rapidly than light ions. The flow velocity remains primarily in the co-rotational direction essentially all the way to the magnetopause, but the speed is lower than full co-rotation, as discussed below in the Transport section. Combined with the higher-energy measurements of MIMI, the CAPS data enabled a comprehensive survey of the total plasma pressure throughout the magnetosphere and thus an understanding of the currents that distort the dipole field within the plasma sheet and ring current region [Sergis et al. 2010, 2017]. A more recent survey of plasma moments calculated with a forward modeling approach that includes anisotropic temperatures explores both the radial and local time variations of the plasma (Figure CAPS-21) [Wilson et al. 2017].

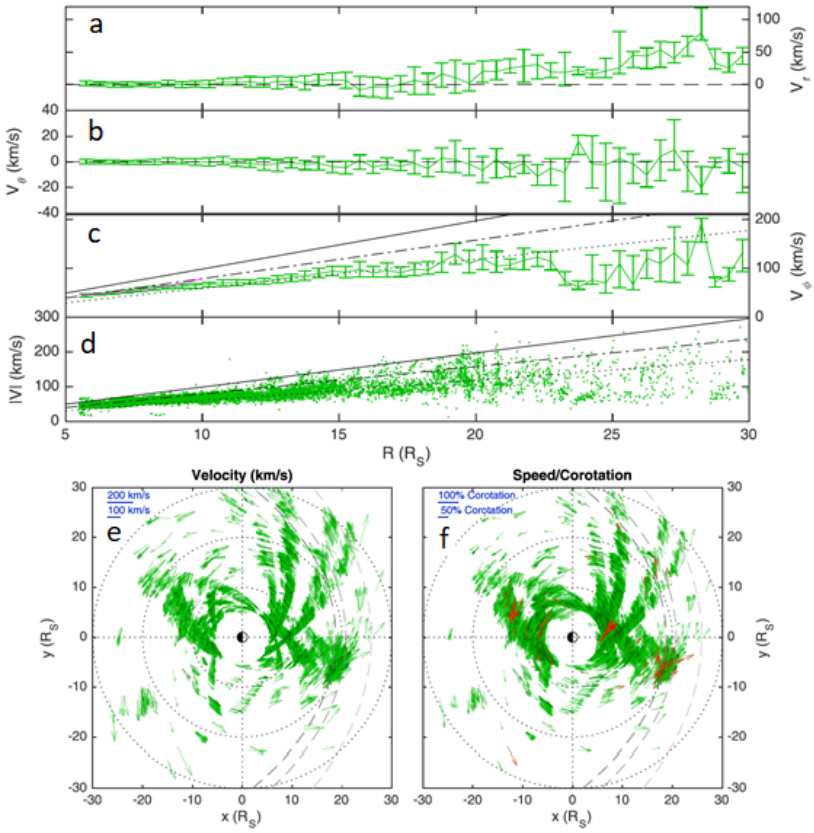

Figure CAPS-21. A low-latitude heavy ion layer displaying narrow substructures, and a higher-latitude, smooth, broad ion layer composed dominantly of light ions. *Panels a–c:* Radial profiles of plasma velocity components, in 0.5-R_S bins. *Panel d:* All measured flow speeds. *Panel e:* Equatorial plane projections of flow vectors with length proportional to flow speed. *Panel f:* Same as panel e, but with length proportional to the fraction of co-rotation. All data points are shown in green, while dark green shows every thirtieth data point. Figure from Wilson et al. [2017].

Disk structure, low-latitude confinement. Because of strong centrifugal forces on co-rotating plasma, Saturn's magnetosphere is flattened into a disk shape, especially on the night side and during times of relatively low solar wind dynamic pressure—for example, Arridge et al. [2007, 2008]. CAPS data allow determination of the latitudinal scale heights of H^+, W^+, and H_2^+ and show

that the heavy ions are more strongly confined to the equatorial plane—for example, Thomsen et al. [2010]. In the magnetotail, the magnetodisk structure is particularly prominent, with the current flowing in a relatively thin region of dense plasma separating the lobes of oppositely directed magnetic field. The magnetodisk consists of a structured plasma sheet: a low-latitude heavy ion layer displaying narrow substructures, and a higher-latitude, smooth, broad ion layer composed predominantly of light ions (Figure CAPS-22) [Szego et al. 2011]. The density and azimuthal flow speed decline with increasing latitude [Nemeth et al. 2015] as a direct consequence of the sub-corotation of the plasma in the outer magnetosphere—for example, McAndrews et al. [2009]; Thomsen et al. [2013, 2014b]; Wilson et al. [2017]. Highest speeds occur on field lines at lowest latitudes mapping to the rapidly rotating inner regions of the plasma sheet, and the speed falls as one moves to higher latitudes where the field lines are connected to strongly sub-co-rotating plasma at large radial distances.

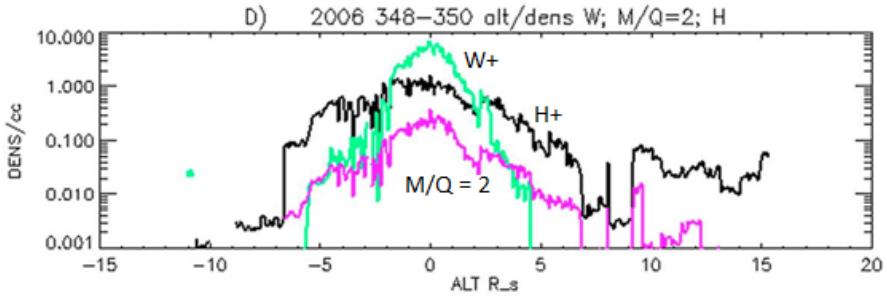

Figure CAPS-22. Density of three species: water W^+ (green), hydrogen H^+ (black), and mass/charge 2 (magenta); as a function of distance from the equatorial plane for a crossing of the magnetic equator at ~9 R_S. W^+ is more confined to the equator than light ions, so the relative composition varies with latitude. Figure from Szego et al. [2011].

Local time dependence. Although CAPS had relatively little low-latitude coverage with appropriate viewing near dawn, several observations were made of the local time dependence of plasma properties. For example, interchange injections (see the section entitled Magnetosphere Dynamics and Radial Transport) appear to be stronger and penetrate more deeply into the inner magnetosphere on the night side compared to the dayside [DeJong et al. 2011]. Also, in the inner magnetosphere, there is a day-night asymmetry in both ion and electron temperatures [Thomsen et al. 2012], which is further discussed in the section entitled Magnetosphere Dynamics and Radial Transport. The day-night asymmetry in the hot electron component extends to high latitudes, but there is no such asymmetry in the plasma sheet thickness, at least in the cold electron population [Carbary and Rymer 2014]. At larger radial distances, there is only modest variation with local time [Wilson et al. 2017].

Cusp and Polar Cap. As seen already during SOI [Young et al. 2005], at latitudes above the extended plasma-sheet/ring-current there is a region that is largely devoid of plasma, known as the magnetospheric lobe. The lobe is commonly seen in the magnetotail—for example, Thomsen et al. 2015b]—as the plasma sheet rocks and flaps up and down (see discussion in the section entitled Periodicities). Lobe field lines are thought to be connected by magnetopause reconnection into the solar wind and have thus lost their magnetospheric contents. At low altitudes, the lobe maps into

the polar cap. The polar cap boundary is identified based on a sharp drop in ELS electron fluxes and corresponding signatures in other data sets (Figure CAPS-23)—e.g., Jinks et al. [2014]. A survey of polar cap boundary crossings showed that the main upward field-aligned currents associated with the aurorae reside equatorward of the open-closed boundary [Jinks et al. 2014].

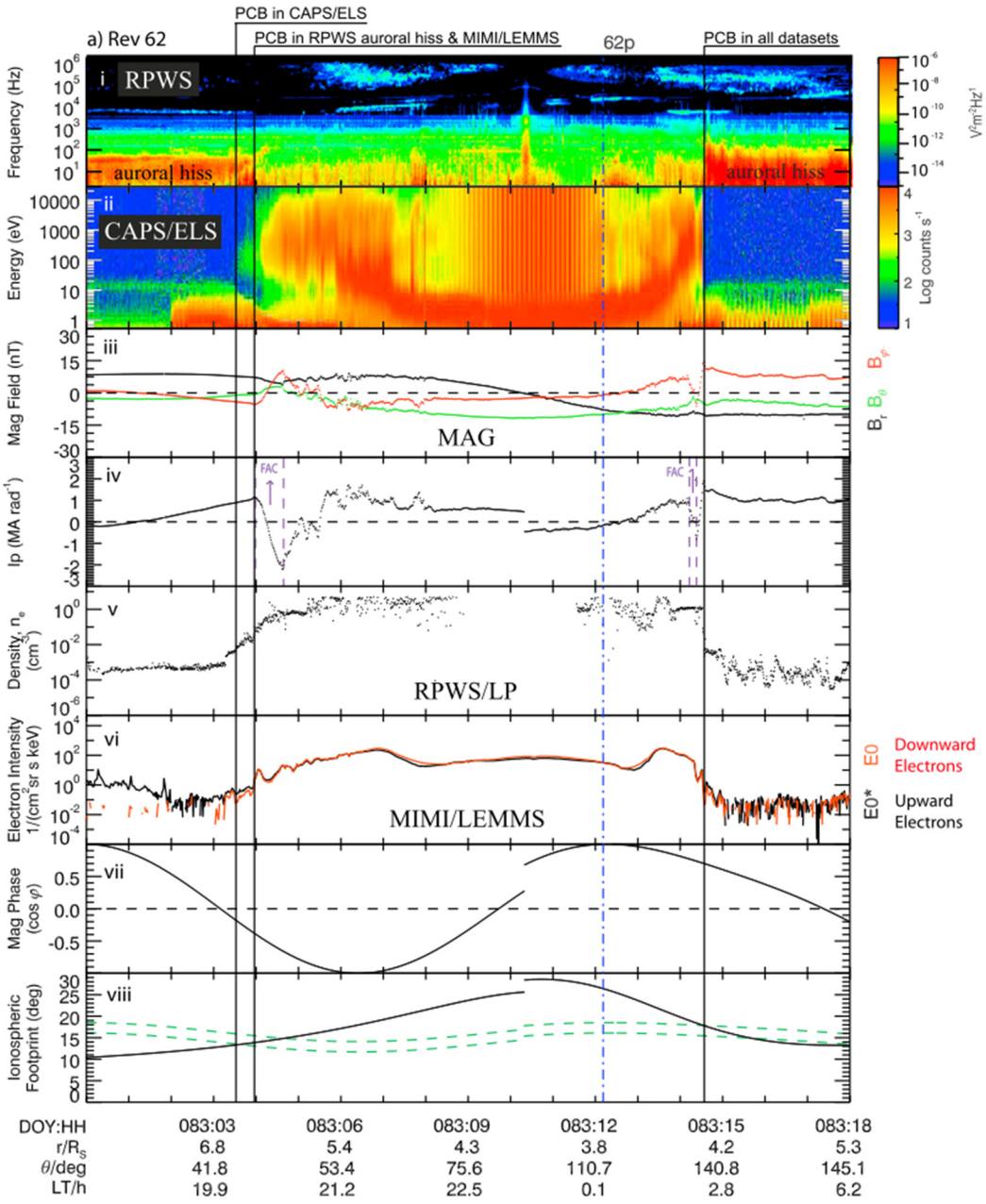

Figure CAPS-23. Polar cap boundary as seen in several different Cassini data sets. The sharp change in the ELS electron spectrum is the most definitive signature. The polar cap is largely devoid of electrons (counts below ~20 eV are due to spacecraft photoelectrons). Figure from Jinks et al. [2014].

Near noon, open magnetic field lines (which will ultimately become the lobe/polar cap) are filled with incoming magnetosheath plasma, which penetrates down to low altitudes. CAPS observations of this region, known as the cusp, demonstrate that the process of reconnection occurs at Saturn's magnetopause, with indications that the reconnection is pulsed [Jasinski et al. 2014]. The first cusp observation was associated with the arrival of a solar wind shock front, which compressed the magnetosphere and probably provided more favorable conditions for magnetopause reconnection [Jasinski et al. 2014]. Evidence for both bursty and more continuous reconnection is observed during different cusp events, and the locations of the reconnection site vary along the subsolar magnetopause. Magnetic reconnection and plasma injection into the cusp can occur for a variety of upstream conditions [Jasinski et al. 2016, 2017; Arridge et al. 2016].

Temporal variability

Seasonal and long-time scale. On the time scale of months to years, most of Saturn's magnetospheric plasma does not exhibit strong variability—less than a factor of three [Wilson et al. 2017]—in spite of the fact that the Enceladus plume source (see Figure CAPS-17) does appear to vary on the scale of several months [Smith et al. 2010; Elrod et al. 2014]. In the innermost magnetosphere, just outside the main rings, heavy ion densities (O_2^+ and W^+) show a seasonal dependence, as could be expected for a ring source that depends on the solar illumination angle [Elrod et al. 2012, 2014] (see the section entitled Rings in Plasma Sources).

Short time scale. On the scale of minutes to hours or days, there is significant variability in plasma properties (Figure CAPS-24)—for example, Young et al. [2005]; Gombosi et al. [2009], Figures 9.28 and 9.29; Thomsen et al. [2015a], Figure 1. Variability at this scale may be due to the

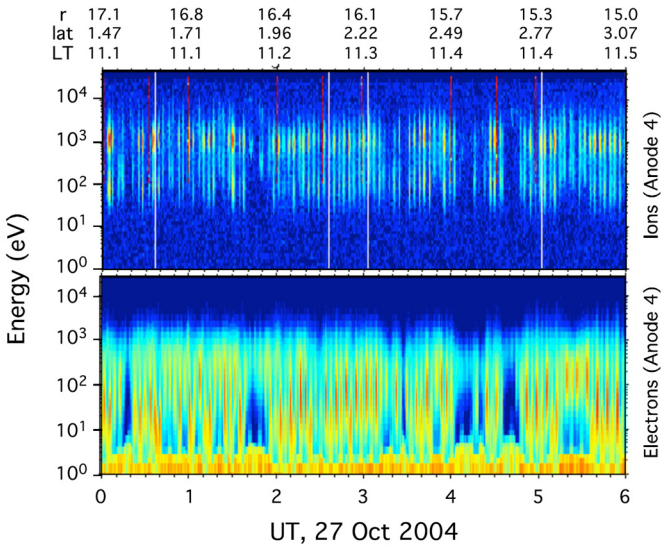

Figure CAPS-24. Temporal variability in plasma found in the middle magnetosphere ~16 R_S. Both panels show CAPS count rate as a function of energy and time for ions (*top panel*) and electrons (*bottom panel*). Regularly periodic variations are due to the CAPS actuator scanning the instrument into different look directions. Aperiodic variations show frequent changes in the spectral shape and intensity of magnetospheric plasma. Figure from Gombosi et al. [2009].

outward transport of interchanged flux tubes from the inner magnetosphere (see the section entitled Magnetosphere Dynamics). At the orbit of Titan, the ambient plasma environments are variable but can be organized into four types by the nature of the electron populations [Rymer et al. 2009a; Smith and Rymer 2014]. The plasma environment at Titan's orbit appears to be determined by the motion of the magnetodisk current sheet [Arridge et al. 2008; Szego et al. 2011].

Periodicity. Many properties of Saturn's magnetosphere exhibit periodicities at approximately the planetary rotation rate, a significant puzzle given the near-alignment of the magnetic and rotational axes. In the plasma data, the periodicities are clearest in the plasma sheet region. The density varies by more than an order of magnitude, depending on the SLS3 longitude [Arridge et al. 2008]. This variability is likely due to periodic up-and-down motion of the plasma sheet. The temporal and spatial variations in plasma and field parameters are well organized by the flapping of the plasma disk about a periodically varying position [Arridge et al. 2008; Szego et al. 2011, 2012, 2013; Nemeth et al. 2016]. Asymmetries in Cassini's periodic plasma sheet crossings [Thomsen et al. 2017] are consistent with predictions of plasma sheet rocking and thickness variation made both by the global magneto-hydrodynamic (MHD) models that incorporate the effects of hypothesized atmospheric vortices [Jia and Kivelson 2012] and by the closely-related dual rotating current systems inferred from magnetic field observations—for example, Cowley et al. [2017] and references therein.

In the inner to middle magnetosphere, evidence was found for a plasma cam in which the plasma density varies roughly sinusoidally with SLS3 (Figure CAPS-25) [Burch et al. 2008, 2009; Goldstein et al. 2016]. Theoretical arguments suggest that asymmetric ring-current pressure coupled to Saturn's ionosphere can initiate a rotating two-cell interchange potential that is long-lived and stable [Goldstein et al. 2014]. Outflow from the dense sector was suggested as the driver of recurrent tail reconnection and plasmoid production (see sections entitled Plasma Sources and Magnetosphere Dynamics) inferred from periodic magnetic field variations in the tail [Burch et al. 2009], but subsequent authors argued that the field variations were more consistent with simple wave-like motion or periodic rocking of the plasma sheet rather than plasmoid formation [Jackman et al. 2009]. In the more recent forward-modeling dataset of ion densities [Wilson et al. 2017], the cam is not seen, so there remain questions about its existence and its consequences.

Response to Solar Wind. Because of its strong magnetic field, rapid rotation, and internal plasma source, most magnetospheric dynamics appear to be internally driven (see the section entitled Magnetosphere Dynamics). Nonetheless, evidence has been found for significant dynamical effects attributable to solar wind variability. CAPS observations in the pre-dawn tail outbound from SOI, showed sudden energization of plasma associated with a field dipolarization, which was interpreted as evidence of a solar wind compression-related tail collapse via magnetic reconnection. Under conditions of high solar wind dynamic pressure, the magnetotail appears to enter a state of sustained lobe reconnection, resulting in a more Dungey-like configuration [Thomsen et al. 2015b]. In the inner magnetosphere, there is no apparent relation between the depth of electron penetration and solar wind properties [Thomsen et al. 2016a], although the energization of ions in a large-scale standing wave might be caused by a solar wind pressure impulse [Thomsen et al. 2017].

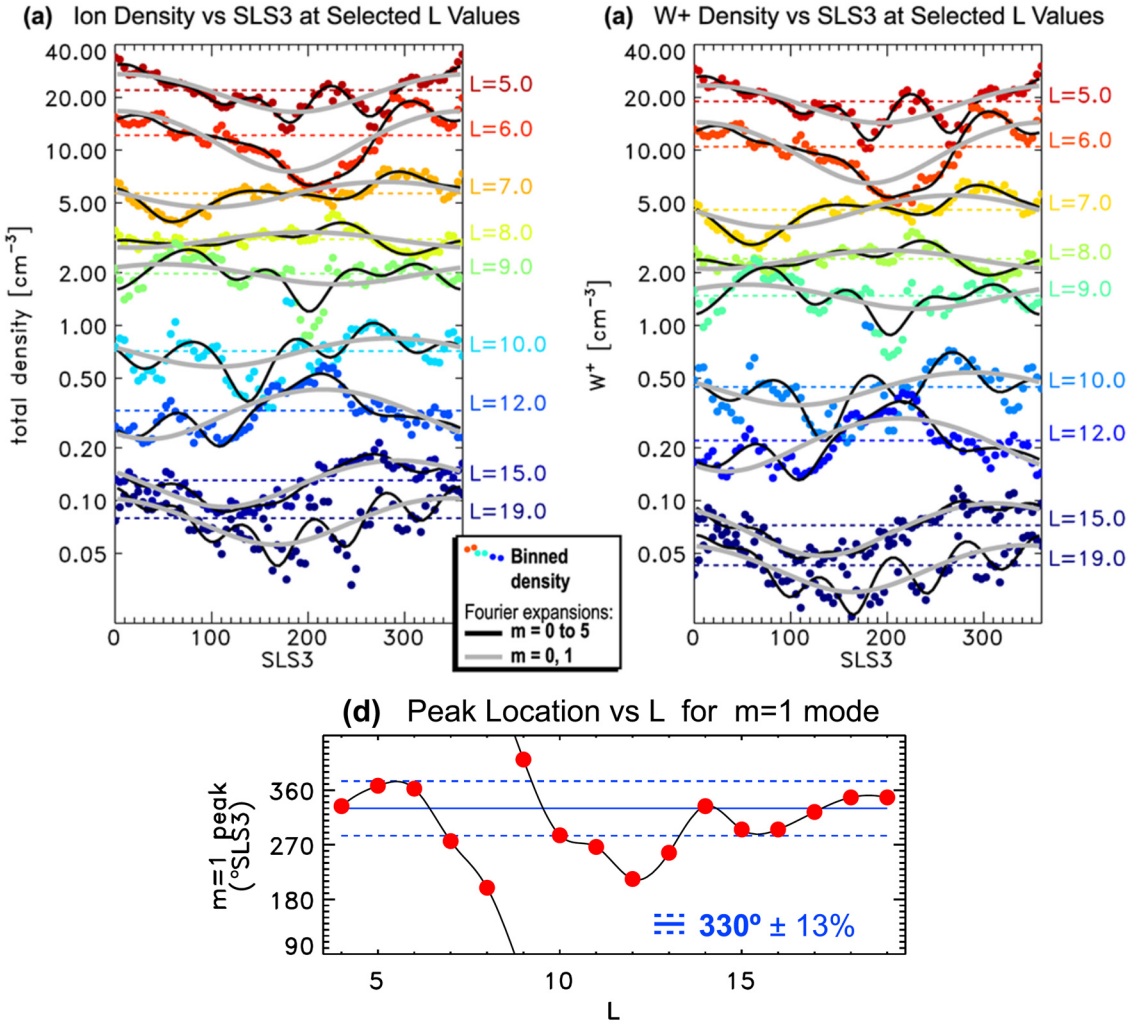

Figure CAPS-25. Evidence for the existence of a plasma cam, in which the density is generally highest in a particular SLS3 longitude sector. Figure from Goldstein et al. [2016].

Plasma sources

Clues from Composition. The composition of plasma ions is one of the best pointers to the source of the plasma. CAPS findings that the dominant magnetospheric ions are W^+, H^+, and H_2^+ [Young et al. 2005; Thomsen et al. 2010] were well explained by the later discovery of the prodigious output of water from the south-polar plumes of Enceladus. It was noted by Young et al. [2005] that the presence of H_3O^+ within the W^+ ion group indicated ion-molecule reactions occurring in a water-rich atmosphere, attributed to the E-ring and inner icy satellites, which ultimately was determined to be Enceladus. A careful separation of the individual components of the water-group species and determination of the radial distance dependence of their relative proportions [Tokar et al. 2008; Wilson et al. 2015] provided vital constraints on models of the physics and chemistry of Enceladus-originating material.

Another example of source determination through composition is N^+ [Smith et al. 2005, 2007, 2008]. Originally expected from Titan, the radial dependence of the N^+ phase space density and the energy of this population suggested instead an inner magnetosphere source [Sittler et al. 2006b], probably Enceladus, with both molecular nitrogen and ammonia emitted there (Figure CAPS-26). Surprisingly little N^+ has been found in the outer magnetosphere, indicating that nitrogen ions coming from Titan do not accumulate to significant densities [Smith and Rymer 2014].

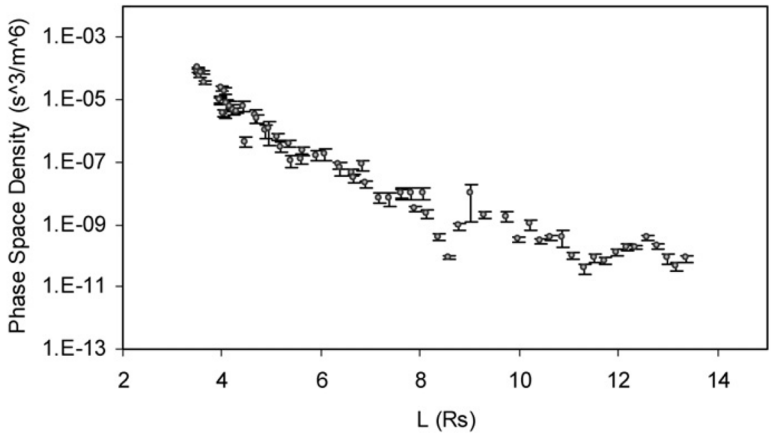

Figure CAPS-26. Nitrogen ion phase space density averaged over energy and angle, as a function of distance from Saturn. Clear decline with distance indicates a source in the inner region, inconsistent with a Titan source in the outer magnetosphere (L ~20). Figure from Smith et al. [2007].

Clues from Energy and Pitch-Angle Distributions. Examples of how the energy distribution illuminates plasma sources were noted above. For example, the way ion energies in the inner magnetosphere track the co-rotational energy was strong evidence for local pick-up from a distributed neutral gas source [Young et al. 2005; Thomsen et al. 2010]. Similarly, the different radial dependence of the two electron populations suggested a local pick-up source with subsequent collisional heating of the cold electrons, while the hot electrons are more likely adiabatically transported inward from the outer magnetosphere (Figure CAPS-27)—for example, Schippers et al. [2008]; Rymer et al. [2007]; Rymer [2010]. Butterfly angular distributions found in inner magnetosphere electrons adjacent to interchange injections (see the section entitled Hot Plasma Injections in Magnetosphere Dynamics) suggest an origin near Dione and Tethys [Burch et al. 2007] but might also be consistent with a hot electron circulation process associated with the injections, rather than an inner magnetospheric source [Rymer et al. 2008].

Enceladus. As can be seen from Figure CAPS-20 and Figure CAPS-22, the dominant ion species seen throughout the magnetosphere are well explained by ionization of material from the water plumes of Enceladus. CAPS observations of the plumes themselves are detailed in the section entitled Enceladus. CAPS data also showed Enceladus to be the probable source of most of the N^+ observed in Saturn's inner magnetosphere (Figure CAPS-26), and CAPS measurements further helped reveal the existence of temporal variability in the plume source [Smith et al. 2010].

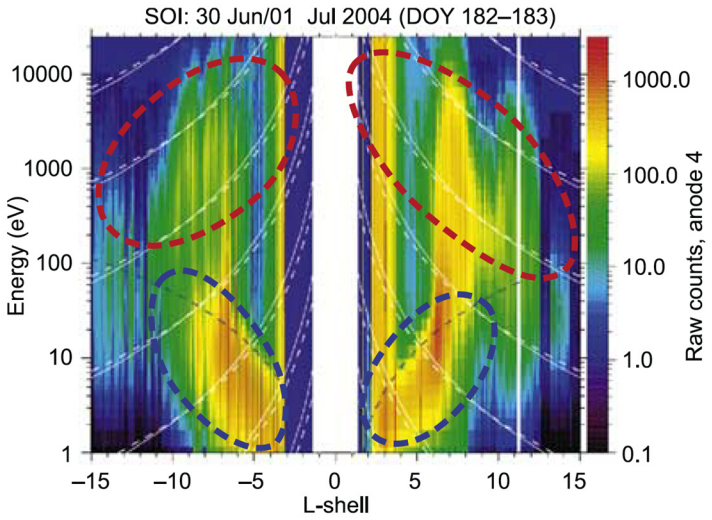

Figure CAPS-27. Two-component electron spectra from the part of the orbit insertion trajectory passing through the inner magnetosphere. White dotted curves show expected L dependence of the energy of particles conserving their first adiabatic invariant. Blue dotted lines show expected energy for local pickup of H^+. The cold electrons are most consistent with non-adiabatic collisional coupling to pick up H^+, whereas the hotter electrons are consistent with adiabatic transport from outside the inner region. Figure from Rymer et al. [2007].

Titan. A summary of CAPS observations during the many encounters with Titan are described elsewhere. The primary tracers of Titan's contributions to magnetospheric plasma, have been N^+ and H_2^+. The finding of very little N^+ in the outer magnetosphere [Smith et al. 2005] indicates that Titan's contribution to the heavy-ion plasma is limited, whereas the fact that H_2^+ becomes comparable to H^+ and W^+ in the outer magnetosphere [Thomsen et al. 2010] indicates that Titan is an important source of lighter ions in that region. From observations during passage through Titan's wake region, the total mass loss rate from Titan is estimated to be a few × 10^{25} amu/q/sec (~0.8 kg/s) [Coates et al. 2012], compared to estimates of ~60-100 kg/s from Enceladus [Fleshman et al. 2013].

Rings. CAPS was turned off before the F-Ring and Proximal Orbits, so the only direct exploration of ring-associated plasma occurred during SOI, where a layer of O^+ and O_2^+ was discovered over the A-ring and B-ring [Young et al. 2005]. Subsequent analysis of the SOI data [Tokar et al. 2005] produced densities and temperatures of these two species (Figure CAPS-28). The ring atmosphere and ionosphere are likely produced by UV photosputtering of the icy rings and subsequent photoionization of O_2^+. Significant O_2^+ was also detected outside the main rings, near the F-ring [Tokar et al. 2005], and analysis of the O_2^+ and W^+ profiles showed the seasonal dependence mentioned above, consistent with a ring source that depends on the solar illumination angle [Elrod et al. 2012, 2014; Tseng et al. 2010]. The result indicates that the rings are an important source of O_2^+ and O^+ ions inside the orbit of Mimas.

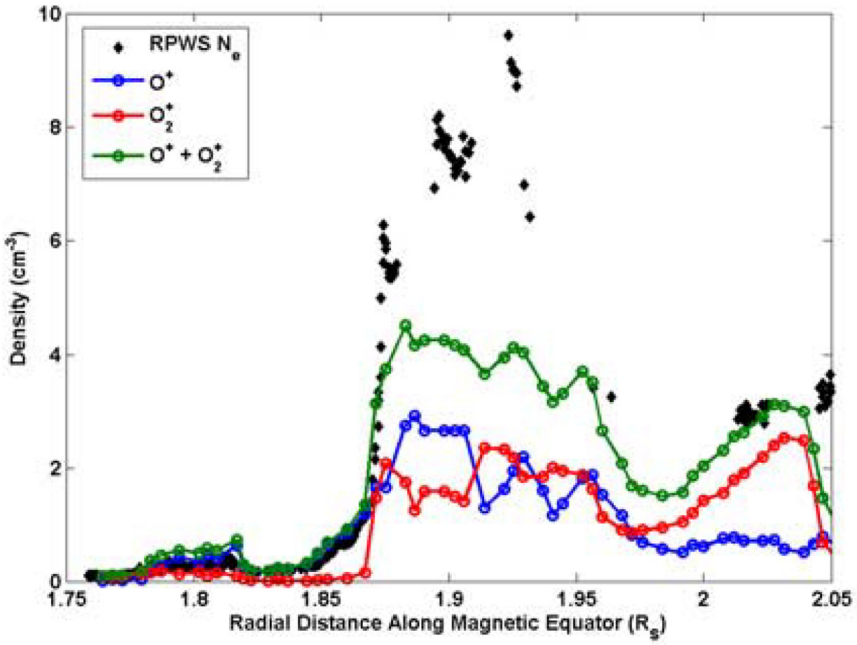

Figure CAPS-28. Radial dependence of O^+ and O_2^+ densities from CAPS observations over the main rings during SOI. Figure from Tokar et al. [2005].

Other satellites. CAPS has also detected O_2^+ in the vicinity of Dione [Tokar et al. 2012], and the observed radial dependence of the ratio O_2^+/W^+ suggested that there is a neutral O_2 source in the vicinity of Rhea [Martens et al. 2008]. Although the evidence for oxygen from Rhea is somewhat skimpy, CAPS has clearly detected non-gyrotropic outflowing CO_2^+ there, as well as another negatively charged species, previously thought to be O^- but now found to be closer to mass 23 [Desai et al. 2018]. The latter is perhaps a carbon-based ion deriving from implanted exogenic compounds. Examination of the plasma conditions on flybys of Rhea [Wilson et al. 2010] revealed that the plasma flowing near it had no radial component on the Saturn-side of the moon but had a radially outward component on the anti-Saturn-side. This is potentially due to an electric field enhancement near the moon, which is suggested in hybrid simulations.

Saturn ionosphere. Observation of probable plasma outflows from the ionosphere at the outer edge of the night side plasma sheet and extending into the lobes led to an estimate of some tens of kg/s lofted from the ionosphere (Figure CAPS-29) [Felici et al. 2016].

The observations occurred during a probable solar wind dynamic pressure enhancement, which may be important for producing significant outflow. It is not yet clear how often such outflow occurs, nor whether the outflow is captured into the closed region of the magnetosphere, rather than just escaping into the solar wind. Additionally, the field-aligned angular distributions of the suprathermal electrons within the plasma sheet/ring current region may indicate an ionospheric origin [Schippers et al. 2008], but no supporting evidence from the ion data has been reported.

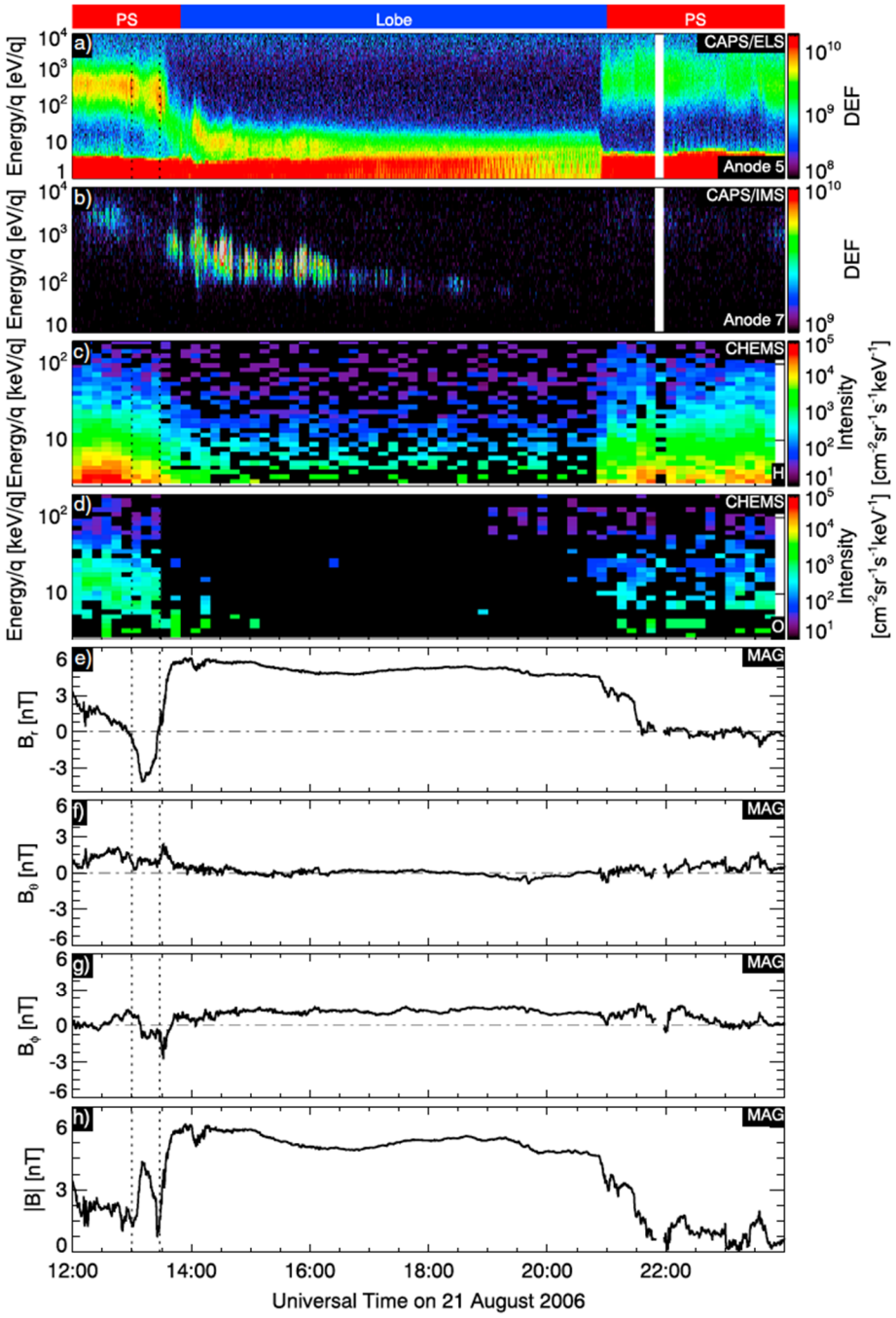

Figure CAPS-29. CAPS observations of an outflowing H^+ population from Saturn's ionosphere, seen in the lobe near the plasma sheet boundary at 36 R_J down tail. Figure from Felici et al. [2016].

Solar wind. Regarding dayside entry of solar wind plasma via reconnection or the Kelvin-Helmholtz instability, there is considerable evidence that both processes take place (see the section entitled Bow Shock, Magnetosheath, and Outer Magnetosphere). Magnetopause encounters frequently exhibit a low-latitude boundary layer (LLBL), in which magnetosheath

plasma can be found just inside the magnetopause. From a survey of 354 crossings of the LLBL [Masters et al. 2011a, 2011b], the estimated thickness is only of the order of one Saturn radius, with no clear dawn-dusk asymmetry. Thus, while solar wind plasma can and does enter the magnetosphere on the dayside, it does not get very far in. This is supported by the fact that the ratio of m/q = 2 to H^+ ions in the outer magnetosphere is almost always significantly greater than the values of 1 to 10% typically seen within the solar wind [Thomsen et al. 2010], indicating that plasma in the outer magnetosphere is predominantly of inner magnetospheric and/or Titan origin, with very little contribution from solar wind plasma.

On the night side, plasma with solar wind-like composition has been observed at 37 R_S near local midnight [Thomsen et al. 2015b]. In that event, it appeared that prolonged high solar wind dynamic pressure may have caused erosion of the tail plasma sheet through ongoing Vasyliunas-type reconnection that then involved open lobe field lines and created a more Earth-like, Dungey-style outer plasma sheet predominantly of solar wind origin. Other evidence for Dungey-style reconnection following a Vasyliunas-style reconnection event is the post-plasmoid plasma sheet— for example, Jackman et al. [2011]. One other event that showed the possibility of a Dungey region, in which field lines were probably closed but the densities were quite low and there was very little O^+, was seen in a rapid high-latitude pass near dawn with clear evidence of Vasyliunas-type reconnection at latitudes just equatorward of the Dungey region [Thomsen et al. 2015a].

One unanticipated discovery of the Cassini mission is the existence of an inner magnetospheric convection pattern superimposed on the dominant co-rotation pattern.

Transport

Inner Magnetosphere. As noted in the section entitled Magnetosphere Structure and in Figure CAPS-21, CAPS measurements consistently show that plasma flow in the inner magnetosphere is predominantly in the co-rotation direction, with a magnitude near full co-rotation at low radial distances but tending toward a fraction (~60%) of full co-rotation by 10 R_S—see Sittler et al. [2005]; Wilson et al. [2008, 2009, 2017]; Thomsen et al. [2010]; Livi et al. [2014]. Radial velocities are much smaller and difficult to measure [Wilson et al. 2008].

There is widespread agreement that the primary mechanism for radial transport within the inner magnetosphere, which is needed to remove the continuously-produced plasma from Enceladus, is the process of centrifugally-driven flux-tube interchange. This process is described in detail in the section entitled Magnetosphere Dynamics, but CAPS data have been instrumental in the discovery [Young et al. 2005; Hill et al. 2005; Burch et al. 2005] and diagnosis [Andre et al. 2007; Chen and Hill 2008; Menietti et al. 2008; Rymer et al. 2009b; Chen et al. 2010; DeJong et al. 2010; Thomsen et al. 2014b; Paranicas et al. 2016] of hot-plasma injection events that are the inward-moving half of the flux-tube interchange. There has been only one reported observation of outward-moving cold plasma fingers that should form the other half of the process [Thomsen et al.

2015a]. Estimates of the inflow speeds within the injection channels range from a few km/s to ~260 km/s [Burch et al. 2005; Rymer et al. 2009b; Chen et al. 2010; Paranicas et al. 2016]. Composition suggests that the plasma inside the injection channels comes from the outer magnetosphere [Thomsen et al. 2014b].

One unanticipated discovery of the Cassini mission is the existence of an inner magnetospheric convection pattern superimposed on the dominant co-rotation pattern [Andriopoulou et al. 2012, 2014; Thomsen et al. 2012; Wilson et al. 2013]. The pattern consists of a general dusk-to-dawn drift, such that particles drift inward while they co-rotate from noon to midnight and outward as they return from midnight to noon (Figure CAPS-30). The result is an inward displacement at midnight compared to noon. Several hypotheses regarding this convection have been advanced, but it remains an unsolved puzzle.

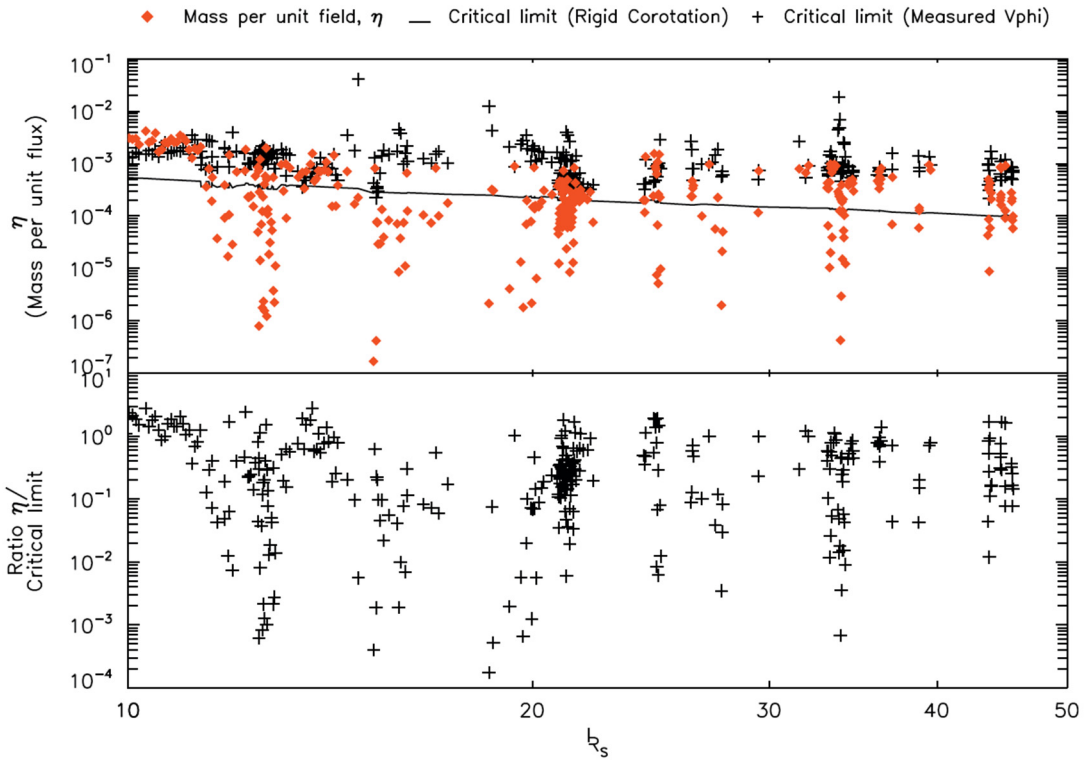

Figure CAPS-30. Comparison of night-side flux-tube content (red ♦), estimated from CAPS/IMS data, with the theoretical critical limit above which the flux tube will pinch off and release a plasmoid downtail (black +). The observed flux-tube content is roughly bounded by the critical limit, suggesting that night-side reconnection and plasmoid formation keep the tail near marginal stability. Figure from McAndrews et al. [2009].

Outer Magnetosphere. Beyond 10 R_S, CAPS measurements show consistently that the plasma flow overwhelmingly remains in the co-rotational direction at essentially all local times, indicating continued influence of connection to the co-rotating ionosphere, but the speed of the flow is well below full co-rotation—for example, McAndrews et al. [2009]; Thomsen et al. [2010, 2013, 2014a]; Wilson et al. [2017]. Beyond about 15–20 R_S, there is little evidence for inflowing plasma

on the night side, where, particularly near the flanks, flows tend to have more of an outward component. From the lack of inward flow in the pre-dawn sector, it appears that dense plasma is not often able to make the turn and return sunward to the dayside magnetosphere at distances beyond ~15 R_S (see Figure CAPS-21).

Plasma loss

Plasmoid formation. One of the principal ways in which plasma produced in the inner magnetosphere can be shed to the solar wind is through the process of magnetic reconnection in the tail. This is covered in greater detail later in the section entitled Magnetosphere Dynamics. Essentially, flux tubes loaded with inner magnetospheric plasma are transported via interchange to the outer magnetosphere. Strong centrifugal forces distend them radially, especially near the equatorial plane. On the dayside, the pressure of the solar wind helps confine the distended flux tubes, but when they rotate into the night side, that confinement goes away, and centrifugal force can overwhelm the magnetic tension. The result is that the flux tubes pinch off (or reconnect), shedding a plasmoid that is no longer connected to the planet and which carries away the load of plasma the flux tube bore before reconnection occurred (Figure CAPS-30). This is the so-called Vasyliunas cycle. CAPS data have been instrumental in identifying the resulting down-tail flows of the disconnected plasmoids [Hill et al. 2008; McAndrews et al. 2009; Jackman et al. 2014, 2015; Arridge et al. 2015; Smith et al. 2016, 2018]. There is ongoing debate as to whether plasmoids can carry away enough plasma to balance new production in the inner magnetosphere.

Magnetopause processes. Magnetic reconnection and nonlinear Kelvin-Helmholtz waves at the magnetopause could both potentially allow magnetospheric mass loss. Evidence for the operation of both processes has been seen—for example, McAndrews et al. [2008]; Masters et al. [2009, 2010, 2012]; Wilson et al. [2012]; Delamere et al. [2013]; Fuselier et al. [2014]; Jasinski et al. [2016]. However, to date the contribution of neither process to the overall mass balance problem has been quantitatively assessed. While energetic W^+ ions are commonly seen in the dayside magnetosheath, there is no evidence for thermal W^+ there [Sergis et al. 2013] or in the upstream region [Thomsen et al. 2007].

Planetary wind. As mentioned above, plasma flows along the night side flanks of the magnetosphere tend to have an outward component, suggesting the likelihood that plasma is lost as a planetary wind down the flanks. An estimate of total mass loss from the tail (excluding plasmoids) [Thomsen et al. 2014a] is within the range of previous estimates of the total mass-loading rate from ionization of water gas from Enceladus.

Magnetosphere Dynamics

Radial transport – centrifugal interchange instability

Magnetospheric plasma motion transverse to the magnetic field, usually called magnetospheric convection, is key to dynamics in any magnetosphere. As discussed in the section entitled

Magnetosphere Composition, Sources, Transport and Losses, such motion in Saturn's magnetosphere is dominated throughout the equatorial region by (partial) co-rotation with the planet. This was widely expected before the Cassini encounter, and although the expectation was not universally held, the basic result was no big surprise.

The surprises are in the details. It is now clear that the dominant source of plasma for Saturn's entire equatorial magnetosphere is the inner icy satellites, in particular, the south-polar geyser plumes of Enceladus orbiting Saturn at L = 3.95, where L is the planet-centered distance normalized to Saturn's equatorial radius, $R_S \approx 60{,}300$ km—see the section entitled Magnetosphere Composition, Sources, Transport and Losses; and Young et al. [2005]. If tiny Enceladus is to dominate the source of Saturnian plasma, and hence its dynamics, there must be a mechanism for transporting this plasma radially from its inner-magnetospheric source to a sink in the outer magnetosphere and ultimately to the downstream solar wind. This transport mechanism is now known to be the centrifugal interchange instability.

A schematic illustration of this process, projected on the equatorial plane, is shown in Figure CAPS-31 [Hill et al. 2005].

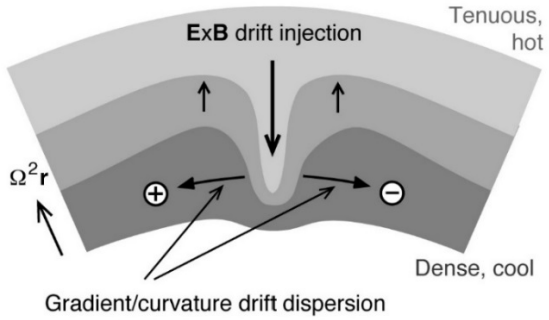

Figure CAPS-31. In the centrifugally driven interchange convection process, flux tubes containing hot but tenuous plasma (*light gray shading*) from an exterior source move inward, toward Saturn, and are replaced by outward moving flux tubes of cooler but denser plasma (*dark gray shading*) moving outward from an interior source.

The centrifugal acceleration Ω^2/r is outward and exceeds Saturn's inward gravitational acceleration beyond L ~2. Outward moving flux tubes release centrifugal potential energy from the system at a rate Ω^2/r per unit mass, and inward moving flux tubes add centrifugal potential energy to the system at the same rate per unit mass. Because of the inward density gradient of the combined plasma distribution (per unit magnetic flux), the combined flux-tube interchange process releases potential energy from the system and is therefore gravitationally unstable. The reverse would be true if the background density gradient (per unit magnetic flux) were reversed. In this sense the interchange motion is centrifugally driven. Flux-tube interchange motions, by definition, involve no net radial transport of magnetic flux.

Hot plasma injections

Figure CAPS-31 also illustrates the azimuthal gradient and curvature drifts of the hot tenuous plasma injected inward by the interchange process, relative to a co-rotating frame of reference. This drift is prograde (eastward) for positive ions and retrograde (westward) for negative ions and electrons. Its speed at a given distance is proportional to particle thermal energy. The injection process thus gives rise to an energy-longitude dispersion signature of the injected plasma, which has been called the smoking gun of interchange convection. This signature was repeatedly observed by CAPS on every Cassini pass through the inner magnetosphere, (L between ~5 and ~12), where the magnetic configuration is well described by an aligned dipole model [Burch et al. 2005; Hill et al. 2005; Young et al. 2005; Chen and Hill 2008; Chen et al. 2010; Rymer et al. 2008, 2009]. An early example of this injection-dispersion signature, appropriate to this off-equatorial orbit, is shown in Figure CAPS-32 from Hill et al. [2005]. In the inner magnetosphere the interchange convection scenario accounts for all key aspects of the morphology and composition results summarized in the section entitled Magnetosphere Composition, Sources, Transport and Losses.

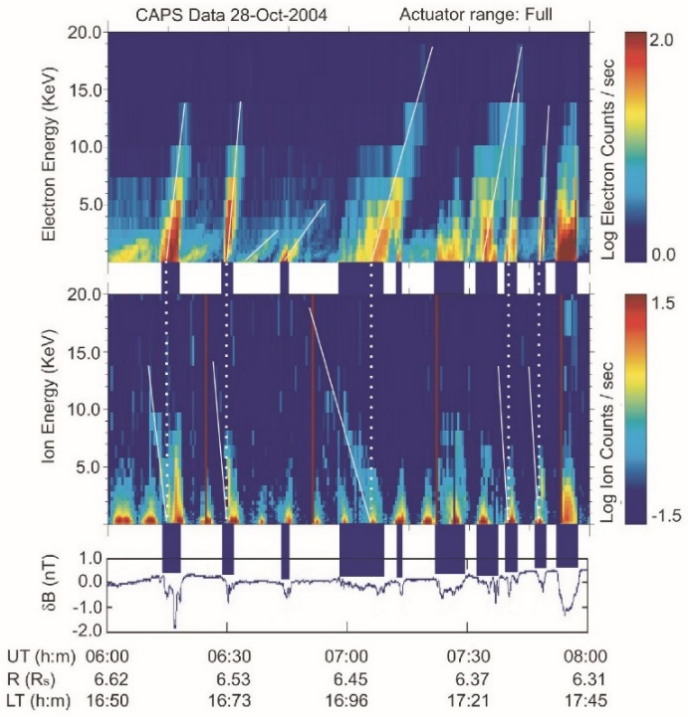

Figure CAPS-32. Energy-longitude dispersion signature of injected plasma. Linear energy-time spectrograms for electrons (*top panel*) and positive ions (*middle panel*) from the CAPS detectors during the second Cassini orbit of Saturn. The *bottom panel* shows simultaneous magnetic-field magnitude perturbations.

One unexpected feature of these observations is that Saturn's inflow channels (containing hot tenuous plasma) are always narrower in longitude than the neighboring outflow channels (containing cooler denser plasma), by a factor ~10 [Chen and Hill 2008; Chen et al. 2010]. All

previous theoretical models of interchange convection had inflow and outflow channels of equal width, because of assumptions made for analytical convenience. Recent numerical simulations using the more flexible Rice Convection Model (RCM), driven by CAPS observational inputs [Liu et al. 2010; Liu and Hill 2012; Hill 2016, 2017; Hill et al. 2018], have clarified the reason for this apparent discrepancy between observation and theory. At Saturn (unlike at Jupiter) the source region for newly injected plasma, both from new ionization and from charge-exchange reactions with ambient neutral molecules, is broadly distributed throughout the radial range in which the resultant interchange radial transport occurs (L between ~5 and ~12).

Co-rotation lag and plasma loading

There are useful and well-established relationships between the local rate of plasma mass or momentum loading (through new ionization, charge exchange, or outward mass transport), on one hand, and the radial variation of the rotational lag behind rigid co-rotation with the planet, on the other. Rates of ionization, charge exchange, and net outward mass transport are difficult if not impossible to measure directly. But the co-rotation lag is straightforward to measure directly if one has access to reliable in situ plasma measurements. If one side of the equation is measurable, it can provide proxy information about the other side of the equation that is not. This method of data analysis has been developed and employed successfully at Jupiter for several decades using Voyager, Galileo, and even Earth-based spectroscopic data, and has now been generalized and employed successfully by the CAPS team.

Tokar et al. [2006] reported surprisingly strong and asymmetric plasma flow perturbations during the distant and highly inclined July 2005 Cassini encounter with Enceladus. The flow measurements are depicted by arrows in Figure CAPS-33, projected onto the equatorial plane. The background flow contours are provided by an analytical model [Pontius and Hill 2006] that is based on earlier Jupiter-Io models, but generalized to account for, among other things, the fact that the Enceladus plasma source is centered, not at Enceladus, but at a position clearly southward of Enceladus, thus anticipating the more-or-less concurrent discovery of the south polar Enceladus plumes. This study also concluded that plasma mass is added to Saturn's magnetosphere at a rate > ~100 kg/s in the near vicinity of Enceladus, a conclusion that was controversial at the time but was subsequently verified by many independent analyses—for example, Chen et al. [2010].

Pontius and Hill [2009] applied a similar analysis, not to the localized plasma loading in the immediate vicinity of Enceladus, but to the much broader region ~3 < L < ~10 where significant co-rotation lag was reported by Wilson et al. [2008, 2009] from their analysis of CAPS data. This study utilized the modeled neutral gas distribution of Johnson et al. [2006b], also based on CAPS results. The red symbols in Figure CAPS-34 [Wilson et al. 2009, Figure 4] show the co-rotation lag as a fraction of the local rigid co-rotation speed. The data-model comparison of Pontius and Hill [2009] concludes that the plasma loading rate in this much larger volume is also > ~100 kg/s, comparable to that in the near vicinity of Enceladus.

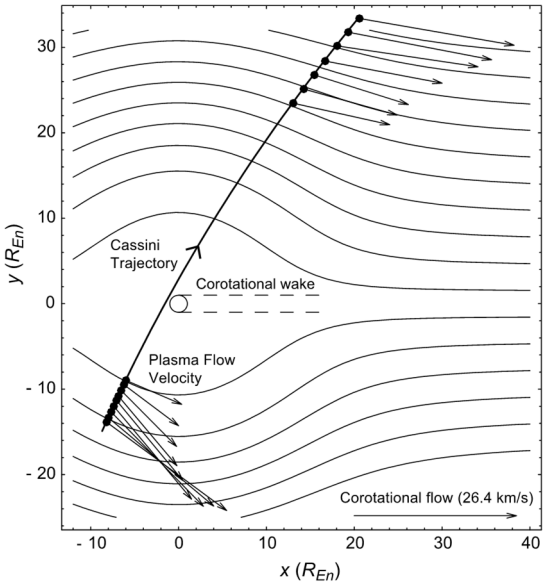

Figure CAPS-33. Strong and asymmetric plasma flow perturbation measurements. Observed plasma flow vectors (arrows), projected onto the equatorial plane, during the July 2005 Cassini encounter with Enceladus, at times (indicated by large dots) when the Cassini orientation was favorable for detection of such flows [Tokar et al. 2006]. The background flow contours are from the theoretical model of Pontius and Hill [2006] as described in the text.

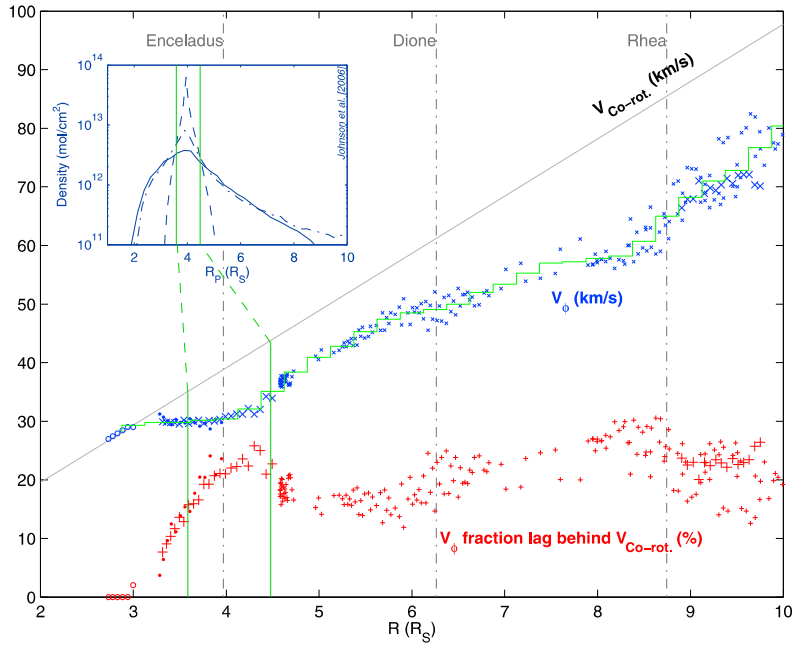

Figure CAPS-34. CAPS plasma flow measurements. Data for L > 5.5 are from forward modeling of thermalized ion velocity moments [Wilson et al. 2008]. Data for L < 5.5 are obtained from analysis of freshly picked-up charge-exchange products under the assumption of gyrotropy. Red symbols at the bottom show azimuthal speeds as a fraction of the local co-rotation speed. Figure from Wilson et al. [2009], Figure 4.

Magnetotail plasmoids and their consequences

Magnetic reconnection in the magnetotail current sheet can produce plasmoids, magnetic flux ropes (or closed magnetic loops) that are disconnected from the planet at one (or both) ends. These structures have been routinely observed in the magnetotails of Earth and Jupiter. Observations at Saturn were limited by orbital geometry because the deep magnetotail passes in 2006 occurred near Saturn's northern winter solstice, when the warped magnetotail current sheet was presumably displaced well northward of Cassini's orbital plane—see Figure CAPS-35. Despite this problem, three plasmoid-like magnetic signatures were identified in the Cassini magnetometer data [Jackman et al. 2007]. Two of these events crossed the current sheet, where ion fluxes were sufficient to permit composition and velocity-moment information to be extracted from CAPS data. These two events were analyzed in detail by Hill et al. [2008]. The most dramatic event occurred on March 4, 2006 at a planet-centered distance of 44 R_S and at 0300 local time (LT). Results are shown in Figure CAPS-36.

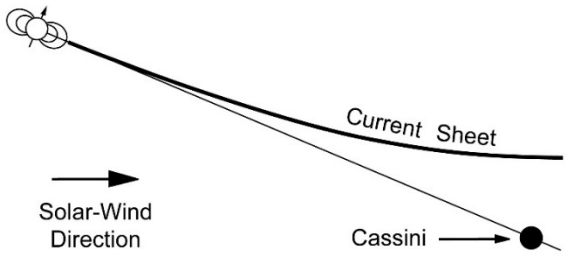

Figure CAPS-35. Orbital geometry during the deep-tail passes of Cassini. Figure from Hill et al. [2008], Figure 1.

Early in this event, before the sharp B_θ reversal near 2300 UT, water-group ions dominated plasma composition, indicating pinching off of a formerly closed flux tube containing plasma from the interior source, as in Vasyliunas-cycle reconnection. At about 23:10 UT the W^+ peak went off-scale above the energy-per-charge range of the CAPS IMS (50 keV), so W^+ velocity moments became unavailable though their flux remained high. The velocity moments (based on H^+ after 23:10) indicate sub-co-rotational azimuthal flow throughout the event and a dramatic tailward acceleration (with V_r increasing up to ~800 km/s) late in the event. Rigid co-rotation at this distance would be 430 km/s in the V_Φ direction.

A particularly interesting feature of this event is that Cassini was in a position to see not only the plasmoid properties observed in situ by CAPS and MAG, but also the plasmoid's earlier initiation closer to Saturn as observed by MIMI in energetic neutral atom (ENA) bursts. The viewing geometry is shown in Figure CAPS-37. The ENAs were hydrogen and oxygen atoms having speeds consistent with covering the distance from source to Cassini (~26.5 R_S) in the allotted time (~25 min). The plasmoid structure itself could also have covered the same distance in the same time interval [Hill et al. 2008].

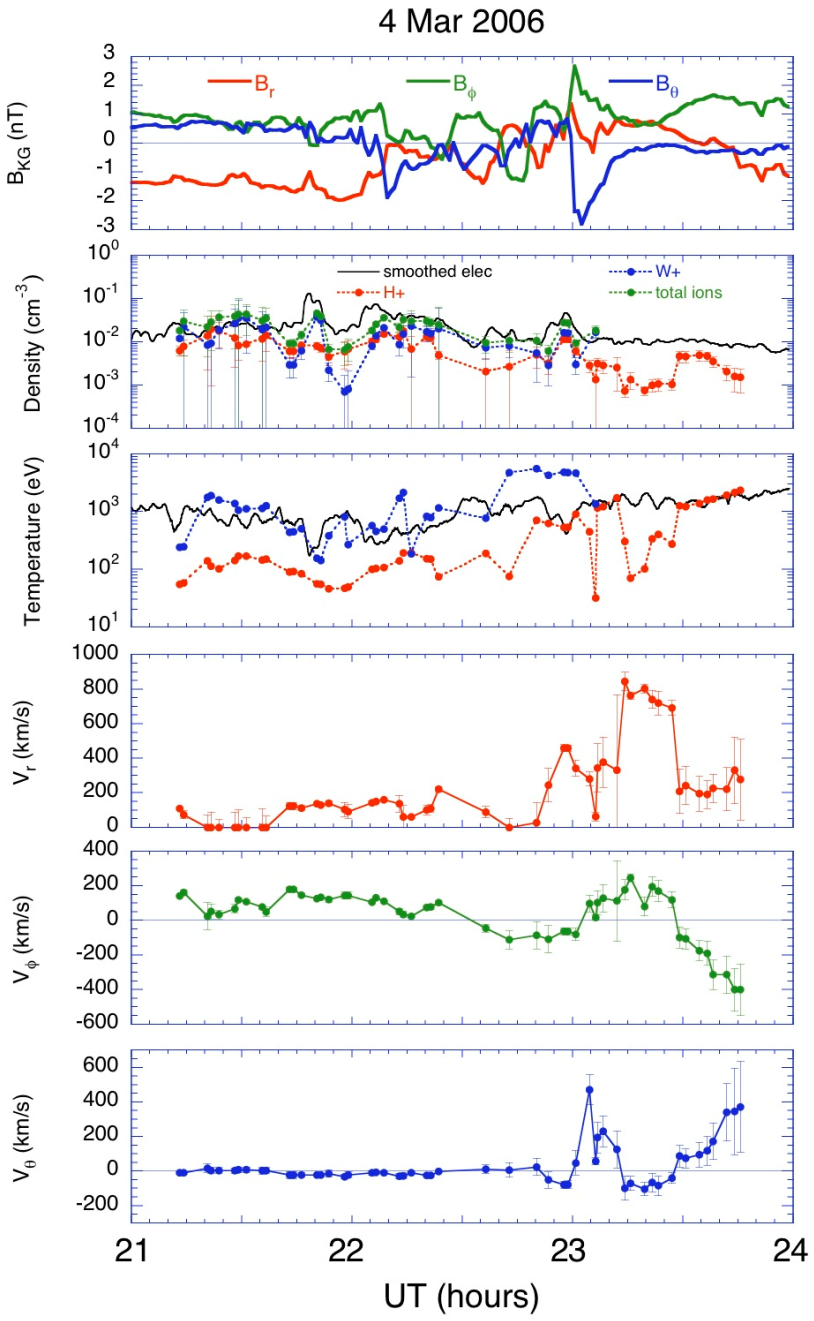

Figure CAPS-36. Magnetic field components and particle velocity moments for the plasmoid encountered by Cassini at 44 R_S near 0300 LT [Hill et al. 2008, Figure 3].

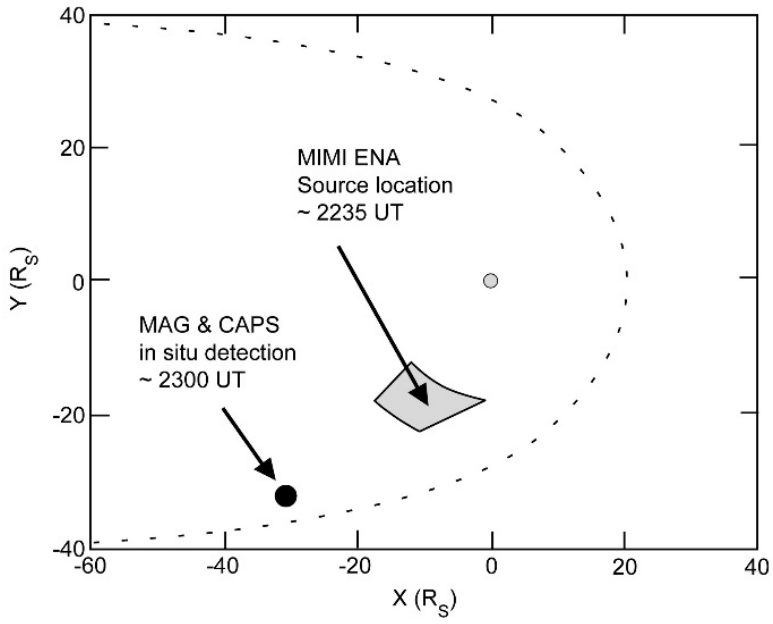

Figure CAPS-37. During the in situ CAPS and MAG plasmoid observations on March 4, 2006 (see Figure CAPS-36 above), Cassini was within the large dot indicated. The ENA bursts observed from the same location ~25 min earlier were deduced to have a source within the quasi-rectangular shaded box. The dashed contour is a cartoon depiction of the typical shape and location of Saturn's magnetopause.

Plasmoid formation provides an escape route for cool W^+ plasma that has accumulated from the interior source region. There remains some controversy as to whether this escape route is adequate to balance the interior source rate, estimated to be roughly 100 kg/s or more. It is plausible, but not yet demonstrated, that an unseen spectrum of smaller but more frequent plasmoids could contribute importantly to the escape rate.

Magnetotail reconnection also provides a fresh source of hot, tenuous plasma to the region planetward of the reconnection site, where it causes a dipolarization signature in the magnetic field. It can also provide seed particles both for the inflow channels of the interchange cells in the inner magnetosphere, as described earlier, and for the intermittent ENA bursts observed by MIMI from the middle and outer magnetosphere, and the associated SKR bursts observed by RPWS from the footprints of the same field lines.

Theoretically, there is a clear distinction between Vasyliunas-cycle reconnection involving the pinching off of formerly closed flux tubes containing cool dense plasma from the inner-magnetosphere source, and the more Earth-like Dungey-cycle reconnection involving the closure of formerly open flux tubes of the magnetotail lobes, containing hotter and more tenuous plasma of magnetosheath origin. The large plasmoid event described above (Figure CAPS-36) is readily explained by the Vasyliunas cycle alone. But two detailed multi-instrument event studies [Thomsen et al. 2015a, 2015b] have also found evidence of both Vasyliunas and Dungey cycles occurring either simultaneously or sequentially.

Thomsen et al. [2015a] examined a high-latitude dawn-side Cassini pass moving from the low-density lobe region into the higher-density closed field-line region. They inferred a stripping of plasma from the outer region of closed magnetic flux tubes as those tubes cross the night side magnetosphere from dusk to dawn, attributable to Vasyliunas-cycle reconnection, together with an interval (or region) of Dungey-cycle reconnection at the high-latitude boundary between open and closed field lines.

Thomsen et al. [2015b] also examined a deep-tail near-equatorial Cassini pass near 37 R_S near midnight LT. They found a prolonged period (~5 hr) of planet-ward plasma-sheet flow attributable to an even more prolonged period of magnetotail compression due to the passage of a recurrent solar-wind structure containing enhanced dynamic pressure. They concluded that Dungey-cycle reconnection takes precedence over Vasyliunas-cycle reconnection when the solar-wind pressure is high.

Bow Shock, Magnetosheath, and Outer Magnetosphere

The Cassini spacecraft crossed Saturn's bow shock for the first time at 09:45 UT on June 27, 2004, at a radial distance of 49.2 R_S from the planet. Clarke et al. [2010] investigated 35 orbits on which the spacecraft crossed Saturn's magnetopause and bow shock during 2004–2007 and concluded that the bow shock and magnetopause oscillate approximately in phase, within a phase uncertainty of about ±25°. The typical amplitude is 1–2 R_S and the period is organized by the phase of the interior magnetic field oscillations, with a period near that of planetary rotation. Saturn's (dayside) bow shocks are predominantly quasi-perpendicular by virtue of the shape of the Parker spiral at 10 AU. Sulaiman et al. [2016], analyzing data between 2004 and 2014, found that Saturn's bow shock, which is principally controlled by the upstream magnetic field strength, exhibits characteristics similar to both terrestrial and astrophysical regimes (Alfven Mach number of order 100). Went et al. [2011] used a semi-empirical model to show that the shock is axisymmetric about the solar wind flow direction.

The Cassini spacecraft crossed the bow shock of Saturn for the first time at 09:45 UT on June 27, 2004, at a radial distance of 49.2 R_S from Saturn.

How stable is the bow shock? Sulaiman et al. [2015] carried out a study of very high Mach number shocks in a parameter space that has been poorly explored previously. They identified re-formation of the shock at 10 AU using in situ magnetic field observations from the MAPS suite of instruments. They found evidence for cyclic re-formation of the shock (Figure CAPS-38) controlled by specular ion reflection occurring on a predicted time scale of ~0.3 τ_C, where τ_C is the ion gyro period. In addition, they showed that the magnetic structure of re-forming shocks at the same M_A, a re-forming shock exhibits stronger magnetic field amplification than a shock that is not re-forming.

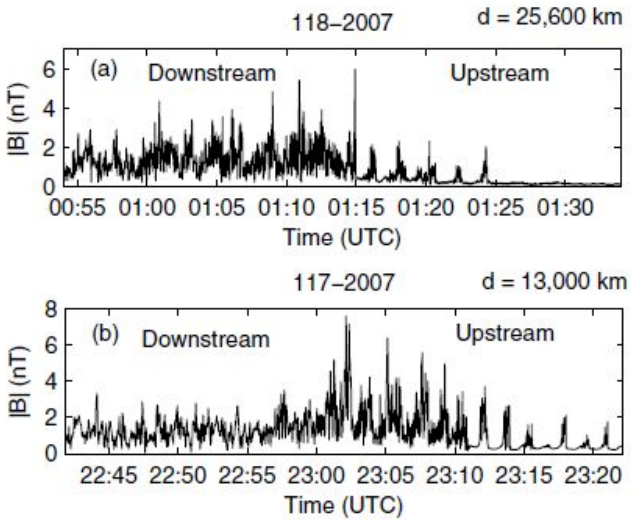

Figure CAPS-38. Magnetic field plots. The panels are two examples of magnetic field plots showing quasi-perpendicular bow shock crossings with re-formation cycles occurring upstream of the shock.

The long-term statistical behavior of the large-scale structure of Saturn's magnetosphere has been investigated by Achilleos et al. [2008]—see also the section entitled Magnetosphere Composition, Sources, Transport and Losses. Statistical techniques established for Jupiter have been applied to the kronian system, employing Cassini magnetometer data and a new empirical model of the shape of the magnetopause based on these data. The resulting distribution of the standoff distance R_{MP} for Saturn, covering a time interval of ~400 days, is well described by a bimodal model—the sum of two normal distributions with different means at ~22 and ~27 planetary radii. Achilleos et al. [2008] also produced a new mathematical model of magnetopause shape. It was noted that the shape of the magnetopause obstacle has an elliptical cross-section with a major (equatorial) axis ~25% larger than its minor (polar) axis. Saturn's bow shock can occasionally reach a high Mach number typical of astrophysical shocks. In this regime Cassini measurements have provided the first in situ evidence for suprathermal electron acceleration under quasi-parallel upstream magnetic conditions [Masters et al. 2016].

Using CAPS and other MAPS data, Sergis et al. [2013] investigated the properties of the magnetosheath. At energies of a few keV the magnetosheath is comprised of shocked solar wind plasma, while at energies above a few keV there is a strong presence of water group ions forming localized structures that are being convected downstream in the plasma flow. Under average magnetic field conditions in the magnetosheath, the kinetic properties of these hot water group ions can enable their escape upstream from the bow shock—see also the section entitled Magnetosphere Composition, Sources, Transport and Losses.

A new magnetosheath data set introduced by Thomsen et al. [2017] is based on a comprehensive survey of intervals in which the observed magnetosheath flow was encompassed within the CAPS plasma analyzers' fields-of-view, and for which the computed numerical moments are accurate. The data extend over eight years from 2004 day 299 to 2012 day 151 and comprise 19,155 measurements of 416 s each. In addition to the plasma ion moments (density, temperature,

and flow velocity), merged values of the plasma electron density and temperature, the energetic particle pressure, and the magnetic field vector are also included in the data set. The magnetosheath population is characterized by ion energies between ~100 eV and ~2 keV and electrons up to about 100 eV. The solar wind is best identified in the electrons, which have energies generally below 10 eV.

The proton-to-electron temperature ratio is very similar to typical values found in Earth's magnetosheath. Approximately 95% of the flows in Saturn's magnetosheath are found to be super-Alfvénic. The proton temperature tracks the predicted solar wind speed well. The clear correspondence between the magnetosheath proton temperature and the predicted solar wind speed suggests that temperature might provide a useful means of monitoring the upstream solar wind flow speed. Although the presence of the magnetosphere obstacle and its influence on the flow certainly affects the overall energy balance, one might nonetheless expect a rough equivalence between the upstream energy per particle and the downstream energy per particle. An analysis of the total magnetosheath energy (defined as magnetosheath bulk flow energy plus thermal energy plus magnetic energy per particle) using CAPS data, compared to the upstream bulk flow energy at several terrestrial bow shock crossings reported by Song et al. [1999], gives ratios ~0.4 to 0.6. This is similar to simulations of the total energy of plasma carried in Saturn's magnetosheath. On average, the solar wind bulk flow energy is ~1.860 ±0.797 times the combined magnetosheath bulk flow energy and proton temperature. Similarly, it is ~1.69 ±0.76 times the total magnetosheath energy.

The large set of magnetosheath electron temperature measurements made by ELS in this dataset, combined with the statistically-based estimates of the upstream flow speed based on IMS data, reveals how the magnetosheath temperature is related to the solar wind bulk flow energy, in a statistical sense. The median ratio of 3.8% is consistent with the findings of Masters et al. [2011a]. Accounting for other factors, the typical fraction of electron heating is probably closer to 4 than 3.5, which is significantly lower than the typical value for lower-Mach number shocks at Earth.

The rotation period of Saturn's magnetosphere was found to vary with time, and changing periodicities were identified in magnetic fields, radio emissions, and charged particles [Andrews et al. 2008, 2011, 2012; Provan et al. 2009, 2011, 2013, 2014]. The motion of the magnetodisk is very much affected by the oscillating magnetic field of Saturn, which is different in the two hemispheres. These planetary period oscillations strongly influence the magnetic and plasma properties of the outer magnetosphere [Andrews et al. 2010; Provan et al. 2012] as well as the density of thermal ions [Nemeth et al. 2011; Szego et al. 2011]. The thermal plasma sheet properties are different for the different ion species. The proton sheet is smoothly modulated by the flapping of the magnetodisk while heavy ions form a narrow sheet surrounding the magnetic equator—see also the section entitled Magnetosphere Composition, Sources, Transport and Losses. The periodicity of the observed heavy-ion rich events was found to be close to the SKR period of the southern hemisphere.

Szego et al. [2012] observed that the ion density moments derived by Thomsen et al. [2010] exhibit peaks around zero-crossings of the magnetic field. The proton peaks are broader while the

heavy ion peaks are sharper. They found that the positions of these peaks can be explained by the simple structural model of Arridge et al. [2011a]. Szego et al. [2013] modified this simple structural model to include the dual periodicity of the magnetic field and found an even better agreement for the positions of the ion peaks.

Using numerical ion moments, Nemeth et al. [2015] investigated the azimuthal flow velocities measured by CAPS along with their periodicities. They observed a significant positive correlation between the azimuthal plasma speed and the plasma density, while both are anti-correlated with the magnitude of the radial component of the magnetic field. They found that the dense plasma near the magnetic equator rotates around the planet at high speed, but the dilute plasma of higher latitudes is rotating significantly slower.

Nemeth et al. [2016] analyzed the quasi-periodic variation of several plasma parameters. The variation of the magnetic field was used to recover the position of the magnetodisk, and the position information was further used to model the variation of the density and azimuthal velocity moments of the thermal ions. This simple technique provides very good fits for all three parameters simultaneously.

Synergistic Science

Many plasma observations during the mission featured data collected simultaneously by most, if not all, of the particles and fields instruments (CAPS, INMS, MAG, MIMI, and RPWS), collectively referred to as MAPS. Prior to the Cassini mission it was understood from the experience of Voyager at Saturn and investigations of other magnetospheres, as well as space plasma physics in general, that many of Cassini's science objectives could only be met by synergistic measurements made by the MAPS instrument suite. Many details of synergistic science emerging from these measurements are discussed in the section entitled Detailed Magnetosphere Science Results and can easily be judged by the multitude of references cited in this volume. Below is a short list of the most important contributions made by CAPS to synergistic science.

- CAPS and INMS collaborations to elucidate the composition of neutral and charged particles at Titan and Enceladus. This is undoubtedly one of the most productive examples of synergistic science.
- CAPS, MAG and MIMI collaborations on the acceleration and transport of plasma throughout the magnetosphere.
- CAPS and MAG studies of periodic oscillations of the magnetodisk and plasma sheet, as well as investigations of the properties of shocks at Jupiter and Saturn.
- CAPS data inputs to the Rice Convection Model which was then used to simulate plasma convection throughout the magnetosphere.
- CAPS, RPWS, INMS, and CDA—Investigations of the makeup of charged ions, nano-grains and dust in the Enceladus plume.

Open Questions

Although CAPS operated for only the first eight years of the 13-year Cassini mission (2004 through 2012), as might be expected it left behind numerous open questions. Some of the most significant remaining questions concern the nature of the chemistry and formation of heavy negative ions in the atmosphere of Titan and the plumes of Enceladus. Other issues include the source, acceleration, transport and loss of cold, heavy water group ions, and finally, the role of the magnetodisk in controlling plasma sheet dynamics and generation of plasmoids.

Titan and Titan-magnetosphere interactions

Titan's atmosphere and its interaction with the magnetosphere are so complex that there remain many issues to address. Foremost among them are:

1. Search for methane ions in Saturn's outer magnetosphere which should be detectable if the high outward fluxes of methane estimated by Yelle et al. [2008] and Strobel [2008] are correct.

2. Continue IMS composition measurements of ionospheric outflows initiated by Sittler et al. [2010], and later by Woodson et al. [2015]. Look for evidence of minor species such as N^+, H_2O^+, NH_4^+ and more specific identifications of the mass 12–17 amu/q ions and mass 28–30 amu/q ions.

3. Perform more theoretical modeling of the ion composition of these outflows.

4. The Desai et al. [2017] analysis of negative ions measured by ELS showed that negative long carbon chains are forming in Titan's ionosphere, and that doubly-charged fullerenes could explain the main heavy negative ion peak at ~400 amu/q at lower altitudes. More work is required in this area including studies of the conversion of oxygenated fullerenes on Titan's surface, and on the bottom of its hydrocarbon lakes, into exobiological molecules such as amino acids by galactic cosmic rays.

5. Clearly studies of the kinetic interactions between Titan's upper atmosphere and upstream flow (light or heavy ion dominated) need to be continued, but such analysis will require the continued development of hybrid codes so the observed interaction details can be fully understood.

6. Detailed analysis of pickup ions and ionospheric outflows for Titan flybys at different heights still needs to be carried out, for example using ELS data as Coates et al. [2015] have done.

7. In order to characterize neutral energy distributions in the exosphere region, continued development of rarefied gas dynamics theory is needed in order to

understand the energy deposited by pickup ions and the population of hot recoil atoms and molecules that result.

8. Further calibration of the IMS prototype using molecular ions such as HCN^+, and NO^+ is needed in order to get C/N and N/O efficiency ratios. Calibration measurements of NH_4^+ would also be useful.

9. INMS data indicates that Titan's upper atmosphere is highly variable on timescales less than a Titan day [Cui et al. 2009]. However, the dynamics driving the variability are not well understood. Current ideas include gravity waves propagating from the lower atmosphere [Snowden and Yelle 2014], and/or magnetospheric energy inputs [Sillanpaa and Johnson 2015; Johnson et al. 2016; Jiang et al. 2017]. CAPS measurements of plasma energy spectra can provide constraints for numerical simulations of the effect that precipitation has on the thermal structure and escape of Titan's upper atmosphere. Understanding the physics of escape in Titan's current atmospheric environment will provide insight on how Titan and other bodies have evolved over their lifetimes.

Enceladus, rings, and the icy satellites

1. How are heavy negative ions formed in the plume at Enceladus, and what is their contribution to nano-grain formation?

2. How are ions such as O_2^+ which originate over and near the rings distributed throughout the magnetosphere?

3. What happens to the charged nano-grains? Do they contribute to a dusty plasma near Enceladus orbit, or are they eroded by local energetic plasmas?

4. What processes remove material from icy satellite surfaces to create their exospheres, and are they steady-state?

Magnetosphere structure and dynamics

The CAPS data set is exceedingly rich and has enabled great progress in identifying and understanding the structure and behavior of Saturn's magnetosphere. Further understanding will almost certainly be derived from the data in the future. Some of the findings described in this report have been clear and definitive; others need additional confirmation, either by inclusion of more data or by other means such as modeling. The interpretation of many of the findings need more rigorous examination or development. (Note: Some open questions identified in the sections entitled Magnetosphere Composition, Sources, Transport and Losses and Magnetosphere Dynamics dealing with magnetospheric structure and dynamics and seasonal variations of Saturn's magnetosphere appear in the book, Saturn in the 21st Century, Cambridge, 2019).

1. Are the growth of the Kelvin-Helmholtz instability and magnetic reconnection coupled?

2. What is the dominant mode of solar wind interaction with the magnetosphere, the viscous interaction or the large-scale reconnection interaction?

3. How is plasma transported outward, and magnetic flux returned, in the region between ~12 and ~20 to 25 R_S?

4. Where in the Saturnian system does Vasyliunas-type reconnection take place, and where does Dungey-type reconnection take place? Is there a region in Saturn's magnetosphere where one or the other dominates?

5. Where and how does the magnetosphere unload its cold, dense plasma?

6. How does the solar wind drive magnetospheric dynamics at Saturn? Is solar wind dynamic pressure the primary influence?

7. What causes the inner magnetospheric electric field that drives the noon-midnight asymmetry in plasma temperature, plasma density, energetic particle intensity, etc.?

8. What other solar cycle effects can be found in Saturn's magnetosphere?

9. How important is Titan as a source of magnetospheric H_2^+? What is the fraction of N^+ contributed by Titan?

10. What is the relationship between large-scale, tail-reconnection-driven injections and small-scale interchange injections?

11. What determines the scale size and inflow speed of interchange injections? What determines the apparently variable rate and depth of such injections?

12. What is the nature of the very low density layer often seen in lower energy electrons between the plasma sheet and the lobes? Is it related to ionospheric outflow reported by Felici et al. [2016]?

Cruise Science Results

CAPS took advantage of two gravity-assist flybys to gather data on the magnetospheres of Earth and Jupiter and, particularly at Earth, to perform calibration measurements and analysis. During those two flybys CAPS contributed measurements never made before—at Earth with a high-speed traverse that gave a freeze-frame picture of the magnetosphere in addition to real-time observations of the substorm cycle in progress [Khan et al. 2001]—and at Jupiter by establishing characteristics of its bow shock and magnetosheath.

Solar Wind and Heliosphere

During cruise, the CAPS investigation made its first major discovery with the in situ observation of interstellar pickup ions beyond the orbit of Jupiter …

On October 15, 1997, the Cassini-Huygens spacecraft was launched on an almost seven-year journey to Saturn. On its way, Cassini-Huygens performed gravity-assist maneuvers at Venus (on April 25, 1998 and June 24, 1999), Earth (August 17, 1999), and before arriving at Jupiter (technically) on December 29, 2000. The Jupiter flyby was followed by a ~3-month long exploration down the dusk flank of the magnetosphere. CAPS then operated at programmed intervals between 6.4 and 8.2 AU searching for interstellar pickup ions, before arriving at Saturn on July 1, 2004. During much of the cruise before Jupiter and for two years afterwards CAPS was in hibernation as were other MAPS instruments. The Cruise phase was partly devoted to commissioning the instrument, but also to making measurements in the solar wind that led to new science.

Interstellar pickup ions. During cruise, the CAPS investigation made its first major discovery with in situ observations of interstellar pickup ions beyond the orbit of Jupiter. [Gloeckler et al. [1998] had previously measured pickup ions inside Jupiter's orbit using the Solar Wind Ion Composition Spectrometer (SWICS) instrument onboard Ulysses. This was the first direct detection of mass-resolved interstellar pickup ions. It confirmed the existence of helium focusing at these distances caused by the solar gravitational field (Figure CAPS-39). CAPS also made the first direct, in situ, measurements of a large shadow in the interstellar atomic hydrogen population downstream from the Sun caused by its motion through the interstellar medium [McComas et al. 2004]. The shape of the distribution function of He^{+} as a function of energy was characteristic of a pickup distribution with a flat top and cut off at about four times of the solar wind energy.

Saturn's aurora. Geomagnetic storms and associated auroral activity at Earth are tied to the interaction of the disturbed solar wind with the magnetosphere. Saturn's magnetosphere is dominated by co-rotating plasma out to large distances from the planet, and it is unclear to what extent the solar wind plays a role in high latitude phenomena such as the aurora. Crary et al. [2005] combined Hubble Space Telescope (HST) images of Saturn's aurora taken over one month in 2004, with solar wind data from IBS taken while Cassini was ~3 × 10^7 km (~500 R_S) upstream from Saturn, to show that Saturn's aurora responds strongly to changes in solar wind conditions. Auroral power was best correlated with solar wind dynamic pressure (which is similar to that found at Earth) rather than the direction of the interplanetary field. This is a finding apparently unique to Saturn.

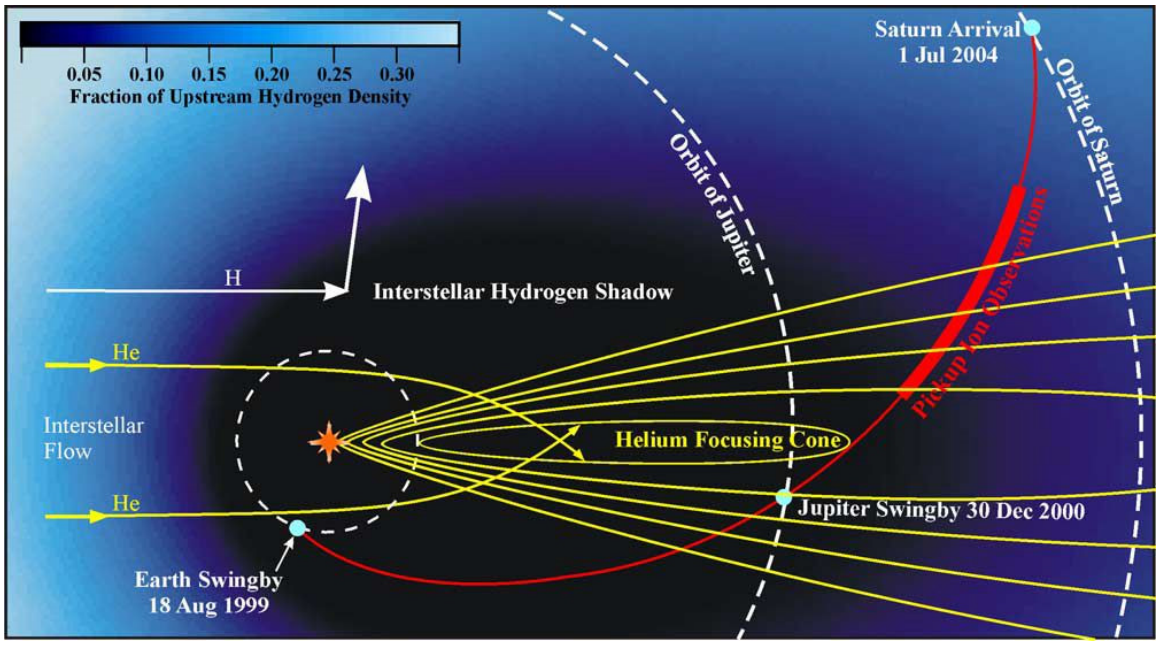

Figure CAPS-39. Schematic diagram of Cassini's trajectory between Earth swing-by and arrival at Saturn. Pickup ion measurements were made between 6.4 and 8.2 AU (heavy line) as Cassini emerged from the down-stream direction. Simulation results show: 1) the gravitational focusing of interstellar He in contours of 5/3, 2, 7/3, 8/3, and 3 times the upstream He density; and 2) the color-coded H density as a fraction of the interstellar value. The dark region downstream from the Sun represents the interstellar hydrogen shadow. Figure from McComas et al. [2004].

Venus

CAPS was not operating during the Venus encounters.

Earth

Earth's gravity-assist encounter on August 18, 1999, was the fastest traversal of Earth's magnetosphere to date. It was effectively a freeze-frame picture of the magnetosphere and an important chance to sample phenomena and boundaries that could later be compared with Saturn's. Inter-comparison of planetary magnetospheres, including that of Jupiter, was a critical, but usually overlooked, feature of the Cassini mission. Most of the following discussion is a condensed version of the definitive study by Rymer [2004] and Rymer [2001].

The spacecraft trajectory allowed CAPS, and particularly ELS, to make measurements of all large structures within the magnetosphere. Since Earth's magnetosphere is a well-known object, the flyby was also an excellent opportunity to calibrate CAPS sensors, particularly ELS, which is subject to spacecraft-plasma interactions that obscure part of its FOV. Figure CAPS-40 shows the Cassini trajectory through the magnetosphere.

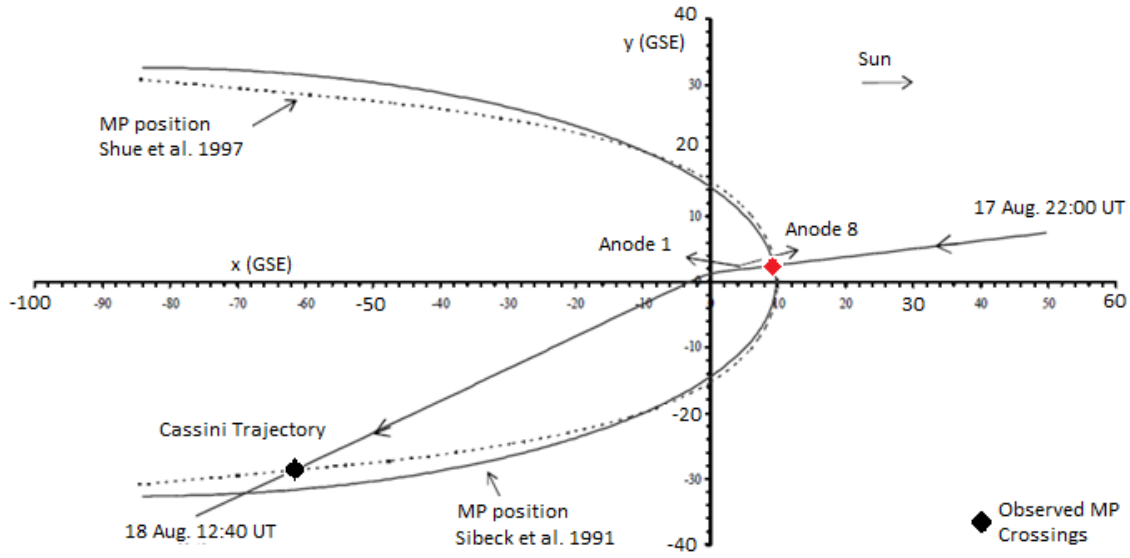

Figure CAPS-40. The Cassini trajectory through the magnetosphere in the x-y Geocentric Solar Ecliptic (GSE) co-ordinate plane showing a model for expected magnetopause shape and position based on Sibeck et al. [1991] and Shue et al. [1997] together with the positions of magnetopause crossings observed by ELS.

During the encounter ELS collected almost ten hours of solar wind data upstream of Earth, and almost nine hours inside the magnetosphere. During the pass ELS sampled electrons in the solar wind, bow shock, magnetosheath, magnetopause, radiation belts, an eclipse, the plasmasphere, plasma sheet, and lobes, and made several crossings of the tail magnetopause. Although this was a period of enhanced solar activity, results were mainly consistent with previous observations of various parts of the magnetosphere with a few exceptions. In addition, two substorms were taking place and there was evidence for low-energy field-aligned electron beams in the plasma sheet [Khan et al. 2001].

A spectacular energy-time spectrograph from ELS covering the entire pass and magnetosphere structures (Figure CAPS-41) can be used to briefly discuss magnetosphere features.

Data taken in the solar wind demonstrated ELS response to photoelectrons down to 0.5 eV, and solar wind electrons up to ~110 eV. Cassini then crossed the very sharp bow shock into the magnetosheath, jumping from solar wind conditions (energy ~10 eV) to the magnetosheath (~52 eV). The radial standoff distance of the bow shock was measured at 15.18 R_E while the magnetopause was at 9.88 R_E, a ratio of 1.55, in good agreement with theoretical predictions of 1.53 [Rymer 2004].

Inside the magnetosheath the core electron population was heated to between 20 eV and 110 eV. The photoelectron flux increased while the energy dropped, which is typical of spacecraft charge becoming more positive. The shift in spacecraft potential was typical of what would be seen

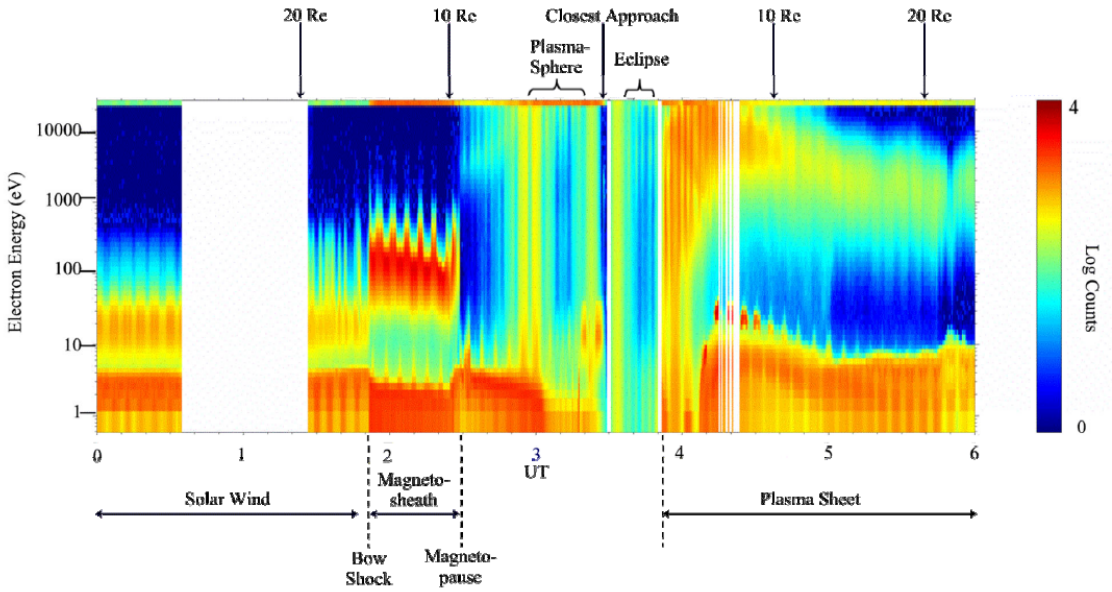

Figure CAPS-41. Six hour energy versus time spectrogram of ELS data from 0000–0600 UT August 18, 1999, for one central anode (out of eight). Counts per accumulation interval (23.4 ms) are indicated by the color scale. Modulation visible in the spectrogram is caused by actuator sweep cycles lasting four minutes.

later at Saturn. Thickness of the magnetopause boundary appears to be rather sharp (956 ±32 km) but its speed past the spacecraft position has an effect on the measurement and is unknown. The LLBL (an appendage of the magnetosheath electron population) is an important feature also seen at Saturn (see the section entitled Bow Shock, Magnetosheath, and Outer Magnetosphere). It carries a mix of both magnetosheath and magnetosphere plasmas and is an important loss process in both magnetospheres.

Once inside the magnetosphere at ~2:30 UT at a distance of 9.38 R_E, Cassini encountered the plasmapause, another feature also seen regularly at Saturn [Young et al. 2005]. The spectrum shows the plasma temperature dropping, which is characteristic of the response expected in the relatively cold plasma of the plasmasphere. Just prior to the encounter Cassini passed through the trapped radiation belts, confirming that shielding of ELS and the other CAPS sensors is effective.

Following the geometric encounter at 03:28 UT, Cassini entered an eclipse period, and then entered the plasma sheet just before local midnight. Electron energies within the plasmapause extended from ~100 eV (identified as accelerated photoelectrons), to above the ELS energy rage of 26 keV. The latter is identified as the plasma sheet distribution calculated to have a density of 0.2 cm^{-3} and a temperature of 2.4 keV about as expected and in agreement with values found with other measurements—for example, Lui et al. [1987].

Starting at 07:27 UT at 36.7 R_E Cassini crossed into and then out of (07:35 UT, 37.9 R_E) the magnetosphere lobe region [Abel et al. 2001]. Finally, at ~6000 R_E downstream from Earth and 12:00 to 22:00 UT, about where the extended magnetotail might be expected under the then current

solar wind conditions, data from several MAPS instruments suggested an encounter with the extended magnetotail. Unfortunately, the measurements were all at the extreme limits of detection and the issue was never resolved [Lagg et al. 2001].

Jupiter

Cassini carried out a gravity assist maneuver at Jupiter on December 30, 2000 at 10:05 UT. The closest approach brought Cassini to within about 9.7 million km of Jupiter's cloud tops. The science it made possible was an additional bonus, more so because Cassini had much superior instrumentation compared to that that of the previous two Voyagers, Ulysses and Galileo missions. The Galileo probe was still active during the flyby (Figure CAPS-42) and joint MAPS measurements provided a chance to study the dynamic effects of the solar wind perturbations on the global configuration of the Jovian magnetosphere [Joy et al. 2002]. The dual Cassini/Galileo spacecraft measurements by MAPS showed clearly that magnetospheric particles leak directly into the interplanetary medium from the closed magnetosphere and are the source for upstream particle events [Krupp 2002].

Cassini made at least five bow shock crossings, one at ~1929 LT and four more between 2100 and 2130 LT on DOY 21. During the flyby, shock activity was high and variable making a moving target for Cassini instruments. Cassini found that the shock is enormous, extending at least 700 R_J down the flank.

All three CAPS sensors were used to identify shock conditions and the times at which Cassini crossed into and out of it—see Szego et al. [2003] for a full description of shock studies based on all Cassini observations. By combining RPWS identification of Langmuir waves and IBS energy spectra, the upstream density could be measured at 0.5 to 1 cm^{-3} while at the same time ELS provided a measure of electron temperature at 2.6 eV. The data allowed the team to solve the Rankine-Hugoniot relations for transitions between the upstream and downstream conditions, deriving plasma density ratios of 2.74, and a downstream ion bulk energy of ~360 eV. The calculated downstream electron bulk temperature prediction was ~44 eV whereas ELS data gave ~11 eV and IMS ~24 eV, in decent agreement with the total energy jump predicted by theory.

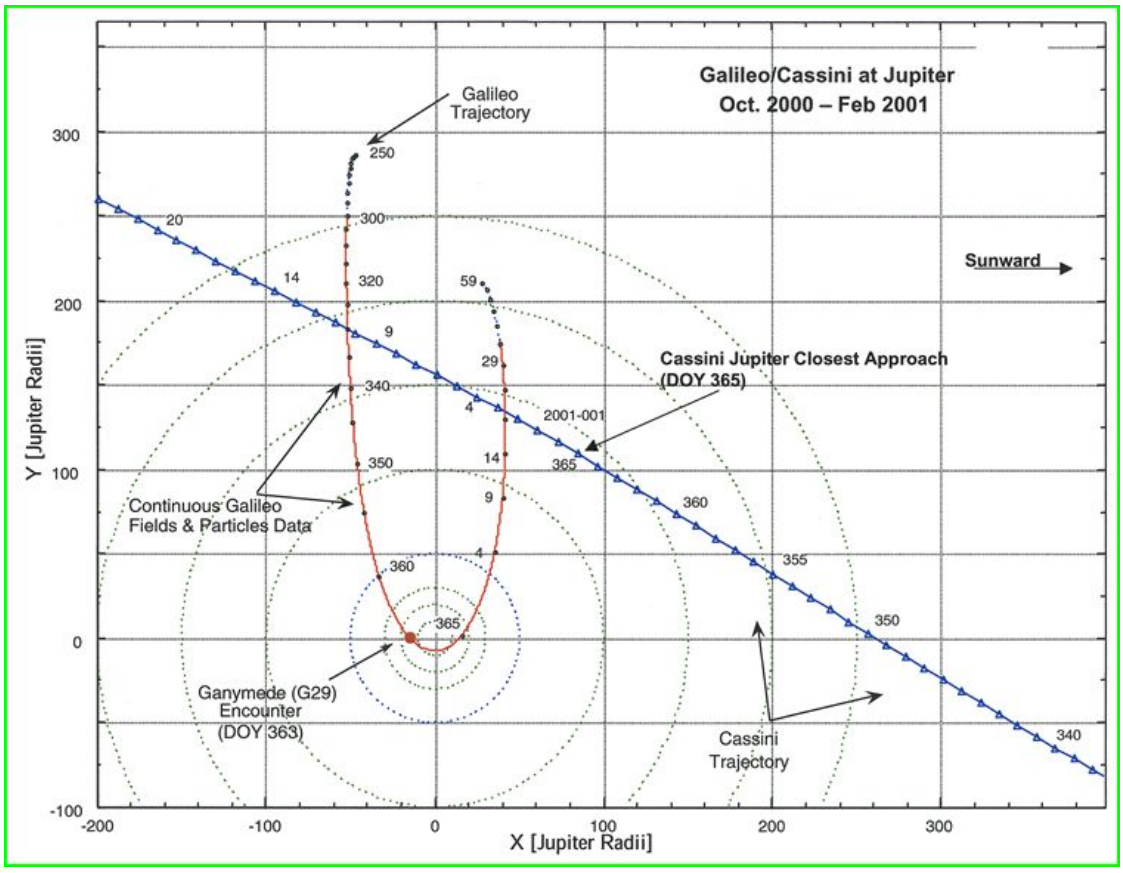

Figure CAPS-42. The orbits of Galileo and Cassini at Jupiter.

IBS energy-time spectrograms were used to easily identify shock crossings far down the flank of the magnetosphere. Figure CAPS-43 is one example of four that were observed at 576, 618, 744, and 770 R_J [Szego et al. 2003].

Using primarily IBS and ELS data in addition to MAG and RPWS, Bebesi et al. [2010] were able to investigate features of the downstream Jovian shock and magnetosheath out to ~700 R_J; a region not previously visited by any other spacecraft. As might be expected, the shock transition layer was broad and turbulent at that distance, but the transits were always easily observed using IBS data.

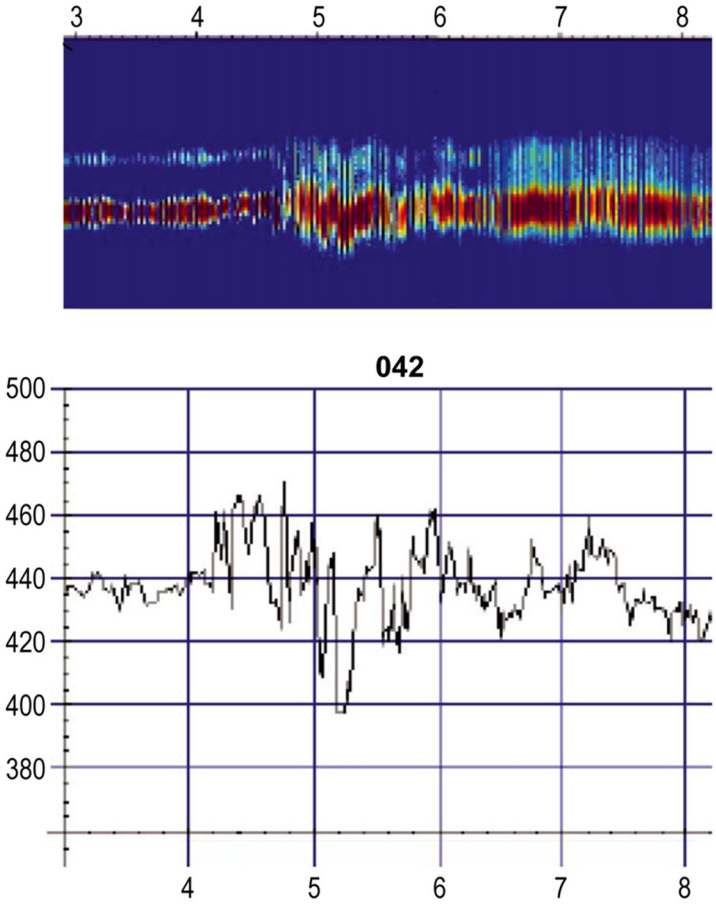

Figure CAPS-43. IBS data taken on DOY 042, 2000, 0300 to 0900 UT along the flanks of the Jovian magnetosphere. The velocity jump across the shock shows up as a jump in the velocity measured by IBS beginning at approximately 0420 UT. The most apparent feature is at ~4:40 UT when Cassini is inside the sheath and density and temperature both increase.

ACRONYMS

Note: For a complete list of Acronyms, refer to Cassini Acronyms – Attachment A.

ACT	actuator
amu	atomic mass unit
AO	Announcement of Opportunity
au	astronomical unit
C/A	closest approach
CAPS	Cassini Plasma Spectrometer
CSM	Cassini Solstice Mission
DPU	data processing unit
DSMC	Direct Simulation Monte Carlo
ELS	Electron Spectrometer
ENA	energetic neutral atom
ESA	electrostatic energy analyzer
eV	electron volt
FOV	field-of-view
GSE	Geocentric Solar Ecliptic
HST	Hubble Space Telescope
IBS	Ion Beam Spectrometer
IMS	Ion Mass Spectrometer
INMS	Ion and Neutral Mass Spectrometer
IR	Independent Review
keV	kiloelectron volt
kg	kilograms
km	kilometer
LEF	linear electric field
LLBL	low-latitude boundary layer
LP	Langmuir Probe
LT	local time
MAG	Magnetometer
MAPS	Magnetospheres and Plasma Science
MHD	magneto-hydrodynamic
MIMI	Magnetospheric Imaging Instrument
MLI	multi-layer insulation
NESC	NASA Engineering and Safety Center
NESC	National Electrical Safety Code
RCM	Rice Convection Model
RPWS	Radio and Plasma Wave Science
R_S	Saturn radii

s	seconds
SKR	Saturn Kilometric Radiation
SOI	Saturn Orbit Insertion
ST	straight through
SWICS	Solar Wind Ion Composition Spectrometer
TM	Traceability Matrix
TOF	time-of-flight
UT	universal time
UV	ultraviolet
UVIS	Ultraviolet Imaging Spectrograph

REFERENCES

Disclaimer: The partial list of references below correspond with in-text references indicated in this report. For all other Cassini references, refer to Attachment B – References & Bibliographies; Attachment C – Cassini Science Bibliographies; the sections entitled References contributed by individual Cassini instrument and discipline teams located in Volume 1 Sections 3.1 and 3.2 Science Results; and other resources outside of the Cassini Final Mission Report.

Abel, G. A., A. J. Coates, A. M. Rymer, D. R. Linder, M. F. Thomsen, D. T. Young, M. K. Dougherty, (2001), Cassini Plasma Spectrometer observations of bidirectional lobe electrons during the Earth flyby, August 18, 1999, Journal of Geophysical Research, 106(A12), 30199–30208, doi: 10.1029/2001JA900076.

Achilleos, N., C. S. Arridge, C. Bertucci, C. M. Jackman, M. K. Dougherty, K. K. Khurana, C. T. Russell, (2008), Large-scale dynamics of Saturn's magnetopause: Observations by Cassini, Journal of Geophysical Research, 113, A11209, doi: 10.1029/2008JA013265.

Ågren, K., N. J. T. Edberg, J.-E. Wahlund, (2012), Detection of negative ions in the deep ionosphere of Titan during the Cassini T70 flyby, Geophysical Research Letters, 39, L10201.

Ali, A., E. C. Sittler Jr., D. Chornay, B. R. Rowe, C. Puzzarini, (2013), Cyclopropenyl cation – the simplest Huckel's aromatic molecule – and its cyclic methyl derivatives in Titan's upper atmosphere, Planetary and Space Science, 109, 46.

André, N., A. M. Persoon, J. Goldstein, J. L. Burch, G. R. Lewis, A. M. Rymer, A. J. Coates, W. S. Kurth, E. C. Sittler Jr., M. F. Thomsen, M. K. Dougherty, D. A. Gurnett, D. T. Young, (2007), Magnetic signatures of plasma-depleted flux tubes in the Saturnian inner magnetosphere, Geophysical Research Letters, 2007GL030374R, doi: 10.1029/2007GL030374.

Andrews, D. J., S. W. H. Cowley, M. K. Dougherty, et al., (2012), Planetary period oscillations in Saturn's magnetosphere: Evolution of magnetic oscillation properties from southern summer to post-equinox, Journal of Geophysical Research, 117, p. A04224, doi: 10.1029/2011JA017444.

Andrews, D. J., B. Cecconi, S. W. H. Cowley, et al., (2011), Planetary period oscillations in Saturn's magnetosphere: Evidence in magnetic field phase data for rotational modulation of Saturn kilometric radiation emissions, Journal of Geophysical Research, 116, p. A09206, doi: 10.1029/2011JA016636.

Andrews, D. J., S. W. H. Cowley, M. K. Dougherty, G. Provan, (2010), Magnetic field oscillations near the planetary period in Saturn's equatorial magnetosphere: Variation of amplitude and phase with radial distance and local time, Journal of Geophysical Research, 115, A04212, doi: 10.1029/2009JA014729.

Andrews, D. J., E. J. Bunce, S. W. H. Cowley, et al., (2008), Planetary period oscillations in Saturn's magnetosphere: Phase relation of equatorial magnetic field oscillations and SKR modulation, Journal of Geophysical Research, 113, p. A09205, doi: 10.1029/2007JA012937.

Andriopoulou, M., E. Roussos, N. Krupp, C. Paranicas, M. Thomsen, S. Krimigis, M. K. Dougherty, K.-H. Glassmeier, (2014), Spatial and temporal dependence of the convective electric field in Saturn's inner magnetosphere, Icarus, 229, 57.

Andriopoulou, M., E. Roussos, N. Krupp, C. Paranicas, et al., (2012), A noon-to-midnight electric field and nightside dynamics in Saturn's inner magnetosphere, using microsignature observations, Icarus, 220, 503, doi: 10.1016/j.icarus.2012.05.010.

Arridge, C. S., J. M. Jasinski, N. Achilleos, Y. V. Bogdanova, et al., (2016), Cassini observations of Saturn's southern polar cusp, Journal of Geophysical Research, 121, 3006–3030, doi: 10.1002/2015JA021957.

Arridge, C. S., J. Eastwood, C. Jackman, G. K. Poh, J. Slavin, M. F. Thomsen, N. André, X. Jia, A. Kidder, L. Lamy, A. Radioti, N. Sergis, M. Volwerk, A. Walsh, P. Zarka, A. Coates, M. Dougherty, (2015), Cassini in situ observations of long duration magnetic reconnection in Saturn's magnetotail, Nature Physics, doi: 10.1038/nphys3565.

Arridge, C. S., N. Andrew, K. K. Khurana, C. T. Russell, S. W. H. Cowley, G. Provan, et al., (2011a), Periodic motion of Saturn's nightside plasma sheet, Journal of Geophysical Research, 116, 11205, doi: 10.1029/2011JA016827.

Arridge, C. S., N. André, H. J. McAndrews, E. J. Bunce, M. H. Burger, K. C. Hansen, H.-W. Hsu, R. E. Johnson, G. H. Jones, S. Kempf, K. K. Khurana, N. Krupp, W. S. Kurth, J. S. Leisner, C. Paranicas, E. Roussos, C. T. Russell, P. Schippers, E. C. Sittler, H. T. Smith, M. F. Thomsen, M. K . Dougherty, (2011b), Mapping magnetospheric equatorial regions at Saturn from Cassini prime mission observations, Space Science Review, 164, 1, doi: 10.1007/s11214-011-9850-4.

Arridge, C. S., C. T. Russell, K. K. Khurana, N. Achilleos, S. W. H. Cowley, M. K. Dougherty, E. J. Bunce, (2008), Saturn's magnetodisc current sheet, Journal of Geophysical Research, 113, A04214, doi: 10.1029/2007JA012540.

Arridge, C. S., C. T. Russell, K. K. Khurana, N. Achilleos, N. André, A. M. Rymer, M. K. Dougherty, A. J. Coates, (2007), Mass of Saturn's magnetodisc: Cassini observations, Geophysical Research Letters, vol 34, CiteID L09108, doi: 10.1029/2006GL028921.

Bebesi, Z., K. Szego, A. Balogh, G. Erdos, M. K. Dougherty, D. T. Young, (2010), Slow-mode shock candidates in the Jovian magnetosheath, Planetary and Space Science, 58, pp. 807–813.

Bell, J. M., J. H. Waite, B. A. Magee, K. E. Mandt, J. Westlake, (2009), Simulating the 3-D structure of Titan's upper atmosphere, American Geophysical Union (AGU), Spring Meeting 2009, abstract P11A-04.

Bouhram, M., R. E. Johnson, J.-J. Berthelier, J.-M. Illiano, R. L. Tokar, D. T. Young, F. J. Crary, (2006), A test-particle model of the atmosphere/ionosphere system of Saturn's main rings, Geophysical Research Letters, 33, L05106, doi: 10.1029/2005GL025011.

Brown, W.L., W. M. Augustyniak, E. Simmons, K. J. Marcantonio, L. J. Lanzerotti, R. E. Johnson, J. W. Boring, C. T. Reimann, G. Foti, V. Pirronello, (1982), Erosion and molecule formation in

condensed gas films by electronic energy loss of fast ions, Nuclear Instruments and Methods in Physics Research, vol. 198, issue 1 pp. 1–8, doi: 10.1016/0167-5087(82)90043-6.

Brünken, S., H. Gupta, C. A. Gottlieb, M. C. McCarthy, P. Thaddeus, (2007), Detection of the carbon chain negative ion C_8H^- in TMC-1, The Astrophysical Journal Letters, 664, L43−L46.

Burch, J. L., A. D. Dejong, J. Goldstein, D. T. Young, (2009), Periodicity in Saturn's magnetosphere: Plasma cam, Geophysical Research Letters, doi: 10.1029/2009GL039043.

Burch, J. L., J. Goldstein, P. Mokashi, W. S. Lewis, C. Paty, D. T. Young, A. J. Coates, M. K. Dougherty, N. André, (2008), On the cause of Saturn's plasma periodicity, Geophysical Research Letters, 35, L14105, doi: 10.1029/2008GL034951.

Burch, J. L., J. Goldstein, W. S. Lewis, D. T. Young, A. J. Coates, M. K. Dougherty, N. André, (2007), Tethys and Dione as sources of outward flowing plasma in Saturn's magnetosphere, Nature, Vol 447, doi: 10.1038/nature05906.

Burch, J. L., J. Goldstein, T. W. Hill, D. T. Young, F. J. Crary, A. J. Coates, N. André, W. S. Kurth, E. C. Sittler, (2005), Properties of local plasma injections in Saturn's magnetosphere, Geophysical Research Letters, 32, L14S02, doi: 10.1029/2005GL02261.

Carbary, J. F. and A. M. Rymer, (2014), Meridional maps of Saturn's thermal electrons, Journal of Geophysical Research, 119, 1721–1733, doi: 10.1002/2013JA019436.

Cassidy, T. A. and R. E. Johnson, (2010), Collisional spreading of Enceladus' neutral cloud, Icarus 209, 696–703.

Cassini Plasma Spectrometer (CAPS), (2019), Cassini Final Mission Report Voloume 1: Mission Overview, Science Objectives, and Science Results.

Cassini Plasma Spectrometer (CAPS), (2019), Cassini Final Mission Report Volume 3: Instrument Performance Assessment.

Cassini Plasma Spectrometer (CAPS), (2019), Cassini Final Mission Report Volume 5: Mission Operations System Performance Assessment.

Cassini Plasma Spectrometer (CAPS), (2019) Cassini Final Mission Report Volume 6: Lessons Learned.

Chen, Y., T. W. Hill, A. M. Rymer, R. J. Wilson, (2010), Rate of radial transport of plasma in Saturn's inner magnetosphere, Journal of Geophysical Research, 115, A10211, doi: 10.1029/2010JA015412.

Chen, Y. and T. W. Hill, (2008), Statistical analysis of injection/dispersion events in Saturn's inner magnetosphere, Journal of Geophysical Research, 113, A07215, doi: 10.1029/2008JA013166.

Clarke, K. E., D. J. Andrews, A. J. Coates, S. W. H. Cowley, A. Burch, (2010), Magnetospheric period oscillations of Saturn's bow shock, Journal of Geophysical Research, 115, A05202, doi: 10.1029/2009JA015164.

Coates, A. J., A. Wellbrock, J. H. Waite, G. H. Jones, (2015), A new upper limit to the field-aligned potential near Titan, Geophysical Research Letters, vol. 42, issue 12, pp. 4676–4684, doi: 10.1002/2015GL064474.

Coates, A. J., A. Wellbrock, G. R. Lewis, C. S. Arridge, F. J. Crary, D. T. Young, M. F. Thomsen, D. B. Reisenfeld, E. C. Sittler Jr., R. E. Johnson, K. Szego, Z. Bebesi, G. H. Jones, (2012), Cassini in Titan's tail: CAPS observations of plasma escape, Journal of Geophysical Research, vol. 117, issue A5, doi:10.1029/2012JA017595.

Coates, A. J., A. Wellbrock, G. R. Lewis, G. H.Jones, D. T. Young, F. J. Crary, J. H. Waite, R. E. Johnson, T. W. Hill, E. C. Sittler Jr., (2010a), Negative ions at Titan and Enceladus: recent results, Faraday Discussion, vol. 147(1), 293–305, doi: 10.1039/C004700G.

Coates, A.J., G. H. Jones, G. R. Lewis, A. Wellbrock, D. T. Young, F. J. Crary, R. E. Johnson, T. A. Cassidy, T. W. Hill, (2010b), Negative Ions in the Enceladus Plume, Icarus, 206, no. 2, pp. 618–622, doi: 10.1016/j.icarus.2009.07.013.

Coates, A. J., A. Wellbrock, G. R. Lewis, G. H. Jones, D. T. Young, F. J. Crary, J. H. Waite Jr., (2009), Heavy negative ions in Titan's ionosphere: altitude and latitude dependence, Planetary and Space Science, 57, Issues 14–15, 1866–1871, doi: 10.1016/j.pss.2009.05.009.

Coates, A.J ., F. J. Crary, G. R. Lewis, D. T. Young, J. H. Waite Jr., E. C. Sittler Jr., (2007a), Discovery of heavy negative ions in Titan's ionosphere, Geophysical Research Letters, 34, L22103, doi: 10.1029/2007GL030978.

Coates, A. J., F. J. Crary, D. T. Young, K. Szego, C. S. Arridge, Z. Bebesi, E. C. Sittler Jr., R. E. Hartle, T. W. Hill, (2007b), Ionospheric electrons in Titan's tail: plasma structure during the Cassini T9 encounter, Geophysical Research Letters, 34, L24S05, doi: 10.1029/2007GL030919.

Coates, A. J., H. J. McAndrews, A. M. Rymer, D. T. Young, F. J. Crary, S. Maurice, R. E. Johnson, R. A. Baragiola, R. L. Tokar, E. C. Sittler, G. R. Lewis, (2005), Plasma electrons above Saturn's main rings: CAPS observations, Geophysical Research Letters, 32, 14S09, doi: 10.1029/2005GL022694.

Cooper, J. F, E. C. Sittler, R. E. Johnson, P. Kollman, E. Roussos, Atmospheric, ionospheric, and energetic radiation environments of Saturn's rings, (2015), American Geophysical Union (AGU) Fall Meeting, abstract P51B-2064.

Coustenis, A., S. K. Atreya, T. Balint, R. H. Brown, et al., (2009), Titan and Enceladus Mission, Experimental Astronomy, vol. 23, issue, pp. 893–946, doi: 10.1007/s10686-008-9103-z.

Coustenis, A., A. Salama, E. Lellouch, T. Encrenaz, G. L. Bjoraker, R. E. Sameulson, T. de Graauw, H. Feuchtgruber, M. F. Kessler, (1998) Evidence for water vapor in Titan's atmosphere from ISO/SWS data, Astronomy & Astrophysics, 336, L85–L89.

Cowley, S. W. H., G. Provan, G. J. Hunt, C. M. Jackman, (2017), Planetary period modulations of Saturn's magnetotail current sheet: A simple illustrative mathematical model, Journal of Geophysical Research: Space Physics, 122, 258–279, doi:10.1002/2016JA023367.

Cowley, S. W. H., C. S. Arridge, E. J. Bunce, J. T. Clarke, A. J. Coates, M. K. Dougherty, J.-C. Gérard, D. Grodent, J. D. Nichols, D. L. Talboys, (2008), Auroral current systems in Saturn's magnetosphere: Comparison of theoretical models with Cassini and HST observations, Annales Geophysicae, 26, pp. 2613–2630.

Crary, F.J., B. A. Magee, K. Mandt, J. H. Waite Jr., J. Westlake, D. T. Young, (2009), Heavy ions, temperatures and winds in Titan's ionosphere: Combined Cassini CAPS and INMS observations, Planetary Space Science, 57, 1847–1856, doi: 10.1016/j.pss.2009.09.006.

Crary, F. J., J. T. Clarke, M. K. Dougherty, P. Hanlon, K. C. Hansen, J. T. Steinberg, B. L. Barraclough, A. J. Coates, J.-C. Gérard, D. Grodent, W. S. Kurth, D. G. Mitchell, A. M. Rymer, D. T. Young, (2005), Solar wind dynamic pressure and electric field as main factors controlling Saturn's aurorae, Nature, 433, 720–722.

Cravens, T. E., R. V. Yelle, J.-E. Wahlund, D. E. Shemansky, A. F. Nagy, (2009), Composition and structure of the ionosphere and thermosphere, In Titan from Cassini-Huygens, Chapter 11, (eds.) R. E. Brown, J.-P. Lebreton, J. H. Waite, Springer, Dordrecht, pp. 259–295, doi: 10.1007/978-1-4020-9215-2_11.

Cravens, T. E., I. P. Robertson, S. A. Ledvina, D. Mitchell, S. M. Krimigis, J. H. Waite Jr., et al., (2008), Energetic ion precipitation at Titan, Geophysical Research Letters, 35, no. 3, doi: 10.1029/2007GL032451.

Cravens, T. E., I. P. Robertson, J. H. Waite Jr., R. V. Yelle, W. T. Kasprzak, C. N. Keller, S. A. Ledvina, et al., (2006), The composition of Titan's ionosphere, Geophysical Research Letters, 33, L07105, doi: 10.1029/2005GL025575.

Cui, J., M. Galand, R. V. Yelle, V. Vuitton, J.-E. Wahlund, P. P. Lavvas, I. C. F. Muller-Wodarg, T. E. Cravens, W. T. Kasprzak, J. H. Waite Jr., (2009), Diurnal variations of Titan's ionosphere, Journal of Geophysical Research, vol. 114, issue A6, doi: 10.1029/2009JA014228.

Cui, J., R. V. Yelle, K. Volk, (2008), Distribution and escape of molecular hydrogen in Titan's thermosphere and exosphere,Journal of Geophysical Research: Planets 113, no. E10.

Cuzzi, J., R. Clark, G. Filacchione, R. French, R. Johnson, E. Marouf, L. Spilker, (2009), Ring particle composition and size distribution, Chapter 15, In Saturn from Cassini- Huygens (eds.) M. K. Dougherty, Springer, Dordrecht, pp. 459–509, doi: 10.1007/978-1-4020-9217-6_15.

de Kok, R., P. G. J. Irwin, N. A . Teanby, E. Lellouch, B. Bézard, S. Vinatier, C. A. Nixon, L. Fletcher, C. Howett, S. B. Calcutt, N. E. Bowles, F. M. Flasar, F. W. Taylor, (2007), Oxygen compounds in Titan's stratosphere as observed by Cassini CIRS, Icarus 186, 354–363.

De La Haye, V., J. H. Waite Jr., T. E. Cravens, A. F. Nagy, R. V. Yelle, R. E. Johnson, S. Lebonnois, I. P. Robertson, (2007a), Titan's corona: the contribution of exothermic chemistry, Icarus, 191, 236–250.

De La Haye, V., J. H. Waite Jr., R. E. Johnson, et al., (2007b), Cassini ion and neutral mass spectrometer data in Titan's upper atmosphere and exosphere: observations of a suprathermal corona, Journal of Geophysical Research, vol. 112, issue A7, doi: 10.1029/2006JA0122.

DeJong, A. D., J. L. Burch, J. Goldstein, A. J. Coates, F. Crary, (2011), Day-night asymmetries of low-energy electrons in Saturn's inner magnetosphere, Geophysical Research Letters, 38, L08106, doi:1 0.1029/2011GL047308.

DeJong, A. D., J. L. Burch, J. Goldstein, A. J. Coates, D. T. Young, (2010), Low-energy electrons in Saturn's inner magnetosphere and their role in interchange injections, Journal of Geophysical Research, vol. 115, issue A10, doi: 10.1029/2010JA015510.

Delamere, P. A., R. J. Wilson, S. Eriksson, F. Bagenal, (2013), Magnetic signatures of Kelvin-Helmholtz vortices on Saturn's magnetopause: Global survey, Journal of Geophysical Research: Space Physics, 118, 393–404, doi: 10.1029/2012JA018197.

Desai, R. T., S. A. Taylor, L. H. Regoli, A. J. Coates, T. A. Nordheim, M. A. Cordiner, B. D. Teolis, et al., (2018), Cassini CAPS identification of pickup ion compositions at Rhea, Geophysical Research Letters, vol. 45, issue 4, pp. 1704–1712, doi: 10.1002/2017GL076588.

Desai, R. T., A. J. Coates, A. Wellbrock, V. Vuitton, F. J. Crary, D. González-Caniulef, O. Shebanits, G. H. Jones, G. R. Lewis, J. H. Waite, M. Cordiner, S. A. Taylor, D. O. Kataria, J.-E. Wahlund, N. J. T. Edberg, E. C. Sittler, (2017), Carbon chain anions and the growth of complex organic molecules in Titan’s ionosphere, Astrophysical Journal Letters, 844, L18, doi: 10.3847/2041-8213/aa7851.

Dong, Y., T. W. Hill, S.-Y. Ye, (2015), Characteristics of ice grains in the Enceladus plume from Cassini observations, of Geophysical Research: Space Physics, vol. 120, issue 2, pp. 915–937, doi: 10.1002/2014JA020288.

Elrod, M. K., W.-L. Tseng, A. K. Woodson, R. E. Johnson, (2014), Seasonal and radial trends in Saturn's thermal plasma between the main rings and Enceladus, Icarus 242, 130–137.

Elrod, M. K., W.-L. Tseng, R. J. Wilson, R. E. Johnson, (2012), Seasonal variations Saturn's plasma between the main rings and Enceladus, Journal of Geophysical Research, vol. 117, issue A3, doi: 10.1029/2011JA017332.

Felici, M., C. S. Arridge, A. J. Coates, S. V. Badman, M. K. Dougherty, C. M. Jackman, W. S. Kurth, H. Melin, D. G. Mitchell, D. B. Reisenfeld, et al., (2016), Cassini observations of ionospheric plasma in Saturn's magnetotail lobes, Journal of Geophysical Research, 121, 338–357, doi: 10.1002/2015JA021648.

Fleshman, B. L., P. A. Delamere, F. Bagenal, T. Cassidy, (2013), A 1-D model of physical chemistry in Saturn's inner magnetosphere, Journal of Geophysical Research: Planets, 118, 1567–1581, doi: 10.1002/jgre.20106.

Fuselier, S. A., R. Frahm, W. S. Lewis, A. Masters, J. Mukherjee, S. M. Petrinec, I. J. Sillanpaa, (2014), The location of magnetic reconnection at Saturn's magnetopause: A comparison with Earth, Journal of Geophysical Research: Space Physics, 119, 2563–2578, doi: 10.1002/2013JA019684.

Galand, M., A. J. Coates, T. E. Cravens, J.-E. Wahlund, (2013), Titan's ionosphere, In Titan: Surface, atmosphere and magnetosphere, (eds.) I. Mueller-Wodarg, C. Griffith, E. Lellouch, T. Cravens, Cambridge Planetary Science Series, Cambridge University Press.

Garnier, P., M. K. G. Holmberg, J.-E. Wahlund, G. R. Lewis, S. Grimald, M. F. Thomsen, D. A. Gurnett, A. J. Coates, F. Crary, I. Dandouras, (2013), The influence of the secondary electrons induced by energetic electrons impacting the Cassini Langmuir probe at Saturn, Journal of Geophysical Research: Space Physics 118, no. 11, 7054–7073.

Gloeckler, G. and J. Geiss (1998), Interstellar and inner source pickup ions observed with SWICS on ULYSSES, Space Science Review 86, 127–159.

Goldstein, J., J. H. Waite, J. L. Burch, R. Livi, (2016), Evidence of m = 1 density mode (plasma cam) in Saturn's rotating magnetosphere, Journal of Geophysical Research: Space Physics, 121, 2335–2348, doi: 10.1002/2015JA022131.

Goldstein, J., T. W. Hill, J. H. Waite, J. L. Burch, (2014), Analytical model of rotating two-cell convection at Saturn, Journal of Geophysical Research, 119, doi: 10.1002/2013JA019615.

Gombosi, T. I., T. P. Armstrong, C. S. Arridge, K. K. Khurana, S. M. Krimigis, N. Krupp, A. M. Persoon, M. F. Thomsen, (2009), Saturn's magnetospheric configuration, In Saturn after Cassini-Huygens, (eds.) M. Dougherty, L. Esposito, S. M. Krimigis, Springer, Dordecht, pp. 203–255.

Hanel, R., B. Conrath, F. M. Flasar, V. Kunde, W. Maguire, J. C. Pearl, J. Pirraglia, R. Samuelson, L. Herath, M. Allison, et al., (1981), Infrared observations of the Saturnian system from Voyager 1, Science, 212, 192–200.

Hartle, R. E., M. Sarantos, E. C. Sittler Jr., (2011), Pickup ion distributions from three-dimensional neutral exospheres, Journal of Geophysical Research, vol. 116, issue A10, doi: 10.1029/2011JA016859.

Hartle, R. E., E. C. Sittler Jr., A. Lipatov, (2008), Ion Escape from the Ionosphere of Titan, European Geosciences Union Annual Meeting, Vienna Austria, 14–18 April 2008.

Hartle, R. E. and E. C. Sittler Jr., (2007), Pickup ion phase space distributions: Effects of atmospheric spatial gradients, Journal of Geophysical Research, vol. 112, issue A7, doi: 10.1029/2006JA012157.

Hartle, R. E., E. C. Sittler Jr., F. M. Neubauer, R. E. Johnson, H. T. Smith, F. Crary, D. J. McComas, D. T. Young, A. J. Coates, D. Simpson, S. Bolton, D. Reisenfeld, K. Szego, J. J. Berthelier, A. Rymer, J. Vilppola, J. T. Steinberg, N. Andre, (2006a), Preliminary interpretation of Titan plasma interaction as observed by the Cassini plasma spectrometer: Comparisons with Voyager 1, Geophysical Research Letters, 33, L08201, doi: 10.1029/2005GL024817.

Hartle, R. E., E. C. Sittler Jr., F. M. Neubauer, R. E. Johnson, H. T. Smith, F. Crary, D. J. McComas, D. T. Young, A. J. Coates, D. Simpson, S. Bolton, D. Reisenfeld, K. Szego, J. J. Berthelier, A. Rymer, J. Vilppola, J. T. Steinberg, N. Andre, (2006b), Initial interpretation of Titan plasma interaction as observed by the Cassini plasma spectrometer: Comparisons with Voyager 1, Planetary and Space Science, 54, 1211.

Hartle, R. E. and R. Killen, (2006), Measuring pickup ions to characterize the surfaces and exospheres of planetary bodies: applications to the moon, Geophysical Research Letters, 33(5), L05201.

Herbst, E. and Y. Osamura, (2008),Calculations on the formation rates and mechanisms for CnH anions in interstellar and circumstellar media, The Astrophysical Journal 679, no. 2, 1670.

Herbst, E., (1981), Can negative molecular ions be detected in dense interstellar clouds?, Nature 289, no. 5799, 656–657.

Hill, T. W., A. Jaggi, S. Sazykin, R. A. Wolf, (2018), Plasma circulation time scale of Saturn's magnetosphere, in preparation.

Hill, T. W., (2017), Magnetosphere-Ionosphere coupling at Jupiter and Saturn, In Magnetosphere-Ionosphere Coupling in the Solar System, Part VI: Chapter 24, (eds.) C. R. Chappell, R. W. Schunk, P. M. Banks, J. L. Burch, R. M. Thorne, pp. 307–318, doi: 10.1002/9781119066880.ch24.

Hill, T. W., (2016), Penetration of external plasma into a rotation-driven magnetosphere, Journal of Geophysical Research: Space Physics, 121, doi: 10.1002/ 2016JA023430.

Hill, T. W., M. F. Thomsen, R. L. Tokar, A. J. Coates, G. R. Lewis, D. T. Young, F. J. Crary, R. A. Baragiola, R. E. Johnson, Y. Dong, R. J. Wilson, G. H. Jones, J.-E. Wahlund, D. G. Mitchell, M. Hornyi, (2012), Charged nanograins in the Enceladus plume, Journal of Geophysical Research: Space Physics, 117, A05209, doi: 10.1029/2011JA017218.

Hill, T. W., M. F. Thomsen, M. G. Henderson, R. L. Tokar, A. J. Coates, H. J. McAndrews, G. R. Lewis, D. G. Mitchell, C. M. Jackman, C. T. Russell, M. K. Dougherty, F. J. Crary, D. T. Young, (2008), Plasmoids in Saturn's magnetotail, Journal of Geophysical Research, 113, A01214, doi: 10.1029/2007JA012626.

Hill, T. W., A. M. Rymer, J. L. Burch, F. J. Crary, D. T. Young, M. F. Thomsen, D. Delapp, N. André, A. J. Coates, G. R. Lewis, (2005), Evidence for rotationally-driven plasma transport in Saturn's magnetosphere, Geophysical Research Letters, 32, L14S10, doi: 10.1029/2005GL022620.

Hörst, S. M., V. Vuitton, R. V. Yelle, (2008), Origin of oxygen species in Titan's atmosphere, Journal of Geophysical Research, 113, E10006, doi: 10.1029/2008JE003135.

Jackman, C. M., M. F. Thomsen, D. G. Mitchell, N. Sergis, C. S. Arridge, M. Felici, S. V. Badman, C. Paranicas, X. Jia, G. B. Hospodarsky, M. Andriopoulou, K. K. Khurana, A. W. Smith, M. K. Dougherty, (2015), Field dipolarization in Saturn's magnetotail with planetward ion flows and energetic particle flow bursts: Evidence of quasi-steady reconnection, Journal of Geophysical Research, 120, doi: 10.1002/2015JA020995.

Jackman, C. M., J. A Slavin, M. G. Kivelson, D. J. Southwood, N. Achilleos, M. F. Thomsen, G. A. DiBraccio, J. P. Eastwood, M. P. Freeman, M. K. Dougherty, (2014), Saturn's dynamic magnetotail: A comprehensive magnetic field and plasma survey of plasmoids and traveling compression regions and their role in global magnetospheric dynamics, Journal of Geophysical Research, 119, 5465–5494, doi: 10.1002/ 2013JA019388.

Jackman, C. M., J. A. Slavin, S. W. H. Cowley, (2011), Cassini observations of plasmoid structure and dynamics: Implications for the role of magnetic reconnection in magnetospheric circulation at Saturn, Journal of Geophysical Research, 116, A10212, doi: 10.1029/2011JA016682.

Jackman, C. M., C. S. Arridge, H. J. McAndrews, M. G. Henderson, R. J. Wilson, (2009), Northward field excursions in Saturn's magnetotail and their relationship to magnetospheric periodicities, Geophysical Research Letters, 36, L16101, doi: 10.1029/2009GL039149.

Jackman, C. M., C. T. Russell, D. J. Southwood, C. S. Arridge, N. Achilleos, M. K. Dougherty, (2007), Strong rapid dipolarizations in Saturn's magnetotail: In situ evidence of reconnection, Geophysical Research Letters, 34, L11203, doi: 10.1029/2007GL029764.

Jasinski, J. M., C. S. Arridge, A. J. Coates, G. H. Jones, N. Sergis, M. F. Thomsen, N. Krupp, (2017), Diamagnetic depression observations at Saturn's magnetospheric cusp by the Cassini spacecraft, Journal of Geophysical Research, doi: 10.1002/2016JA023738.

Jasinski, J. M., C. S. Arridge, A. J. Coates, G. H. Jones, N. Sergis, M. F. Thomsen, D. B. Reisenfeld, N. Krupp, J. H. Waite Jr., (2016), Cassini plasma observations of Saturn's magnetospheric cusp, Journal of Geophysical Research: Space Physics, 121, 12,047–12,067, doi: 10.1002/2016JA023310.

Jasinski, J. M., C. S. Arridge, L. Lamy, J. S. Leisner, M. F. Thomsen, D. G. Mitchell, A. J. Coates, A. Radioti, G. H. Jones, E. Roussos, N.Krupp, D. Grodent, M. K. Dougherty, J. H. Waite, (2014), Cusp observation at Saturn's high latitude magnetosphere by the Cassini spacecraft, Geophysical Research Letters, 41, doi: 10.1002/2014GL0593.

Jia, X. and M. G. Kivelson, (2012), Driving Saturn's magnetospheric periodicities from the upper atmosphere/ionosphere: Magnetotail response to dual sources, Journal of Geophysical Research, 117, A11219, doi: 10.1029/2012JA018183.

Jiang, F., J. Cui, J. Xu, (2017), The structure of Titan's N_2 and CH_4 coronae, The Astronomical Journal, 154, 271.

Jinks, S. L., E. J. Bunce, S. W. H. Cowley, G. Provan, et al., (2014), Cassini multi-instrument assessment of Saturn's polar cap boundary, Journal of Geophysical Research: Space Physics, 119, 8161–8177, doi: 10.1002/2014JA020367.

Johnson, R. E., W.-L. Tseng, M. K. Elrod, A. M. Persoon, (2017), Nanograin density outside Saturn's A-ring, The Astrophysical Journal Letters 834, L6 (4 pp.) doi: 10.384/2041-8213/834/L6.

Johnson, R. E., O. J. Tucker, W. Waalkes, V. M. Tenishev, et al., (2016), Evolution of an early Titan atmosphere, Icarus, 271, 202–206, doi: 10.1016/j.icarus.2016.01.014.

Johnson, R. E., O. J. Tucker, M. Michael, E. C. Sittler, H. T. Smith, D. T. Young, J. H. Waite, (2009), Mass loss processes in Titan's upper atmosphere, In Titan from Cassini-Huygens, Chapter 15, (eds.) R. H. Brown, J. P. Lebreton, J. H. Waite, Springer, Dordrecht, pp. 373–391, doi: 10.1007/978-1-4020-9215-2_15.

Johnson, R. E., M. Fama, M. Liu, R. A. Baragiola, E. C. Sittler, H. T. Smith, (2008), Sputtering of ice grains and icy satellites in Saturn's inner magnetosphere, Planetary and Space Science, 56, pp. 1238–1243, doi: 10.1016/j.pss.2008.04.003.

Johnson, R. E., H. T. Smith, O. J. Tucker, M. Liu, M. H. Burger, E. C. Sittler, R. L. Tokar, (2006a), The Enceladus and OH tori at Saturn, The Astrophysical Journal Letters, 644, L137-L139, doi: 10.1086/505750.

Johnson, R. E., J. G.Luhmann, R. L. Tokar, M. Bouhram, J. J. Berthelier, E. C. Sittler, J. F. Cooper, T. W. Hill, H. T. Smith, M. Michael, M. Liu, F. J. Crary, D. T. Young, (2006b), Production, ionization and redistribution of O_2 Saturn's ring atmosphere, Icarus180, 393–402.

Johnson, R. E., M. Liu, E. C. Sittler Jr., (2005), Plasma-induced clearing and redistribution of material embedded in planetary magnetospheres, Geophysical Research Letters, 32, L24201, doi: 10.1029/2005GL024275.

Jones, G. H., C. S. Arridge, A. J. Coates, G. R. Lewis, S. Kanani, A. Wellbrock, D. T. Young, F. J. Crary, R. L. Tokar, R. J. Wilson, T. W. Hill, R. E. Johnson, D. G. Mitchell, J. Schmidt, S. Kempf, U. Beckmann, C. T. Russell, Y. D. Jia, M. K. Dougherty, J. H. Waite Jr., B. A. Magee, (2009), Fine jet structure of electrically charged grains in Enceladus' plume, Geophysical Research Letters, 36, L16204, doi: 10.1029/2009GL038284.

Jones, G. H., E. Roussos, N. Krupp, U. Beckmann, A. J. Coates, F. Crary, I. Dandouras, V. Dikarev, M. K. Dougherty, P. Garnier, C. J. Hansen, A. R. Hendrix, G. B. Hospodarsky, R. E. Johnson, S. Kempf, K. K. Khurana, S. M. Krimigis, H. Kröger, W. S. Kurth, A. Lagg, H. J. McAndrews, D. G. Mitchell, C. Paranicas, F. Postberg, C. T. Russell, J. Saur, M. Seiß, F. Spahn, R. Srama, D. F. Strobel, R. Tokar, J.-E. Wahlund, R. J. Wilson, J. Woch, D. Young, (2008), The dust halo of Saturn's largest icy moon, Rhea, Science, vol. 319, issue 5868, pp. 1380–1384, doi: 10.1126/science.1151524.

Joy, S. P., M. G. Kivelson, R. J. Walker, K. K. Khurana, C. T. Russell, T. Ogino, (2002), Probabilistic models of the Jovian magnetopause and bow shock locations, Journal of Geophysical Research, 107(A10), 1309, doi: 10.1029/2001JA009146.

Khan, H., S. W. H. Cowley, E. Kolesnikova, M. Lester, M. J. Brittnacher, T. J. Hughes, W. J. Hughes, et al., (2001), Observations of two complete substorm cycles during the Cassini Earth swing-by: Cassini magnetometer data in a global context, Journal of Geophysical Research, pp. 30141–30175.

Krasnopolsky, V. A., (2012), Titan's photochemical model: Further update, oxygen species, and comparison with Triton and Pluto, Planetary and Space Science, 73, 318–326.

Kroto, H. W., A. W. Allaf, S. P. Balm, (1991), C_{60}: Buckminsterfullerene, Chemical Reviews, 91, 6, pp. 1213–1235, doi: 10.1021/cr00006a005.

Kroto, H. W., J. R. Heath, S. C. O'Brien, R. F. Curl, R. E. Smalley, (1985), C_{60}: Buckminsterfullerene, Nature, 318, 162–163.

Krupp, N., P. Kollmann, M. F. Thomsen, D. G. Mitchell, X. Jia, A. Masters, P. Zarka, (2018), Global configuration an seasonal variations of Saturn's magnetosphere, In Saturn in the 21st Century, (eds.) K. H. Baines, F. M. Flasar, N. Krupp, and T. Stallard, Cambridge University Press, in press.

Krupp, N., J. Woch, A. Lagg, S. Livi, D. G. Mitchell, S. M. Krimigis, M. K. Dougherty, P. G. Hanlon, T. P. Armstrong, S. A. Espinosa, (2004), Energetic particle observations in the vicinity of Jupiter: Cassini MIMI/LEMMS results, Journal of Geophysical Research, vol. 109, issue A9, doi: 10.1029/2003JA010111.

Krupp, N., J. Woch, A. Lagg, S. A. Espinosa, et al., (2002), Leakage of energetic particles from Jupiter's dusk magnetosphere: dual spacecraft observations, Geophysical Research Letters, 29, doi: 10.1029/2001GL014290.

Lagg, A., N. Krupp, S. Livi, J. Woch, S. M. Krimigis, M. K. Dougherty, (2001), Energetic particle measurements during the Earth swing-by of the Cassini spacecraft in August 1999, Journal of Geophysical Research, 106(A12), 30209–30222, doi: 10.1029/2001JA900048.

Lavvas, P., R. V. Yelle, T. Koskinen, A. Bazin, V. Vuitton, E. Vigren, M. Galand, A. Wellbrock, A. J. Coates, J.-E. Wahlund, F. J. Crary, D. Snowden, (2013), Aerosol growth in Titan's ionosphere, PNAS early edition, February 4, 2013, 110, 2729–2734, doi: 10.1073/pnas.1217059110.

Lavvas, P. P., A. Coustenis, I. M. Vardavas, (2008), Coupling photochemistry with haze formation in titan's atmosphere, Part II: Results and validation with Cassini-Huygens data, Planetary and Space Science, 56(1), 67–99.

Liang, M.-C., Y. L. Yung, D. E. Shemansky, (2007), Photolytically generated aerosols in the mesosphere and thermosphere of Titan, The Astrophysical Journal Letters, 661, L199-L202, doi: 10.1086/518785.

Lipatov, A. S., E. C. Sittler Jr., R. E. Hartle, J. F. Cooper, D. G. Simpson, (2014), Titan's plasma environment: 3D hybrid kinetic modeling of the TA flyby and comparison with CAPS-ELS and RPWS LP observations, Planetary and Space Science, 93–94, 119–128.

Lipatov, A. S., E. C. Sittler, R. E. Hartle, J. F. Cooper, D. G. Simpson, (2012), Saturn's magnetosphere interaction with Titan for T9 encounter: 3D hybrid modeling and comparison with CAPS's observations, Planetary and Space Science, 61, 66–78.

Lipatov, E. C., E. C. Sittler Jr., R. E. Hartle, J. F. Cooper, D. G. Simpson, (2011), Background and pickup ion velocity distribution dynamics in Titan's plasma environment: 3D hybrid simulation and comparison with CAPS T9 observations, Advances in Space Research, 48, 1114–1125.

Liu, X. and T. W. Hill, (2012), Effects of finite plasma pressure on centrifugally driven convection in Saturn's inner magnetosphere, Journal of Geophysical Research, 117, A07216, doi: 10.1029/2012JA017827.

Liu, X., T. W. Hill, R. A. Wolf, S. Sazykin, R. W. Spiro, H. Wu, (2010), Numerical simulation of plasma transport in Saturn's inner magnetosphere using the Rice Convection Model, Journal of Geophysical Research, 115, A12254, doi: 10.1029/2010JA015859.

Livi, R. J., J. L. Burch, J. L. Burch, F. Crary, A. M. Rymer, D. G. Mitchell, A. M. Persoon, (2014), Multi-instrument analysis of plasma parameters in Saturn's equatorial, inner magnetosphere using corrections for spacecraft potential and penetrating background radiation, Journal of Geophysical Research: Space Physics, 119, 3683–3707, doi: 10.1002/2013JA019616.

Luhmann, J. G, R. E. Johnson, R. L. Tokar, T. Cravens, (2006), A model of the ionosphere of Saturn's rings and its implications, Icarus 181, 465–474.

Lui, A. T. Y, R. W. McEntire, S. M. Krimigis, (1987), Evolution of the ring current during two geomagnetic storms, Journal of Geophysical Research: Space Physics 92, no. A7, pp. 7459–7470, doi: 10.1029/JA092iA07p07459.

Lunine, J., M. Choukroun, D. Stevenson, G. Tobie, (2009), The origin and evolution of Titan, In Titan from Cassini-Huygens, Chapter 3, (eds.) R. H. Brown, J.-P. Lebreton, J. H. Waite, Springer, Dordrecht, pp. 35–60, doi: 10.1007/978-1-4020-9215-2_3.

Martens, H. R., D. B. Reisenfeld, J. D. Williams, R. E. Johnson, H. T. Smith, (2008), Observations of molecular oxygen ions in Saturn's inner magnetosphere, Geophysical Research Letters, 35, L20103, doi: 10.1028/2008GL035433, 2008.

Masters, A., A. H. Sulaiman, N. Sergis, L. Stawarz, M. Fujimoto, A. J. Coates, M. K. Dougherty, (2016), Suprathermal electrons at Saturn's bow shock, The Astrophysical Journal, vol. 826, np. 1, article 48, 7 pp., doi: 10.3847/0004-637X/826/1/48.

Masters, A., N. Achilleos, J. C. Cutler, A. J. Coates, M. K. Dougherty, G. H. Jones, (2012), Surface waves on Saturn's magnetopause, Planetary and Space Science, 65(1), doi: 10.1016/j.pss.2012.02.007.

Masters, A., D. G. Mitchell, A. J. Coates, M. K. Dougherty, (2011a), Saturn's low-latitude boundary layer: 1. Properties and variability, Journal of Geophysical Research, 116, A06210, doi: 10.1029/2010JA016421.

Masters, A., A. P. Walsh, A. N. Fazakerley, A. J. Coates, M. K. Dougherty, (2011b), Saturn's low-latitude boundary layer: 2. Electron structure, Journal of Geophysical Research, 116, A06211, doi: 10.1029/2010JA016422.

Masters, A., N. Achilleos, M. G. Kivelson, N. Sergis, M. K. Dougherty, M. F. Thomsen, C. S. Arridge, S. M. Krimigis, H. J. McAndrews, S. J. Kanani, N. Krupp, A. J. Coates, (2010), Cassini observations of a Kelvin-Helmholtz vortex in Saturn's outer magnetosphere, Journal of Geophysical Research, 115, A07225, doi: 10.1029/2010JA015351.

Masters, A., N. Achilleos, C. Bertucci, M. K. Dougherty, et al., (2009), Surface waves on Saturn's dawn flank magnetopause driven by the Kelvin–Helmholtz instability, Planetary Space Science, vol. 57, issues 14–15, pp. 1769–1778, doi: 10.1016/j.pss.2009.02.010.

McAndrews, H. J., M. F. Thomsen, C. S. Arridge, C. M. Jackman, et al. (2009), Plasma in Saturn's nightside magnetosphere and the implications for global circulation, Planetary and Space Science, vol. 57, issues 14–15, pp. 1714–1722, doi: 10.1016/j.pss.2009.03.003.

McAndrews, H. J., C. J. Owen, M. F. Thomsen, B. Lavraud, A. J. Coates, M. K. Dougherty, D. T. Young, (2008), Evidence for reconnection at Saturn's magnetopause, Journal of Geophysical Research, 113, A04210, doi: 10.1029/2007JA012581.

McCarthy, M. C., C. A. Gottlieb, H. Gupta, P. Thaddeus, (2006) Laboratory and astronomical identification of the negative molecular ion C_6H^-, The Astrophysical Journal Letters, 652, L141-L144.

McComas, D. J., N. A. Schwardron, F. J. Crary, H. A. Elliott, D. T. Young, J. T. Gosling, M. F. Thomsen, E. Sittler, J. J. Berthelier, K. Szegö, A. J. Coates, (2004), The interstellar hydrogen shadow: Observations of interstellar pickup ions beyond Jupiter, Journal of Geophysical Research: Space Physics, 109, A02104, doi: 10.1029/2003JA010217.

Meier, P., H. Kriegel, U. Motschmann, J. Schmidt, F. Spahn, T. W. Hill, Y. Dong, G. H. Jones, (2014), A model of the spatial and size distribution of Enceladus′ dust plume, Planetary and Space Science 104, 216–233.

Meier, P., U. Motschmann, J. Schmidt, F. Spahn, T. W. Hill, Y. Dong, G. H. Jones, H. Kriegel, (2015), Modeling the total dust production of Enceladus from stochastic charge equilibrium and simulations, Planetary and Space Science 119, 208–221.

Menietti, J. D., O. Santolik, A. M. Rymer, G. B. Hospodorsky, A. M. Persoon, D. A. Gurnett, A. J. Coates, D. T. Young, (2008), Analysis of plasma waves observed within local plasma injections seen in Saturn's magnetosphere, Journal of Geophysical Research, 113, A05213, doi: 10.1029/2007JA012856.

Michael, M., S. N. Tripathi, P. Arya, A. Coates, A. Wellbrock, D. T. Young, (2011), High-altitude charged particles in the atmosphere of Titan, Planetary and Space Science, 59, 880–885.

Millar, T. J., C. Walsh, T. A. Field, (2017), Negative ions in space, Chemical Reviews, 117, 1765−1795 doi: 10.1021/acs.chemrev.

Millar, T. J., C. Walsh, M. A. Cordiner, R. Ní Chuimín, E. Herbst, (2007) Hydrocarbon anions in interstellar clouds and circumstellar envelopes, The Astrophysical Journal Letters, vol. 662, issue 2, L87−L90.

NASA Engineering and Safety Center (NESC), (2014), Cassini Plasma Spepctrometer (CAPS) Short Circuit Anomaly Assessment, Technical Assessment Report NESC-RP-12-00803, August 15, 2014.

NASA Engineering and Safety Center (NESC), (2013), Cassini Plasma Spectrometer (CAPS) Short Circuit Anomaly Assessment, Technical Assessment Report NESC-2013, August 15, 2013.

Nemeth, Z., K. Szego, L. Foldy, S. W. H. Cowley, G. Provan, M. F. Thomsen, (2016), Periodic motion of the magnetodisk as a cause of quasi-periodic variations in the Kronian magnetosphere, Planetary and Space Science, 130, 54.

Nemeth, Z., K. Szego, L. Foldy, M. G. Kivelson, X. Jia, K. M. Ramer, S. W. H. Cowley, G. Provan, M. Thomsen, (2015), The latitudinal structure of the nightside outer magnetosphere of Saturn as revealed by velocity moments of thermal ions, Annales Geophysicae 33(9) pp. 1195–1202.

Nemeth, Z., K. Szego, Z. Bebesi, G. Erdos, L. Foldy, A. Rymer, E. C. Sittler, A. J. Coates, A. Wellbrock, (2011), Ion distributions of different Kronian plasma regions, Journal of Geophysical Research, vol. 116, issue A9, pp.8, doi: 10.1029/2011JA016585.

Paranicas, C., M. F. Thomsen, N. Achilleos, M. Andriopoulou, S. Badman, G. Hospodarsky, C. Jackman, X. Jia, T. Kennelly, K. Khurana, P. Kollmann, N. Krupp, P. Louarn, E. Roussos, N. Sergis, (2016), Effects of radial motion on interchange injections at Saturn, Icarus, 264, 342, doi: 10.1016/j.icarus.2015.10.002.

Pietzak, B., M. Waiblinger, T. A. Murphy, A. Weidinger, et al., (1997) Buckminsterfullerene C_{60}: a chemical Faraday cage for atomic nitrogen, Chemical Physics Letters, 21, 259–263.

Pontius Jr., D. H. and T. W. Hill, (2009), Plasma mass loading from the extended neutral gas torus of Enceladus as inferred from the observed plasma corotation lag, Geophysical Research Letters, 36, L23103, doi: 10.1029/2009GL041030.

Pontius Jr., D. H. and T. W. Hill, (2006) Enceladus: A significant plasma source for Saturn's magnetosphere, Journal of Geophysical Research, 111, A09214, doi: 10.1029/2006JA011674.

Provan, G., L. Lamy, S. W. H. Cowley, et al., (2014) Planetary period oscillations in Saturn's magnetosphere: Comparison of magnetic oscillations and SKR modulations in the post-equinox interval Journal of Geophysical Research, 119, pp. 7380–7401, doi: 10.1002/2014JA020011.

Provan, G., S. W. H. Cowley, J. Sandhu, et al., (2013) Planetary period magnetic field oscillations in Saturn's magnetosphere: Post-equinox abrupt non-monotonic transitions to northern system dominance Journal of Geophysical Research, 118, pp. 3243–3264, doi: 10.1002/jgra.50186.

Provan, G., Andrews D. J., Arridge C. S., et al., (2012), Dual periodicities in planetary period magnetic field oscillations in Saturn's tail, Journal of Geophysical Research, vol. 117, issue A1, doi: 10.1029/2011JA017104.

Provan, G., D. J. Andrews, B. Cecconi, et al., (2011), Magnetospheric period magnetic field oscillations at Saturn: Equatorial phase 'jitter' produced by superposition of southern- and northern-period oscillations Journal of Geophysical Research, vol. 116, issue A4, doi: 10.1029/2010JA016213.

Provan, G., D. J. Andrews, C. S. Arridge, et al., (2009), Polarization and phase of planetary period oscillations on high latitude field lines in Saturn's magnetosphere Journal of Geophysical Research, vol. 114, issue A2, doi: 10.1029/2008JA013782.

Pryor, W. R., A. M. Rymer, D. G. Mitchell, T. W. Hill, D. T. Young, J. Saur, G. H. Jones, S. Jacobsen, S. W. Cowley, B. H. Mauk, A. J. Coates, (2011), The auroral footprint of Enceladus on Saturn, Nature, 472, pp. 331–333.

Remijan, A. J., J. M. Hollis, F. J. Lovas, M. A. Cordiner, T. J. Millar, A. J. Markwick-Kemper, P. R. Jewell, (2007), Detection of C_8H^- and comparison with C_8H toward IRC+10 216, The Astrophysical Journal Letters, vol. 664, issue 1, L47-L50.

Rymer, A. M., D. G. Mitchell, T. W. Hill, E. A. Kronberg, N. Krupp, C. M. Jackman, (2013), Saturn's magnetospheric refresh rate, Geophysical Research Letters, 40, doi: 10.1002/grl.50530.

Rymer, A. M., (2010), Electron-Ion Thermal Equilibration At Saturn: Electron Signatures Of Ion Pick-Up?, In AIP Conference Proceedings, vol. 1302, no. 1, pp. 250–255.

Rymer, A. M., H. T. Smith, A. Wellbrock, A. J. Coates, D. T. Young, (2009a), Discrete classification and electron energy spectra of Titan’s varied magnetospheric environment, Geophysical Research Letters, 36, L15109, doi: 10.1029/2009GL039427.

Rymer, A. M., B. H. Mauk, T. W. Hill, N. André, D. G. Mitchell, C. Paranicas, D. T. Young, H. T. Smith, A. M. Persoon, J. D. Menietti, G. B. Hospodarsky, A. J. Coates, M. K. Dougherty, (2009b), Cassini evidence for rapid interchange transport at Saturn, Planetary and Space Science, doi: 10.1016/j.pss.2009.04.010.

Rymer, A. M., B. H. Mauk, T. W. Hill, C. Paranicas, D. G. Mitchell, A. J. Coates, D. T. Young, (2008), Electron circulation in Saturn's magnetosphere, Journal of Geophysical Research, 113, A01201, doi: 10.1029/2007JA012589.

Rymer, A. M., B. H. Mauk, T. W. Hill, C. Paranicas, N. André, E. C. Sittler Jr., D. G. Mitchell, H. T. Smith, R. E. Johnson, A. J. Coates, D. T. Young, S. J. Bolton, M. F. Thomsen, M. K. Dougherty, (2007), Electron sources in Saturn's magnetosphere, Journal of Geophysical Research, 112, A02201, doi: 10.1029/2006JA012017.

Rymer A. M., F. Crary, D. J. McComas, D. T. Young, D. Reisenfeld, M. Dougherty, N. André, (2005), Preliminary results on Saturn's inner plasmasphere as observed by Cassini: Comparison with Voyager, Geophysical Research Letters, 32, L14S07, doi: 10.1029/2005GL022653.

Rymer, A. M., (2004), Analysis of Cassini plasma and magnetic field mea- surements from 1–7 AU, Ph.D. thesis, University College London, London, United Kingdom.

Rymer, A. M., A. J. Coates, G. A. Abel, D. R. Linder, K. Svenes, B. Narheim, M. Thomsen, D. T. Young, (2001), Cassini CAPS electron spectrometer measurements during the Earth swingby on 18 August 1999, Journal of Geophysical Research, 106, pp. 30177–30198.

Sakai, N., T. Sakai, S. Yamamoto, (2008), Tentative detection of C_4H^- toward the low-mass protostar IRAS 04368+2557 in L1527, The Astrophysical Journal Letters, vol. 673, issue 1, L71–L74.

Sakai, N., T. Sakai, S. Yamamoto, (2007), Detection of C_6H^- toward the low-mass protostar IRAS 04368+2557 in L1527, The Astrophysical Journal Letters, 667, L65–L68.

Schaible, M. J., R. E. Johnson, L. V. Zhigilei, S. Piqueux, (2017), High energy electron sintering of icy regoliths: formation of the PacMan anomalies on the icy Saturnian moons, Icarus 285, pp. 211–123.

Schippers, P, Schenk, P., D. P. Hamilton, R. E. Johnson, W. B. McKinnon, C. Paranicas, J. Schmidt, M. R., N. André, M. Blanc, I. Dandouras, A. J. Coates, S. M. Krimigis, D. T. Young,

(2009), Identification of photoelectron energy peaks in Saturn's inner neutral torus, Journal of Geophysical Research 114, A12212, doi: 10.1029/2009JA014368.

Schippers, P., M. Blanc, N. André, I. Dandouras, G. R. Lewis, L. K. Gilbert, A. M. Persoon, N. Krupp, D. A. Gurnett, A. J. Coates, S. M. Krimigis, D. T. Young, M. K. Dougherty, (2008), Multi-instrument analysis of electron populations in Saturn's magnetosphere, Journal of Geophysical Research, 113, A07208, doi: 10.1029/2008JA013098.

Sergis, N., C. M. Jackman, M. F. Thomsen, S. M. Krimigis, D. G. Mitchell, D. C. Hamilton, M. K. Dougherty, N. Krupp, R. J. Wilson, (2017), Radial and local time structure of the Saturnian ring current revealed by Cassini, Journal of Geophysical Research, 122, 1803.

Sergis, N., C. M. Jackman, A. Masters, S. M. Krimigis, M. F. Thomsen, D. C. Hamilton, D. G. Mitchell, M. K. Dougherty, A. J. Coates, (2013), Particle and magnetic field properties of the Saturnian magnetosheath: Presence and upstream escape of hot magnetospheric plasma, Journal of Geophysical Research: Space Physics, 118, 1620–1634, doi: 10.1002/jgra.50164.

Sergis, N., S. M. Krimigis, E. C. Roelof, C. S. Arridge, A. M. Rymer, D. G. Mitchell, D. C. Hamilton, N. Krupp, M. F. Thomsen, M. K. Dougherty, A. J. Coates, D. Y. Young, (2010), Particle pressure, inertial force, and ring current density profiles in the magnetosphere of Saturn, based on Cassini measurements, Geophysical Research Letters, 37, L02102, doi: 10.1029/2009GL041920.

Shebanits, O., J.-E. Wahlund, N. J. T. Edberg, F. J. Crary, A. Wellbrock, D. J. Andrews, E. Vigren, R. T. Desai, A. J. Coates, K. E. Mandt, J. H. Waite Jr., (2016), Ion & aerosol precursor densities in Titan's ionosphere: a multi-instrument case study, Journal of Geophysical Research, 121, 10,075–10,090, doi: 10.1002.2016JA022980.

Shue, J. H., J. K. Chao, H. C. Fu, C. T. Russell, P. Song, K. K. Khurana, H. J. Singer, (1997), A new functional form to study the solar wind control of the magnetopause size and shape, Journal of Geophysical Research, 102, 9497–9511.

Sibeck, D. G., R. E. Lopez, E. C. Roelof, (1991), Solar wind control of the magnetopause shape, location, and motion, Journal of Geophysical Research, 96(A4), 5489–5495, doi: 10.1029/90JA02464.

Sillanpää, I. J. and Johnson, R. E., (2015), The role of ion-neutral collisions in Titan's magnetospheric interaction, PSS 108, 73–88.

Sillanpää, I., E. Kallio, P. Janhunen, W. Schmidt, K. Mursula, J. Vilppola, P. Tanskanen, (2006), Hybrid simulation study of ion escape at Titan for different orbital positions, Advances in Space Research, 38, 799–805, doi: 10.1016/j.asr.2006.01.005.

Sittler Jr., E. C., R. E. Hartle, R. E. Johnson, J. F. Cooper, A. S. Lipatov, C. Bertucci, A. J. Coates, K. Szego, M. Shappirio, D. G. Simpson, J.-E. Wahlund, (2010), Saturn's magnetospheric interaction with Titan as defined by Cassini encounters T9 and T18: New results, Planetary and Space Science 58, 327–350.

Sittler Jr., E. C., A. Ali, J. F. Cooper, R. E. Hartle, R. E. Johnson, A. J. Coates, D. T. Young, (2009a), Heavy ion formation in Titan's ionosphere: Magnetospheric introduction of free

oxygen and a source of Titan's aerosols?, Planetary and Space Science, 57, 1547–1557, doi: 10.1016/j.pss.2009.07.017.

Sittler Jr., E. C., R. E. Hartle, C. Bertucci, A. Coates, T. Cravens, I. Dandouras, D. Shemansky, (2009b), Energy deposition processes in Titan's upper atmosphere and its induced magnetosphere, In Titan from Cassini-Huygens, Chaper 16, (eds.) R.H. Brown, J. P. Lebreton, J. H. Waite, Springer, Dordrecht, pp, 393-453, doi: 10.1007/978-1-4020-9215-2_16.

Sittler Jr., E. C., N. Andre, M. Blanc, M. Burger, R. E. Johnson, A. Coates, A. Rymer, et al. (2008), Ion and neutral sources and sinks within Saturn's inner magnetosphere: Cassini results, Planetary and Space Science, 56, 3, doi: 10.1016/j.pss.2007.06.006.

Sittler Jr., E. C., M. Thomsen, R. E. Johnson, R. E. Hartle, M. Burger, D. Chornay, M. D. Shappirio, D. Simpson, H. T. Smith, A. J. Coates, A. M. Rymer, D. J. McComas, D. T. Young, D. Reisenfeld, M. Dougherty, N. André, (2006a), Cassini observations of Saturn's inner plasmasphere: Saturn orbit insertion results, Planetary and Space Science, 54, 1197–1210, doi: 10.1016/j.pss.2006.05.038.

Sittler Jr., E. C., R. E. Johnson, H. T. Smith, J. D. Richardson, S. Jurac, M. Moore, J. F. Cooper, B. H. Mauk, M. Michael, C. Paranicas, T. P. Armstrong, B. Tsurutani, (2006), Energetic nitrogen ions within the inner magnetosphere of Saturn, Journal of Geophysical Research 111, A09223, doi: 10.1029/2004JA010509.

Sittler Jr., E. C., M. Thomsen, D. Chornay, M. D. Shappirio, D. Simpson, R. E. Johnson, H. T. Smith, A. J. Coates, A. M. Rymer, F. Crary, D. J. McComas, D. T. Young, D. Reisenfeld, M. Dougherty, N. André, (2005), Preliminary results on Saturn's inner plasmasphere as observed by Cassini: Comparison with Voyager, Geophysical Research Letters, 32, L14S07, doi: 10.1029/2005GL022653.

Smith, A. W., C. M. Jackman, M. F. Thomsen, L. Lamy, N. Sergis, (2018), Multi-instrument investigation of the location of Saturn's magnetotail X-line, Journal of Geophysical Research: Space Physics 123, no. 7, 5494–5505.

Smith, A. W., C. M. Jackman, M. F. Thomsen, (2016), Magnetic reconnection in Saturn's magnetotail: A comprehensive magnetic field survey, Journal of Geophysical Research, 121, 2984, doi: 10.1002/2015JA022005.

Smith, H. T. and A. M. Rymer, (2014), An empirical model for the plasma environment along Titan's orbit based on Cassini plasma observations, Journal of Geophysical Research: Space Physics, 119, 5674–5684, doi: 10.1002/2014JA019872.

Smith, H. T., R. E. Johnson, M. E. Perry, D. G. Mitchell, R. L. McNutt, D. T. Young, (2010), Enceladus plume variability and the neutral gas densities in Saturn's magnetosphere, Journal of Geophysical Research, 115, A10252, doi: 10.1029/2009JA015184.

Smith, H. T., M. Shappirio, R. E. Johnson, D. Reisenfeld, E. C. Sittler, F. J. Crary, D. J. McComas, D. T. Young, (2008), Enceladus: a potential source of ammonia products and molecular nitrogen for Saturn's magnetosphere, Journal of Geophysical Research 113, A11206, doi: 10.1029/2008JA013352.

Smith, H. T., R. E. Johnson, E. C. Sittler, M. Shappirio, D. Reisenfeld, O. J. Tucker, M. Burger, F. J. Crary, D. J. McComas, D. T. Young, (2007), Enceladus: The likely dominant nitrogen source in Saturn's magnetosphere, Icarus, 188, 356–366, doi: 10.1016/j.icarus.2006.12.007.

Smith, H. T., M. Shappirio, E. C. Sittler, D. Reisenfeld, R. E. Johnson, R. A. Baragiola, F. J. Crary, D. J. McComas, D. T. Young, (2005), Discovery of nitrogen in Saturn's inner magnetosphere, Geophysical Research Letters 32, L14S03, doi: 10.1029/2005GL022654.

Snowden, D. and R. V. Yelle, (2014), The thermal structure of Titan's upper atmosphere, II: Energetics Icarus, 228, pp. 64–77.

Snowden, D., R. V. Yelle, J. Cui, et al., (2013), The thermal structure of Titan's upper atmosphere, I: Temperature profiles from Cassini INMS observations, Icarus, 226, pp. 522–582.

Song, P., C. T. Russell, X. X. Zhang, S. S. Stahara, J. R. Spreiter, T. I. Gombosi, (1999), On the processes in the terrestrial magnetosheath 2. Case study. Journal of Geophysical Research, 104, 22357, doi: 10.1029/1999JA900246.

Strobel, D. F., (2008), Titan’s hydrodynamically escaping atmosphere, Icarus, 193, 588–594.

Sulaiman, A. H., A. Masters, M. K. Dougherty, (2016), Characterization of Saturn’s bow shock: Magnetic field observations of quasi-perpendicular shocks, Journal of Geophysical Research: Space Physics, 121, 4425–4434, doi: 10.1002/2016JA022449.

Sulaiman, A., H., A. Masters, M. K. Dougherty, D. Burgess, M. Fujimoto, G. B. Hospodarsky, (2015), Quasiperpendicular high mach number shocks, Physical Review Letters, 115, 125001, doi: 10.1103/PhysRevLett.115.125001.

Szegö, K., Z. Nemeth, L. Foldy, S. W. H. Cowley, G. Provan, (2013), Dual periodicities in the flapping of Saturn's magnetodisk, Journal of Geophysical Research 118:(6) pp. 2883–2887.

Szegö, K., Z. Nemeth, G. Erdos, L. Foldy, Z. Bebesi, M. Thomsen, D. Delapp, (2012), Location of the magnetodisk in the nightside outer magnetosphere of Saturn near equinox based on ion densities, Journal of Geophysical Research, 117, A09225, doi: 10.1029/2012JA017817.

Szegö, K., Z. Nemeth, G. Erdos, L. Földy, M. Thomsen, D. Delapp, (2011), The plasma environment of Titan: The magnetodisk of Saturn near the encounters as derived from ion densities measured by the Cassini/CAPS plasma spectrometer, Journal of Geophysical Research: Space Physics, 116, A10219, doi: 10.1029/2011JA016629.

Szegö, K., D. T. Young, B. Barraclough, J.-J. Berthelier, et al., (2003) Cassini plasma spectrometer measurements of Jovian bow shock structure, Journal of Geophysical Research, 108, 1287, doi: 10.1029/2002JA009517.

Teolis, B. D., G. H. Jones, P. F. Miles, R. L. Tokar, B. A. Magee, J. H. Waite, E. Roussos, D. T. Young, et al., (2010), Cassini finds an oxygen–carbon dioxide atmosphere at Saturn’s icy moon Rhea, Science, vol. 330, issue 6012, pp. 1813–1815, doi: 10.1126/science.1198366.

Thaddeus, P., C. A. Gottlieb, H. Gupta, S. Brünken, M. C. McCarthy, M. Agundez, M. Guélin, J. Cernicharo, (2008), Laboratory´ and astronomical detection of the negative molecular ion C_3N^-, The Astrophysical Journal, 677, pp. 1132−1139.

Thomsen, M. F., S. V. Badman, C. M. Jackman, X. Jia, M. G. Kivelson, W. S. Kurth, (2017), Energy-banded ions in Saturn's magnetosphere, Journal of Geophysical Research, 122, doi: 10.1002/2017JA024147.

Thomsen, M. F., A. J. Coates, E. Roussos, R. J. Wilson, K. C. Hansen, G. R. Lewis, (2016a), Suprathermal electron penetration into the inner magnetosphere of Saturn, Journal of Geophysical Research, 121, 5436, doi: 10.1002/2016JA022692.

Thomsen, M. F., C. M. Jackman, S. W. H. Cowley, X. Jia, M. G. Kivelson, G. Provan, (2016b), Evidence for periodic variations in the thickness of Saturn's nightside plasma sheet, Journal of Geophysical Research, 121, doi: 10.1002/2016JA023368.

Thomsen, M. F., D. G. Mitchell, X. Jia, C. M. Jackman, G. Hospodarsky, A. J. Coates, (2015a), Plasmapause formation at Saturn, Journal of Geophysical Research, 120, 2571, doi: 10.1002/2015JA021008.

Thomsen, M. F., C. M. Jackman, D. G. Mitchell, G. Hospodarsky, W. S. Kurth, K. C. Hansen, (2015b), Sustained lobe reconnection in Saturn's magnetotail, Journal of Geophysical Research, doi: 10.1002/2015JA021768.

Thomsen, M. F., C. M. Jackman, R. L. Tokar, R. J. Wilson, (2014a), Plasma flows in Saturn's nightside magnetosphere, Journal of Geophysical Research, 119, 4521–4535.

Thomsen, M. F., D. B. Reisenfeld, R. J. Wilson, M. Andriopoulouet, et al., (2014b), Ion composition in interchange injection events in Saturn's magnetosphere, Journal of Geophysical Research: Space Physics, 119, 9761–9772, doi: 10.1002/2014JA020489.

Thomsen, M. F., R. J. Wilson, R. L. Tokar, D. B. Reisenfeld, C. M. Jackman, (2013), Cassini/CAPS observations of duskside tail dynamics at Saturn, Journal of Geophysical Research, 118, 5767, doi: 10.1002/jgra.50552.

Thomsen, M. F., (2013), Saturn's magnetospheric dynamics, Geophysical Research Letters, vol. 40, issue 20, pp. 5337–5344, doi: 10.1002/2013GL057967.

Thomsen, M. F., E. Roussos, M. Andriopoulou, P. Kollmann, C. S. Arridge, C. P. Paranicas, D. A. Gurnett, R. L. Powell, R. L. Tokar, D. T. Young, (2012), Saturn's inner magnetospheric convection pattern: Further evidence, Journal of Geophysical Research, vol. 117, issue A9, doi: 10.1029/2011JA017482.

Thomsen, M. F., D. B. Reisenfeld, D. M. Delapp, R. L. Tokar, D. T. Young, F. J. Crary, E. C. Sittler, M. A. McGraw, J. D. Williams, (2010), Survey of ion plasma parameters in Saturn's magnetosphere, Journal of Geophysical Research, vol. 115, issue A10, doi: 10.1029/2010JA015267.

Thomsen, M. F., J. P. DiLorenzo, D. J. McComas, D. T. Young, F. J. Crary, D. Delapp, D. B. Reisenfeld, N. André, (2007), Assessment of the magnetospheric contribution to the

suprathermal ions in Saturn's foreshock region, Journal of Geophysical Research, vol. 112, issue A5, doi: 10.1029/2006JA012084.

Tobie, G., N. A. Teanby, A. Coustenis, R. Jaumann, F. Raulin, J. Schmidt, N. Carrasco, A. J. Coates, D. Cordier, R. De Kok, W. D. Geppert, J.-P. Lebreton, A. Lefevre, T. A. Livengood, K. E. Mandt, G. Mitri, F. Nimmo, C. A. Nixon, L. Norman, R. T. Pappalardo, F. Postberg, S. Rodriguez, D. Schulze-Makuch, J. M. Soderblom, A. Solomonidou, K. Stephan, E. R. Stofan, E. P. Turtle, R. J. Wagner, R. A. West, J. H. Westlake, (2014), Science goals and mission concept for the future exploration of Titan and Enceladus, Planetary and Space Science, 104, pp. 59–77.

Tokar, R. L., R. E. Johnson, M. F. Thomsen, E. C. Sittler, A. J . Coates, R. J. Wilson, F. J. Crary, D. T. Young, G. H. Jones, (2012), Detection of exospheric O_2^+ at Saturn's moon Dione, Geophysical Research Letters 39, L03105, doi: 10.1029/2011GL050452.

Tokar, R. L., R. E. Johnson, M. F. Thomsen, R. J. Wilson, D. T. Young, F. J. Crary, A. J. Coates, G. H. Jones, C. S. Paty, (2009), Cassini detection of Enceladus' cold water-group plume ionosphere, Geophysical Research Letters 36, L13203, doi: 10.1029/2009GL038923.

Tokar, R. L., R. J. Wilson, R. E. Johnson, M. G. Henderson, M. F. Thomas, M. M. Cowee, E. C. Sittler Jr., D. T. Young, H.J . McAndrews, H. T. Smith, (2008), Cassini detection of water-group pick-up ions in the Enceladus torus, Geophysical Research Letters 35, L14202, doi: 10.1029/2008GL034749.

Tokar, R. L, R. E. Johnson, T. W. Hill, D. H. Pontius, W. S. Kurth, F. J. Crary, D. T. Young, M. F. Thomsen, D. B. Reisenfeld, A. J. Coates, G. R. Lewis, E. C. Sitter, D. A. Gurnett, (2006), The interaction of the atmosphere of Enceladus with Saturn’s plasma, Science 311, 1409–1412.

Tokar, R. L., R. E. Johnson, M. F. Thomsen, D. M. Delapp, R. A. Baragiola, M. F. Francis, D. B. Reisenfeld, B. A. Fish, D. T. Young, F. J. Crary, A. J. Coates, D. A. Gurnett, W. S. Kurth, (2005), Cassini observations of the thermal plasma in the vicinity of Saturn's main rings and the F and G rings, Geophysical Research Letters, 32, L14S04, doi: 10.1029/2005GL022690.

Tseng, W.-L., R. E. Johnson, M. K. Elrod, (2013a), Modeling the seasonal variability of the plasma environment in Saturn's magnetosphere between main rings and Mimas, Planetary and Space Science 77, 126–135.

Tseng, W.-L., R. E. Johnson, W.-H. Ip, (2013b), The atomic hydrogen cloud in the Saturnian system, Planetary and Space Science 85, 164–174.

Tseng, W.-L., R. E. Johnson, M. F. Thomson, T. A. Cassidy, Meredith K. Elrod, (2011), Neutral H2 and H2+ ions in the Saturnian magnetosphere, Journal of Geophysical Research, vol. 116, issue A3, doi: 10.1029/2010JA016145.

Tseng, W.-L., W.-H. Ip, R. E. Johnson, T. A. Cassidy, M. K. Elrod, (2010), The Structure and time variability of the ring atmosphere and ionosphere, Icarus 206, 382–389.

Tucker, O. J., W. Waalkes, V. M. Tenishev, et al., (2016), Examining the exobase approximation: DSMC models of Titan's upper atmosphere, Icarus, 272, 290–300.

Tucker, O. J., R. E. Johnson, J. I. Deighan, et al., (2013), Diffusion and thermal escape of H2 from Titan's atmosphere: Monte Carlo simulations, Icarus 222, 149–158.

Turtle, E. P., J. W. Barnes, M. G. Trainer, R. D. Lorenz, S. M. MacKenzie, et al., (2017), Dragonfly: Exploring Titan's prebiotic organic chemistry and habitability, vol. 48, id. 1958, 48th Lunar and Planetary Science Conference, March 20–24, 2017, TX.

Volkov, A. N., O. J. Tucker, J. T. Erwin, et al., (2011), Kinetic simulations of thermal escape from a single component atmosphere, Physics of Fluids, vol. 23, issue 6, 1–16, doi: 10.1063/1.3592253.

Vuitton, V., P. Lavvas, R. V. Yelle, M. Galand, A. Wellbrock, G. R. Lewis, A. J. Coates, J.-E. Wahlund, (2009), Negative ion chemistry in Titan's upper atmosphere, Planetary and Space Science, 57, 1558−1572.

Vuitton, V., R. V. Yelle, M. J. McEwan, (2007), Ion chemistry and N-containing molecules in Titan's upper atmosphere, Icarus, 191, 722–742.

Wahlund, J.-E., M. Galand, I. Müller-Wodarg, J. Cui, R. V. Yelle, F. J. Crary, K. Mandt, B. Magee, J. H. Waite Jr, D. T. Young, A. J. Coates, P. Garnier, K. Ågren, M. André, A. I. Eriksson, T. E. Cravens, V. Vuitton, D. A. Gurnett, W. S. Kurth, (2009), On the amount of heavy molecular ions in Titan's ionosphere, Planetary and Space Science, 57, 1857–1865, doi: 10.1016/j.pss.2009.07.014.

Waite Jr., J. H., D. T. Young, A. J. Coates, F. J. Crary, B. Magee, K. Mandt, J. Westlake, (2008), The source of heavy organics and aerosols in Titan's atmosphere, Proceedings of the International Astronomical Union, vol. 4, issue S251, February 2008, pp. 321–326, doi: 10.1017/S1743921308021844.

Waite Jr., J. H., D. T. Young, T. E. Cravens, A. J. Coates, F. J. Crary, B. Magee, J. Westlake, (2007), The process of Tholin formation in Titan's upper atmosphere, Science 316, 870, doi: 10.1126/science.1139727.

Waite, J. H., H. Niemann, R. V. Yelle, W. Kasprzak, T. Cravens, et al., (2005), Ion Neutral Mass Spectrometer (INMS) results from the first flyby of Titan, Science, 308, 982–986.

Wang, X.-B. and Wang, L.-S., (2009), Photoelectron spectroscopy of multiply charged atoms, Annual Review of Physical Chemistry, vol. 60, pp. 105–126.

Wellbrock, A., A. J. Coates, G. H. Jones, V. Vuitton, P. Lavvas, J. H. Waite, (2018), Heavy negative ions in Titan's ionosphere: The effect of polar winter conditions, submitted.

Wellbrock, A., A. J. Coates, G. H. Jones, G. R. Lewis, J. H. Waite, (2013), Cassini CAPS-ELS observations of negative ions in Titan's ionosphere: Trends of density with altitude, Geophysical Research Letters, vol. 40, issue 17, pp. 4481–4485, doi: 10.1002/grl.50751.

Wellbrock A., A. J. Coates, I. Sillanpää, G. H. Jones, C. S. Arridge, G. R. Lewis, D. T. Young, F. J. Crary, A. D. Aylward, (2012), Cassini observations of ionospheric photoelectrons at large distances from Titan: Implications for Titan's exospheric environment and magnetic tail, Journal of Geophysical Research, vol. 117, issue A3, doi: 10.1029/2011JA017113.

Went, D. R., G. B. Hospodarsky, A. Masters, K. C. Hansen, M. K. Dougherty, (2011), A new semiempirical model of Saturn's bow shock based on propagated solar wind parameters. Journal of Geophysical Research: Space Physics 116, issue A7.

Wilson, R. J., F. Bagenal, A. M. Persoon, (2017), Survey of thermal plasma ions in Saturn's magnetosphere utilizing a forward model, Journal of Geophysical Research: Space Physics, 122, 7256–7278, doi: 10.1002/2017JA024117.

Wilson, R. J., F. Bagenal, T. Cassidy, B. L. Fleshman, F. Crary, (2015), The relative proportions of water group ions in Saturn's inner magnetosphere: A preliminary study, Journal of Geophysical Research: Space Physics, 120, 6624–6632, doi: 10.1002/2014JA020557.

Wilson, R. J., F. Bagenal, P. A. Delamere, M. Desroche, B. L. Fleshman, V. Dols, (2013), Evidence from radial velocity measurements of a global electric field in Saturn's inner magnetosphere, Journal of Geophysical Research: Space Physics, vol. 118, issue 5, 2122–2132, doi: 10.1002/jgra.50251.

Wilson, R. J., P. A. Delamere, F. Bagenal, A. Masters, (2012), Kelvin-Helmholtz instability at Saturn's magnetopause: Cassini ion data analysis, Journal of Geophysical Research: Space Physics, vol. 117, issue A3, doi: 10.1029/2011JA016723.

Wilson, R. J., R. L. Tokar, W. S. Kurth, A. M. Persoon, (2010), Properties of the thermal ion plasma near Rhea as measured by the Cassini plasma spectrometer, Journal of Geophysical Research, vol. 115, issue A5, doi: 10.1029/2009JA014679.

Wilson, R. J., R. L. Tokar, M. G. Henderson, (2009), Thermal ion flow in Saturn's inner magnetosphere measured by the Cassini plasma spectrometer: A signature of the Enceladus torus?, Geophysical Research Letters, 36, L23104, doi: 10.1029/2009GL040225.

Wilson, R. J., R. L. Tokar, M. G. Henderson, T. W. Hill, M. F. Thomsen, D. H. Pontius Jr., (2008), Cassini plasma spectrometer thermal ion measurements in Saturn's inner magnetosphere, Journal of Geophysical Research, vol. 113, issue A12, doi: 10.1029/2008JA013486.

Wilson, E. H. and Atreya, S. K., (2004), Current state of modeling the photochemistry of Titan's mutually dependent atmosphere and ionosphere, Journal of Geophysical Research, 109, E06002, doi: 10.1029/2003JE002181.

Woodson, A. K., H. T. Smith, F. J. Crary, R. E. Johnson, (2015), Ion composition in Titan’s exosphere via the Cassini plasma spectrometer I: T40 encounter, Journal of Geophysical Research: Space Physics, 120, 212–234, doi: 10.1002/2014JA020499.

Yelle, R. V., J. Cui, I. C. F. Muller-Wodarg, (2008), Methane escape from Titan’s atmosphere, Journal of Geophysical Research, 113, doi: 10.1029/2007JE003031.

Young, D. T., J-J. Berthelier, M. Blanc, J. L. Burch, S. Bolton, A. J. Coates, F. J. Crary, et al., (2005), Composition and dynamics of plasma in Saturn's magnetosphere, Science, vol. 307, issue 5713, pp. 1262–1266, doi: 10.1126/science.1106151.

Young, D. T., J. J. Berthelier, M. Blanc, J. L. Burch, A. J. Coates, R. Goldstein, M. Grande, et al., (2004), Cassini plasma spectrometer investigation, Space Science Reviews, vol. 114, issues 1–4, pp. 1–112, doi: 10.1007/s11214-004-1406-4.